

PROJECT ADMINISTRATION DATA SHEET

ORIGINAL REVISION NO. _____

Project No. A-3233 DATE 5/3/82

Project Director: Dr. Ron Bohlander ~~Senes~~ Lab EML/RSD

Sponsor: U. S. Army Missile Command; Redstone Arsenal, AL 35898

Type Agreement: Delivery Order No. 51 under Contract No. DAAH01-81-D-A003

Award Period: From 4/21/82 To 8/31/82 (Performance) 8/31/82 (Reports)

Sponsor Amount: \$35,019 Contracted through:

Cost Sharing: None GTRI/~~CDX~~

Title: Government Owned Quasi-Optical Scanning Multiport (QUOSM) Network Analyzer (RDF-44)

ADMINISTRATIVE DATA OCA Contact Linda H. Bowman x4820

1) Sponsor Technical Contact:
Dr. M. M. Hallum
Systems Simulation and Development Directorate
U. S. Army Missile Command
Attn: DRSMI-RDF
Redstone Arsenal, AL 35898
205-876-4141

2) Sponsor Admin/Contractual Matters:
Mr. Thomas A. Bryant
ONR Resident Representative
Georgia Institute of Technology
206 O'Keefe Building
Atlanta, GA 30332

Defense Priority Rating: DO-A2 under DMS Reg. 1 Security Classification: Unclassified

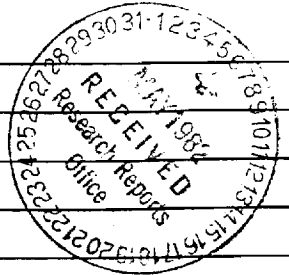
RESTRICTIONS

See Attached Government Supplemental Information Sheet for Additional Requirements.

Travel: Foreign travel must have prior approval - Contact OCA in each case. Domestic travel requires sponsor approval where total will exceed greater of \$500 or 125% of approved proposal budget category.

Equipment: Title vests with Government; except that items costing less than \$1,000 vests with GIT if prior approval to purchase is obtained from the Contracting Officer.

COMMENTS:



COPIES TO:

- Administrative Coordinator
- Research Property Management
- Accounting
- Procurement/EES Supply Services
- FORM OCA 1-781
- Research Security Services
- Reports Coordinator (OCA) ✓
- Legal Services (OCA)
- Library
- EES Public Relations (2)
- Computer Input
- Project File
- Other _____

SPONSORED PROJECT TERMINATION SHEET

Date 6/29/83

Project Title: "Government Owned Quasi-Optical Scanning Multipoint (QUOSM) Network Analyzer, RDF-44"

Project No: A-3233

Project Director: Dr. Ron Bohlander

Sponsor: U. S. Army Missile Command; Redstone Arsenal, AL

Effective Termination Date: 10/31/82

Clearance of Accounting Charges: 10/31/82

Grant/Contract Closeout Actions Remaining:

- Final Invoice ~~and Closing Documents~~
- Final Fiscal Report
- Final Report of Inventions
- Govt. Property Inventory & Related Certificate
- Classified Material Certificate
- Other _____

Assigned to: EML/RSD ~~(School/Laboratory)~~

COPIES TO:

Administrative Coordinator	Research Security Services	EES Public Relations (2)
Research Property Management	Reports Coordinator (OCA)	Computer Input
Accounting	Legal Services (OCA)	Project File
Procurement/EES Supply Services	Library	Other _____

1000 A 1000

QUasi-Optical Scanning Multiport (QUOSM)
Network Analyzer: Solutions to the
Problem of Standing Waves

R.A.Bohlander, A.McSweeney,
V.T.Brady, and R.G.Shackelford

FINAL REPORT

Contract No. DAAH01-81-D-A003
Delivery Order Number 51
(A-3233)

Prepared by
Engineering Experiment Station
Georgia Institute of Technology
Atlanta, Georgia 30332

Prepared for
U.S. Army Missile Command
TMDE Support Group
Redstone Arsenal, Alabama 35898

April 8, 1983

REPORT DOCUMENTATION PAGE		READ INSTRUCTIONS BEFORE COMPLETING FORM
1. REPORT NUMBER A-3233	2. GOVT ACCESSION NO.	3. RECIPIENT'S CATALOG NUMBER
4. TITLE (and Subtitle) Quasi-optical Scanning Multiport (QUOSM) Network Analyzer: Solutions to the Problem of Standing Waves		5. TYPE OF REPORT & PERIOD COVERED FINAL REPORT 21 Apr. 82 - 30 Nov. 82
		6. PERFORMING ORG. REPORT NUMBER A-3233
7. AUTHOR(s) R. A. Bohlander, A. McSweeney, V. T. Brady, and R. G. Shackelford		8. CONTRACT OR GRANT NUMBER(s) DAAH01-81-D-A003 Delivery Order No. 51
9. PERFORMING ORGANIZATION NAME AND ADDRESS Georgia Institute of Technology EES/EML/MMD Atlanta, Georgia 30332		10. PROGRAM ELEMENT, PROJECT, TASK AREA & WORK UNIT NUMBERS
11. CONTROLLING OFFICE NAME AND ADDRESS U.S. Army Missile Command TMDE Support Group Redstone Arsenal, Alabama 35898		12. REPORT DATE 8 Apr. 83
		13. NUMBER OF PAGES 92
14. MONITORING AGENCY NAME & ADDRESS (if different from Controlling Office)		15. SECURITY CLASS. (of this report) UNCLASSIFIED
		15a. DECLASSIFICATION/DOWNGRADING SCHEDULE
16. DISTRIBUTION STATEMENT (of this Report)		
17. DISTRIBUTION STATEMENT (of the abstract entered in Block 20, if different from Report)		
18. SUPPLEMENTARY NOTES		
19. KEY WORDS (Continue on reverse side if necessary and identify by block number) Network Analyzers Reflectometer Millimeter Wave Quasi-Optical Six-Ports		
20. ABSTRACT (Continue on reverse side if necessary and identify by block number) Advanced calibration and data analysis techniques have been developed to compensate for the effect of standing waves in a new type of millimeter wave reflectometer. This instrument, the Quasi-Optical Scanning Multiport, was developed under a previous contract to be an alternative to guided wave Six Port Network Analyzers and one which offers much greater facility at the high frequency end of the millimeter wave spectrum. The present work describes a calibration		

procedure adapted from use with six-ports that involves an eigenvector analysis of detector readings with various calibration devices installed. The calibration devices required are a waveguide load and short, a quasi-optical absorbing load, and a quasi-optical means of delaying signals to and from the test port. A computer simulation has been implemented to demonstrate that the technique works. Tests of pyroelectric detectors have also been made. Recommendations for future work are made.

Table of Contents

	<u>PAGE</u>
1.0 Introduction.....	1
1.1 Statement of Objectives.....	2
2.0 Correction for Standing Waves in Calibration Procedure.....	4
2.1 Introduction.....	4
2.2 Extension of the Phasor Representation to Include Standing Waves.....	10
2.3 Method Adapted from the Analysis of Six-Ports.....	16
2.4 Eigenvalue/vector Analysis.....	34
2.5 Simulation of QUOSM Signals.....	39
2.6 Simulated Calibration.....	47
3.0 Reduction of Standing Waves.....	57
3.1 Experiments with the Detector.....	57
3.2 Isolation by Attenuation.....	59
4.0 Status of Hardware and Software.....	61
5.0 Summary.....	63
6.0 Future Work.....	64
7.0 References.....	67
 Appendices	
A. Software to Simulate QUOSM Signals Including the Effects of Standing Waves.....	69
B. Software to Calculate Eigenvalues and Eigenvectors for Calibrating the QUOSM.....	76
C. Software to Calculate Termination Parameters.....	88
D. Energy Conservation in the QUOSM.....	91

LIST OF FIGURES

<u>FIGURE</u>		<u>PAGE</u>
2.1	Original QUOSM Design.....	5
2.2	Quasi-Optical Scanning Multiport (QUOSM) Network Analyzer.....	6
2.3	Vector Diagram of QUOSM Signals Without Standing Waves.....	8
2.4	Phasor Sum for Standing Wave Case.....	14
2.5	Six-Port Network.....	17
2.6	Calibration Device Required by Eigenvector Method.	22
2.7	Procedure for Calibration of Six-Port.....	24
2.8	Example of a Six-Port Reflectometer Circuit.....	27
2.9	Modified QUOSM Design.....	28
2.10	Emulation of Sliding Transmission Line for QUOSM..	30
2.11	Procedure for Calibration of QUOSM.....	33
2.12	Initial Optical Paths from Source and Detector....	40
2.13	Optical Paths from Beam Splitter to Mirror and Test Port.....	41
2.14	Optical Paths from Mirror and Test Port back to the Beam Splitter.....	42
2.15	Optical Paths back to Source and Detector.....	43
3.1	Type of Pyroelectric Detector Element Tested.....	58

LIST OF TABLES

<u>TABLE</u>		<u>PAGE</u>
2.1	List of Signal Paths.....	12
2.2	Parameters Used in Simulation of Standing Waves....	48
2.3	Test Port Parameters for Case of Standing Waves....	50
2.4	Test Port Parameters for Case of No Standing Waves.	52
2.5	Parameters for Test Port Delays Achieved with Dielectric Plates.....	54
2.6	Test Port Parameters With and Without Noise.....	55

1.0 Introduction

Under contract DAAH01-81-D-A003 delivery order number 51, the Engineering Experiment Station of Georgia Tech (GT/EES) has performed further work on a millimeter wave network analyzer based on quasi-optical rather than guided-wave techniques. An analyzer called a QUasi-Optical Scanning Multiport (QUOSM) was developed under a previous contract (DAAH01-80-C-1634), and the focus of the current work reported here is the development of advanced calibration and data analysis techniques. These address problems with internal standing waves that were found during the previous contract activities. Present results indicate that the problems have been largely overcome and that the QUOSM shows considerable promise. Further work on indicated hardware modifications and on obtaining new data will be recommended.

Automatic network analyzers based on guided-wave six-port circuits had been implemented down to millimeter wavelengths when work on a quasi-optical alternative was initiated under the previous contract. The QUOSM was designed to circumvent the difficulty of constructing guided-wave components, and the increased power losses in them at frequencies higher than 100 GHz. In addition, the four major advantages of automatic network analyzers have been preserved in the design of the QUOSM: (1) Both amplitude and relative phase information for power crossing the test interface are measured utilizing simple power detectors instead of more complex heterodyne systems. (2) Imperfections in the measurement system are found by calibration and are corrected numerically in treating the data. (3) The "circuit" is well-suited to automatic network analysis because it requires little, if any, tuning or modification for each interface to be tested. (4) The "circuit" covers a relatively wide frequency band when calibrated at each test frequency within the band. The working range of the QUOSM is intended to be 90 to 340 GHz with no changes in components within this range except for the need to

change the couplers to the source and to the test device when waveguide sizes change.

Work in the previous contract was divided into three phases:

1) The initial phase [1] culminated in a preliminary design of the QUOSM and included a study of its expected performance based on computer simulations.

2) The second phase of the work [2] consisted of the detailed design, procurement, and fabrication of the components.

3) The system was assembled, aligned, and tested in the third phase [3]. A computer program was written to perform the data acquisition and analysis based on the previous computer simulations.

During the course of testing the QUOSM performance, internal standing waves were discovered that were of such magnitude that the calibration and analysis procedures would have to be revised substantially in order to take them into account. On the basis of measurements made at that time, reasonable steps to reduce the magnitude of the standing wave phenomenon were suggested, but it was judged unlikely that the problem could be essentially eliminated in that way. Thus, consistent with the trend of most modern work on automatic network analyzers, the stress in the present work was on adjustments to the calibration and analysis procedures as a solution to the standing wave problem.

1.1 Statement of Objectives

In summary, the objectives under the present contract (DAAH01-81-D-A003 delivery order 51) were the following:

1. To develop a calibration procedure and an algorithm that corrects for standing wave effects in deriving the reflection properties of a device under test (DUT).
2. To reduce standing wave effects in the QUOSM since this may improve the accuracy afforded by the correction procedures.

3. To provide two horns that add the capability to test WR-10 devices with the QUOSM.
4. To demonstrate the use of the QUOSM on some trial test devices and to demonstrate the effect of flange reflections.

The first three objectives have been met, but the level of effort required to meet the first objective was greater than foreseen, and thus the fourth objective could not be met within the time and funds available. Recommendations for further work will be made in this report.

2.0 Correction for Standing Waves in Calibration Procedure

2.1 Introduction

The QUOSM was originally designed to be similar to the Michelson or Twyman-Green types of optical interferometers. These are generally described as "two-beam" interferometers from the fact that the principal beam splitter divides the beam from the source into two parts which are later recombined at the detector where some degree of interference between the two beams may be seen. The similarity between the QUOSM and these interferometers may be seen in Figure 2.1 in which the principal components are shown in relation to the path of the radiation.

A photograph of the actual system is given in Figure 2.2 and a brief review of the design will be given here. The reader is referred to previous reports [1-3] for more detailed descriptions and explanations. Radiation from a source such as a klystron is launched into the interferometer by the source horn. This in turn feeds a lens which forms a beam that has a Gaussian profile and a minimum lateral width on the principal beam splitter. The beam first falls on another beam splitter, however, that directs a small fraction of the power to a reference detector which was designed to provide a leveling signal to compensate for source fluctuations. Then the signal is split into two beams by the principal beamsplitter, one beam falling on a mirror which can be moved in precisely measured increments along the beam, thereby introducing delay, and another falling on a lens and horn pair which are identical to the source port and which serve as the test device and calibration port. Radiation reflected by a test device as well as that reflected by the movable mirror are recombined then at the principal beam splitter and continue on to a lens which focuses the radiation on the principal detector. The movable mirror and the test port components are designed and positioned such that there is complete symmetry of the Gaussian beam around its intersection with the principal beam splitter.

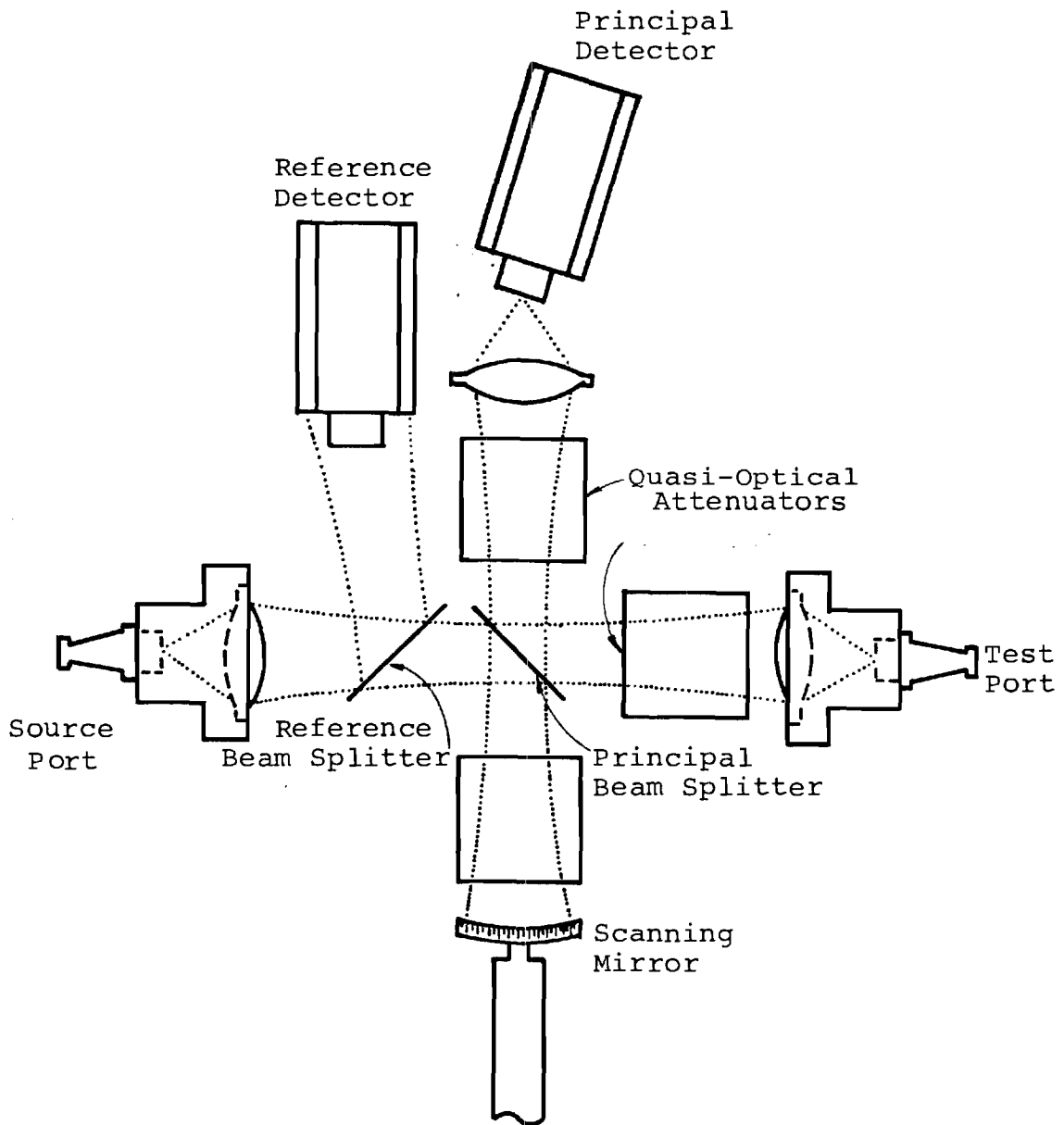
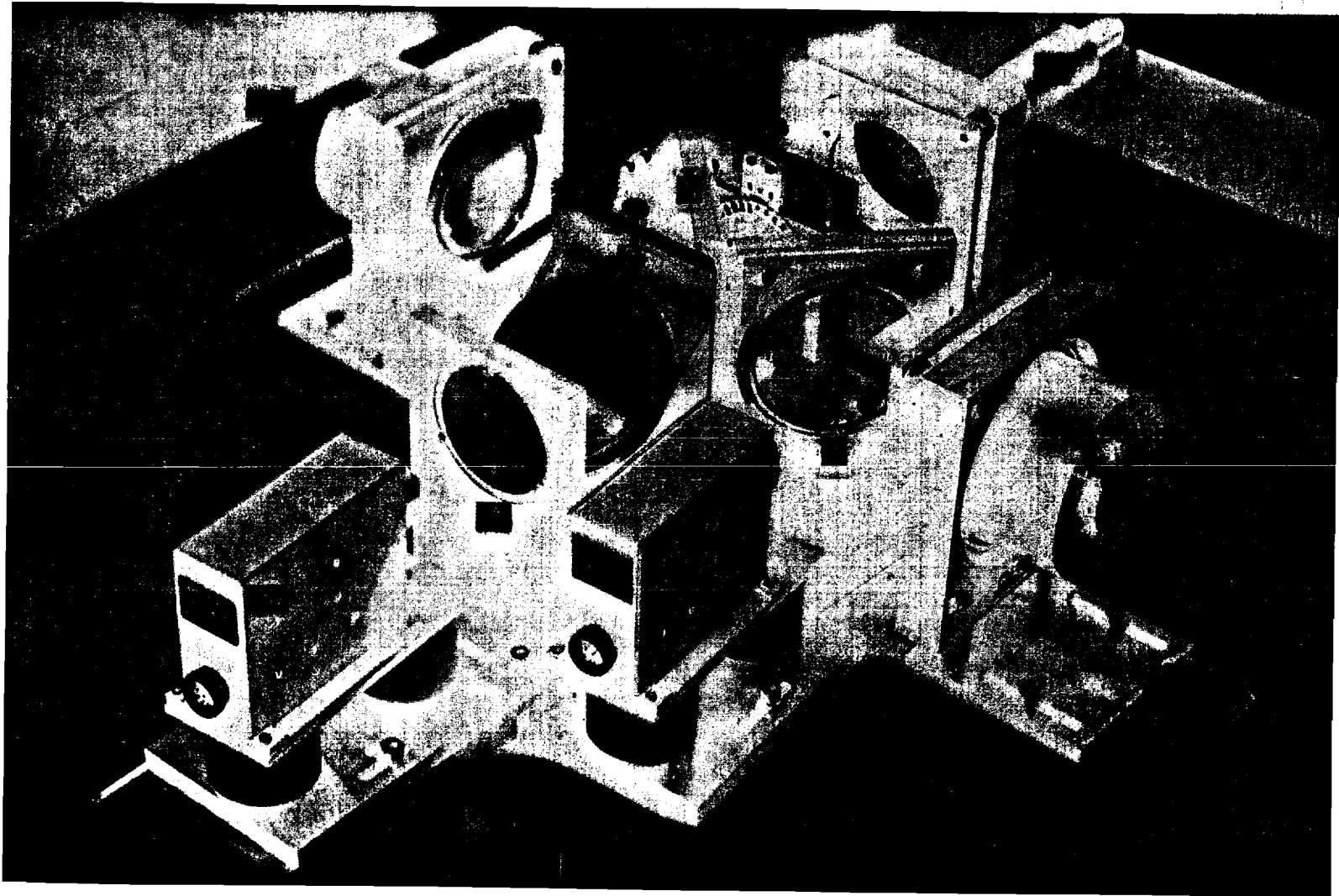


Figure 2.1 Original QUOSM Design.



↑
Change to
page 6

Change to →
Figure 2.2

Fig. 8. Quasi-Optical Scanning Multiport (QOSM) Network Analyzer.
B = Beamsplitter, I = Inchworm, L = Lens
P = Polarizing beamsplitter, PD = Primary Detector,
RD = Reference Detector, S = Source horn, T = Test port

One may notice also that the beam passes through quasi-optical signal attenuators in the mirror, test port, and principal detector arms of the system and these are provided for such signal level adjustments as may be necessary and for some isolation capability, as will be discussed later. Both detectors are of the Golay cell type with 5mm diameter apertures fitted with crystal quartz windows and appropriate optical filters. As configured, they are sensitive to the entire frequency range 90 to 340 GHz required in the use of the QUOSM.

In a previous theoretical model of QUOSM performance [1], the signal arriving at the detector was assumed to be formed by the combination of three signals; namely, that reflected by the scanning mirror, that reflected by the lens-horn transition of the test port, and that reflected by the test device itself. The amplitudes and phases of these signals may be represented by phasor-type vectors, and the combined signal, as a vector sum as shown in Figure 2.3. The dashed line shows the loci of the tips of the detector phasor when the scanning mirror location is moved along the optical beam. This can be used to show that the resulting detector signal power will vary sinusoidally with linear motion of the scanning mirror, and have a period equal to half the source wavelength. Previous analysis showed how to find the phase of the signal reflected by the test port and the relative amplitudes of the signals from the test port and from the scanning mirror [1]. A least squares method was used to fit sinusoidal functions and to obtain the desired parameters. A null reflector (tapered load) was devised for a calibration at the test port that allows one to measure the reflection from the test port horn and lens and thus to separate this signal component from reflections by test devices themselves. The second calibration device is a near perfect reflector that is used as a standard for reflectivity and as a reference for phase.

An essential assumption for the above model to be correct is that the signals falling on the detector are completely absorbed,

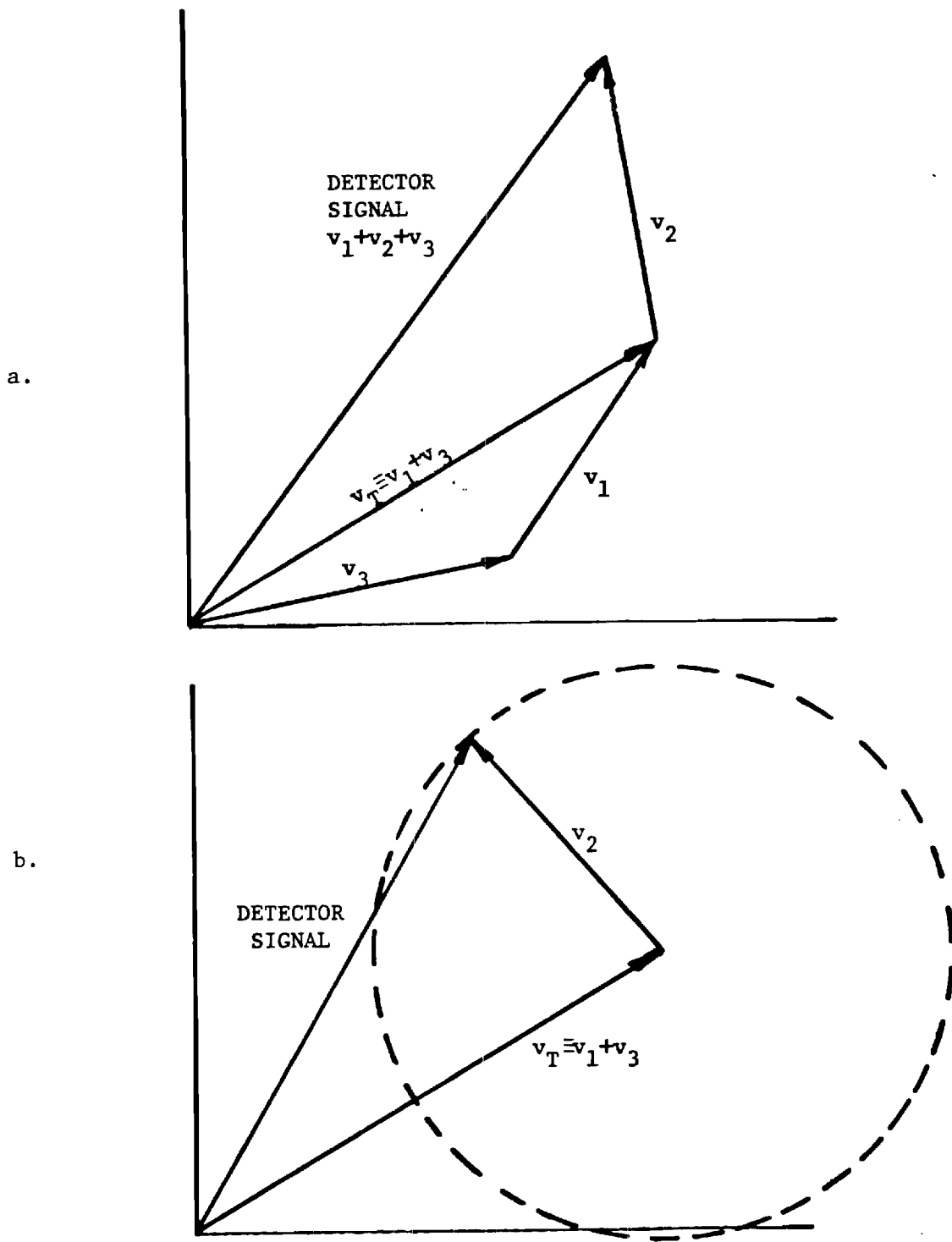


Figure 2.3a. Vector diagram of signals reaching the principal detector in QUOSM. Each vector represents a field strength so that the power reaching the detector is the square of the length of the vector marked "detector signal." The direction of each vector indicates signal phase. v_1 comes from the test port, v_2 from the scanning mirror and v_3 from the horn-lens at the test port. 2.35. The dashed line shows where the tip of vector v_2 lies for all possible positions of the scanning mirror. The tip of the vector representing the detector signal also lies on this circle.

or at least that any residual signal scattered or reflected by the detector does not reenter the interferometric portion of the QUOSM. Since some of the signals reflected by the test port and by the scanning mirror are also returned to the source port, there is a similar requirement that signals scattered by the source port not reenter the interferometric portion of the system. If these conditions are not met, electromagnetic energy is partly trapped between the ends of the four arms of the QUOSM (i.e., in the beams bounded by the source port, the test port, the scanning mirror, and the detector), and in this cavity-like system, standing waves are formed. In the final report of the previous contract activity [3], it was shown that reflections at the detector port were larger than expected and in particular that a tilt of the detector did not suppress the reflections as expected. Apparently, the metal surrounding the detector element acted somewhat like a retro-reflector in its reflection properties. It was demonstrated [3] that this did indeed produce standing waves; for, with the test port blocked by an absorber, one could still observe interference fringes when the scanning mirror was moved.

One approach to solving this problem, in principle, is to devise more thorough ways to suppress the standing waves. Consideration was given to various mechanisms but this was not chosen as the primary line of attack in the present work for several reasons. First, reliance for accuracy on the perfection of components in a network analyzer has been found to be unsatisfactory in general [4] and is contrary to current trends in metrology. Secondly, the problem is not necessarily isolated in just one component. Not only would an improved detector configuration be required, but it is also likely that something would need to be done to reduce back reflections from the lenses. Such a reduction over a wide frequency range, although tractable, is not a negligible undertaking. Moreover, although it could be argued in the particular case studied previously [3] that the

reflections from the detector port were more important than those from the source port, this would not necessarily be true for all frequencies. The beam splitter properties at frequencies other than 94 GHz could be such as to give more weight to the effects of the source port. Measurements of the reflectance of the source port have not been made, so this possible source of standing waves cannot be totally discounted. Since there were these difficulties and complications, the primary effort in the present contract was instead the investigation of ways to allow for the effects of standing waves through mathematical procedures in the analysis of the data and through revisions in the calibration procedures.

The following sections discuss the efficacy of two alternative analytical methods, one of which turned out to be successful. Later, some brief experiments are described that were aimed at whether the standing waves could be reduced in magnitude.

2.2 Extension of the Phasor Representation to Include Standing Waves

Once standing waves are introduced into the interferometric section of the QUOSM, the number of paths which radiation can follow and reach the detector becomes infinite. If the reflectance of the source port and detector port are both sufficiently low, one may argue that radiation which is reflected more than once by either one of these ports (or a combination of them) is too weak to be significant. Unfortunately it has been found that this approximation is not a good one given what are now believed to be reasonable values of the detector or source port reflectances. From modeling efforts which will be described later, it was found that a few multiple reflections generally were significant. Further close examinations of the detector signal obtained when the test port was blocked and the scanning

mirror moved, have suggested that multiple reflections were occurring. Since this is the case, it has been concluded that a meaningful phasor description of the signals in the QUOSM is completely unmanageable as a basis for calibration and analysis.

The reader may if he wishes skip the remainder of this section and proceed to Section 2.3 where a viable alternative is discussed. In the remainder of this section, a phasor description is discussed for the case in which the low detector and low source reflectance approximation mentioned above holds. This serves to show that even this first-order standing wave case is much more complicated than one would like since the number of paths by which radiation can reach the detector is considerably more than two, as shown by the list in Table 2.1.

Each signal path can be represented by a phasor that shows the amplitude and relative phase of the signal that reaches the detector; and then, as before, the net detector signal may be found from the squared modulus of the vector sum of the phasors. Intuitively, some simplification can be made by grouping the phasors as indicated in Table 2.1 and by forming the vector sum of the phasors in each group. There are two ideas behind this: (1) Clearly the paths like S-M-D-T-D and S-T-D-M-D are indistinguishable in terms of detector signal, and the sum is just twice the phasor for one of them. (2) Phasors that come from paths that differ only by whether the source (S) or the detector (D) acts as a partial reflector in the middle can be added without loss of generality. This second point is somewhat subtle. The radiation reflected by the detector and the source merges again when the two beams intersect at the beam splitter, and the final result is the same as if there had been one partial reflector with an effective complex reflectance which is a fixed linear combination of the complex reflectances of the source port and the detector port. This linear combination does not depend on the mirror position nor on the nature of the reflection at the test port, and thus at a given frequency it is constant and may

Table 2.1 List of Signal Paths Connecting the Source to the Detector in the QUOSM

Key

S Source
D Detector
T Test Port
M Scanning Mirror

Zero-Order Paths

S-M-D (means that radiation goes from the source to the mirror to the detector)

S-T-D

First-Order Paths Contributing to Standing Waves

S-M-D-M-D two reflections by the mirror

S-M-S-M-D

S-M-D-T-D one reflection each by the

S-M-S-T-D mirror and the test port

S-T-D-M-D

S-T-S-M-D

S-T-D-T-D two reflections by the

S-T-S-T-D test port

in principle be found by calibration. Therefore, in the case of first-order standing waves, one may represent the detector signal by forming the vector sum of five phasors, two which come from the zero-order paths, and three which come from the first-order groups in Table 2.1.

Even with these simplifications, the picture derived from the phasor sum is quite complicated, as is illustrated in Figure 2.4. The fixed vectors are those which involve only reflections by the test port. The remaining phasors involve reflections from the scanning mirror and will rotate when the mirror moves. The sum of vectors W_3 and W_4 rotates around the foot of W_3 , and the loci of the tips of the sum are on a dashed circle as shown. Finally the tip of signal W_5 moves on an epicycle shown as a dash-dot line in the figure. The squared modulus of the vector sum representing the detector signal can be decomposed into a sum of a constant plus two sinusoidal variations with mirror position, one with a period of half of a wavelength and one with a period of a quarter of a wavelength. This picture is further complicated by the fact that each signal component reflected by the test port, like those represented by W_1 , W_2 , and W_4 , is in reality the vector sum of a signal reflected by the test port horn-lens and one reflected by the test device.

The general method used previously [1] (for the case in which the QUOSM was assumed to have no standing waves) was to use a calibration load in place of the test device to reduce the number of vectors and make it possible to solve for the remaining ones by the least squares method. Then one was able to exchange the load for the test device and use the knowledge gained to solve for the magnitude and phase of the remaining vectors by further application of the least squares method. Since there are many more vectors in the diagram in Figure 2.4 than in Figure 2.3, it is fairly apparent that more calibration steps and devices would be needed to be able to decompose the detector signal into all the component vectors. A large absorber that could be placed

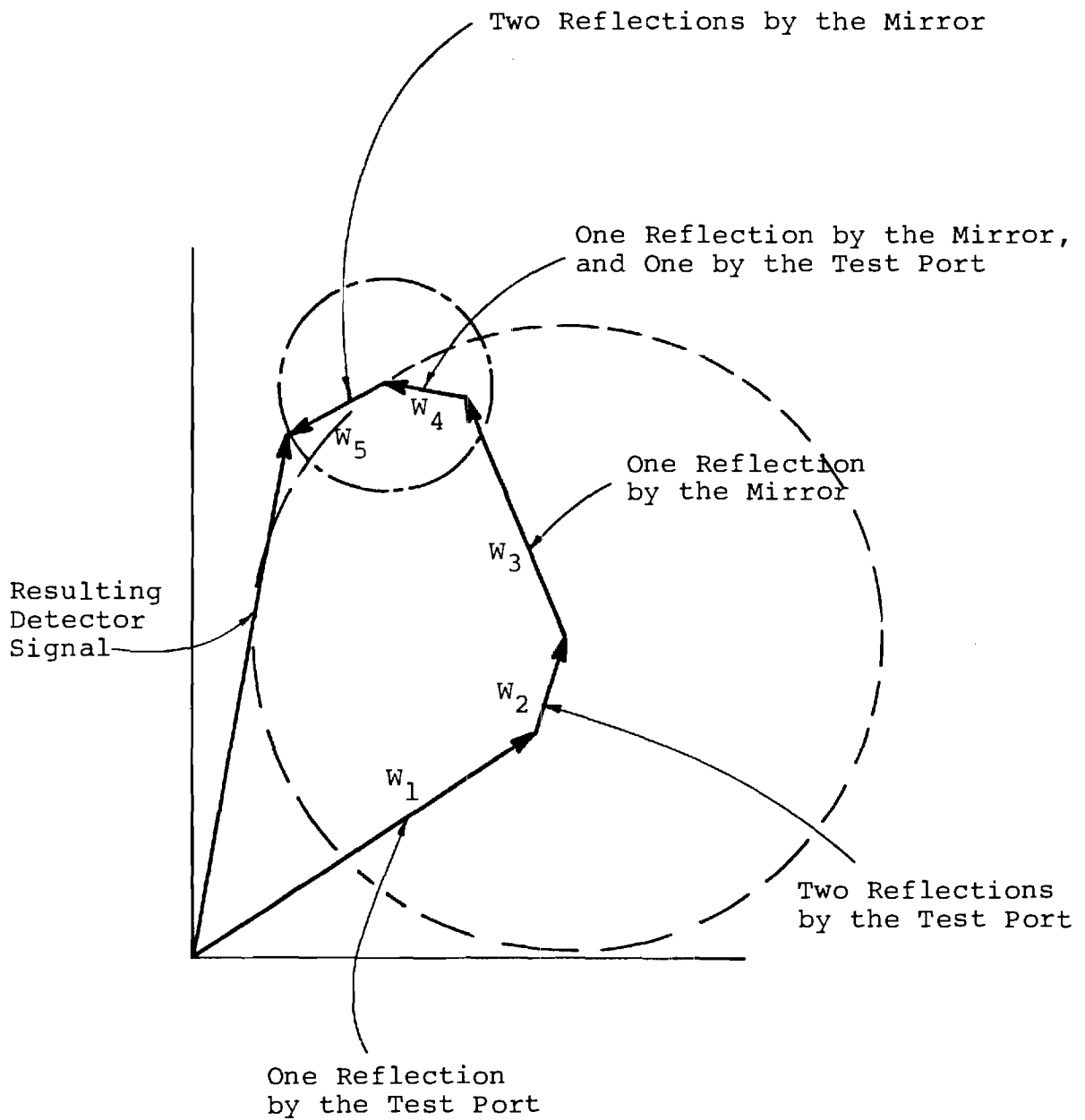


Figure 2.4 Phasor Sum for the Detector Signal in the First-order Standing Wave Case.

alternately in front of the test port and then in front of the scanning mirror would be helpful. However, absorbers alone will not be completely sufficient, since for example, no absorber can remove just one of a pair of signals like W_1 and W_2 , and some other type of calibration device would be needed.

Work on this phasor approach was halted at this point due to the evidence, discussed earlier, that more than one reflection from the detector or source port is likely to be significant. One can readily see from the foregoing discussion that the phasor analysis would be untractable in this case. An alternative method is much better suited, as it turns out, and is described in the following sections.

2.3 Method Adapted from the Analysis of Six-Ports

2.3.1 Review of Findings for Six-Ports

Present-day calibration and data reduction schemes used with six-port reflectometers are based on the concept of the scattering matrix [S]. A significant advantage of this approach compared with phasor analysis of multiport devices is that multiple reflections, and hence standing waves, are more easily handled. The complex S parameters in the matrix [S] relate traveling waves moving away from each port in terms of linear combinations of traveling waves incident upon every port [5], and multiple reflections are implicitly included in these linear combinations. One of the most effective schemes of analysis is that of Cronson and Susman [6,7] who developed an eigenvector analysis derived from scattering matrices for calibrating the single six-port reflectometer.

In the study reported on here, a closer analogy has been drawn between the QUOSM and the six-port reflectometer. From this it may be shown how the analytical tools developed by Cronson and Susman can be adapted to the calibration and reduction of data from a QUOSM regardless of whether or not there are standing waves present. This will be substantiated by simulations described later.

Before consideration is given to the analogy between the six-port reflectometer and the QUOSM, the work of Cronson and Susman on mathematical analyses of six-port reflectometers will be reviewed. Figure 2.5 represents a six-port network with source port (port 1), test port (port 2), and power measurement ports (ports 3-6). Note that port 3 monitors the power incident on the DUT at the test port. It is well known [8] that the wave amplitude incident on each of the four output power meters can be written as a linear combination of the complex scattering variables a and b at the test or measurement port. The complex

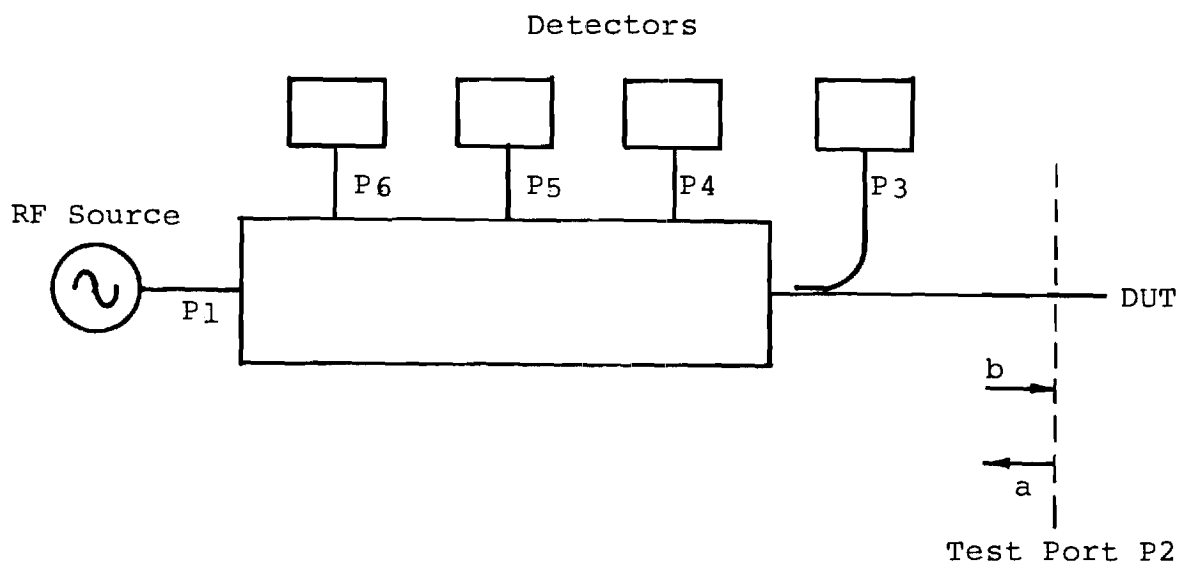


Figure 2.5 Six-port Network.

reflection coefficient at port 2 is defined as:

$$\Gamma = a/b \quad (1)$$

Thus, one may show that an unknown reflection coefficient can be found from four power measurements through the use of a matrix equation which will be given below. The output power at port i , P_i , is a linear combination of four complex quadratic variables: $|b|^2$, ab^* , a^*b , and $|a|^2$. The sets of four power readings and quadratic variables may be expressed as column matrices $[p]$ and $[b_q]$

$$[p] = \begin{bmatrix} P_3 \\ P_4 \\ P_5 \\ P_6 \end{bmatrix} \quad [b_q] = \begin{bmatrix} |b|^2 \\ ab^* \\ a^*b \\ |a|^2 \end{bmatrix}$$

and the matrix equation relating the two may be written as*

$$[p] = [C^{-1}] [b_q] \quad (2)$$

where $[C^{-1}]$ is a 4 by 4 complex matrix of proportionality constants. If $[C^{-1}]$ is invertible the above equation is written in its more useful form:

$$[b_q] = [C] [p]. \quad (3)$$

Thus, once $[C]$ is calculated in the calibration process, an unknown reflection coefficient of a test device

$$\Gamma = a/b = ab^*/|b|^2 \quad (4)$$

can be calculated from the result of multiplying the constant calibration matrix $[C]$ by a set of four power measurements taken with the test device connected to the six-port.

A brief review of the procedure [7] for calibration with known standards follows. Suppose one has a set of m standard reflectors for which the complex values Γ_i are known. Then the column matrices $[b_q]_i$ can be calculated a priori in terms of $|b|_i^2$, the column matrices $[p]_i$ can be measured, and each are

* Throughout the report brackets around a letter will denote a matrix. If the letter symbol is underlined the matrix is square.

related by equation (3). Since the calibration matrix $[C]$ is constant for all the standards, an augmented matrix equation can be constructed:

$$[B_Q] = [C] [P], \quad (5)$$

where

$$[B_Q] = \begin{bmatrix} |b|_1^2 & \cdot & \cdot & \cdot & |b|_m^2 \\ ab_1^* & & & & ab_m^* \\ a^*b_1 & & & & a^*b_m \\ |a|_1^2 & \cdot & \cdot & \cdot & |a|_m^2 \end{bmatrix}$$

$$[P] = \begin{bmatrix} P_{31} & \cdot & \cdot & \cdot & P_{3m} \\ P_{41} & & & & P_{4m} \\ P_{51} & & & & P_{5m} \\ P_{61} & \cdot & \cdot & \cdot & P_{6m} \end{bmatrix}$$

It is helpful for later discussion to note that a $4 \times m$ matrix $[B_Q]$ can be decomposed into the product of an $m \times m$ diagonal matrix whose diagonal elements are the power levels incident on each standard load

$$[B_Q] = \begin{bmatrix} |b|_1^2 & 0 & 0 & \dots & 0 \\ 0 & |b|_2^2 & 0 & & 0 \\ 0 & 0 & & & \\ 0 & 0 & 0 & \dots & |b|_m^2 \end{bmatrix}$$

and a $4 \times m$ matrix $[\Gamma]$ of known reflection coefficients

$$[\Gamma] = \begin{bmatrix} 1 & 1 & \dots & 1 \\ \Gamma_1 & \Gamma_2 & & \Gamma_m \\ \Gamma_1^* & \Gamma_2^* & & \Gamma_m^* \\ |\Gamma_1|^2 & |\Gamma_2|^2 & \dots & |\Gamma_m|^2 \end{bmatrix}$$

Then from equation (5),

$$[B_Q] = [\Gamma][B_Q] = [C][P]. \quad (6)$$

When one only needs to find out the ratio $\Gamma = a/b$ for a test device, it is unnecessary to know the absolute value of the

calibration matrix. Rather it is sufficient to know each element of $[C]$ to within a fixed (but unknown) constant of proportionality. In this case, the calibration matrix is sufficiently determined by equation (6) provided that the following conditions are met:

1. the calibration loads, $[\Gamma_i]$, are known,
2. the power, $|b|^2$, incident on the test port is either kept constant or the relative size of the powers $|b_1|^2$, $|b_2|^2$, ... are known, and
3. at least four columns of $[P]$ are linearly independent.

Condition 3 is required so that $[P][P^t]$ can be inverted in the solution for the calibration matrix $[C]$:

$$[C] = ([B_Q] [P^t]) ([P] [P^t])^{-1}. \quad (9)$$

If fewer than four of the columns of matrix $[P]$ are linearly independent, then the rank of $[P][P^t]$ is less than its order (four) and the matrix is singular or not invertible. Provided that the above conditions are satisfied, Equation (9) can be utilized to calculate the elements of the calibration matrix $[C]$ from the known values of $[B_Q]$ and the measured values of $[P]$. This matrix is constant for a given wavelength, but must be recalculated for substantially different wavelengths.

In practice, the second condition is most easily met by dedicating one of the four detectors (say the one on port 3) to monitoring the power flowing toward the test port. The coupler for this detector is best located near the test port as shown in Figure 2.5 so that the detector is highly isolated from the reflected signal. If both the $[B_Q]$ matrix and the matrix of power readings $[P]$ are multiplied (i.e., normalized) by the matrix

$$[P_{\circ}^{-1}] = \begin{bmatrix} 1/P_{3,1} & 0 & . & . & . & 0 \\ 0 & 1/P_{3,2} & & & & 0 \\ 0 & 0 & & & & 0 \\ \vdots & \vdots & & & & \\ 0 & 0 & . & . & . & 1/P_{3,m} \end{bmatrix}$$

then condition (2) above is fulfilled. Rather than complicate the notation further, it will be understood in the remainder of this report that this normalization will always be done.

Condition 1 on the other hand is difficult to achieve in practice. As the test wavelength is decreased into the low-millimeter range it becomes increasingly difficult to characterize standards accurately enough for the above procedure to be effective. A self-calibration method has been implemented by Cronson and Susman [7] to alleviate this difficulty. Strictly speaking, a self-calibration method would not require any known standards, just calibration devices that are repeatable. In their method, the repeatable calibration devices are a pair of terminations (diagrammed in Figure 2.6) that can be connected to the test port by a sliding transmission line. For best results, the two terminations differ in the signal they reflect by 3 dB and in the phase of the reflection by about 45° [6]. Several repeatable lengths of the sliding transmission line are used, and the two terminations are connected to the sliding section by a switch so that repeatable exchanges can be made. The self-calibration method of Cronson and Susman is almost ideal in that only two other calibration devices are needed which are standards in the usual meaning of the term. These are standards for opposite ends of the reflection scale; namely, a matched load for near-zero reflection and a known short of high reflection. Thus, the number of standards required has been reduced from four or more to only two. The key point in this advance was the realization on the part of Cronson and Susman that the relationship between the power measurements made and the calibration matrix could be formulated as an eigenvector problem.

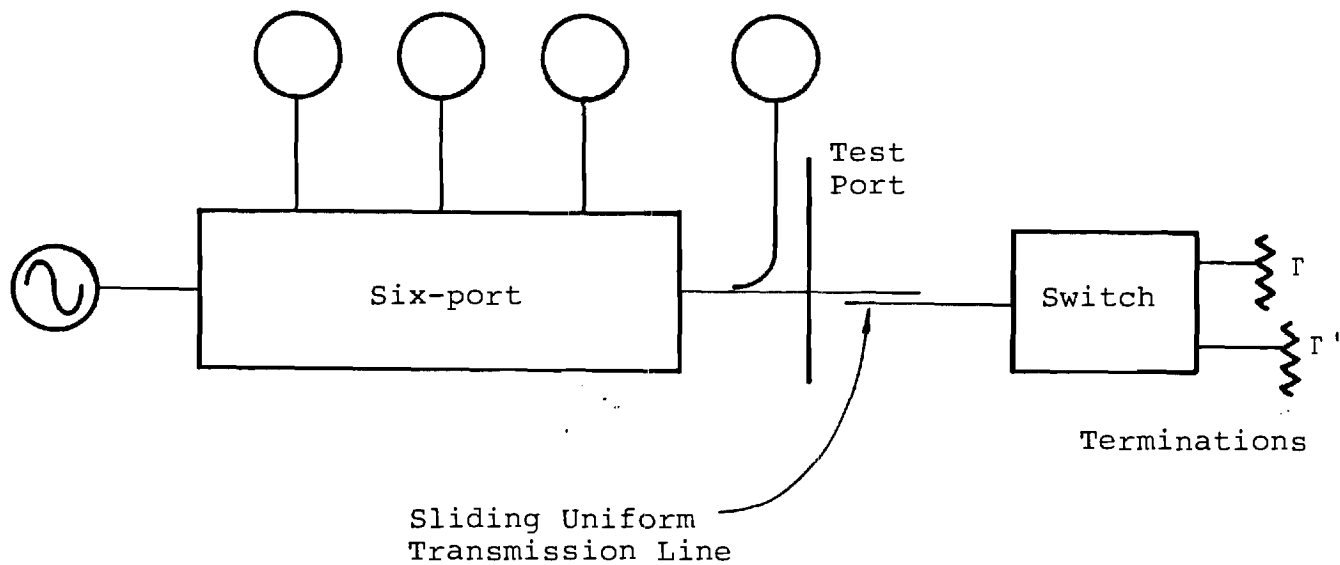


Figure 2.6 A Calibration Device Required by the Eigenvector Method. It comprises two terminations of reflectance, Γ and Γ' , which can be selected by the switch and a sliding transmission line that makes it possible to vary the line length to the termination in a reproducible way.

The following is a review of the self-calibration method for the six-port reflectometer as given by Cronson and Susman [7].* A flow chart of the method is given in Figure 2.7. First, the sliding waveguide section is attached to the test port and one of the terminations selected with a reflection coefficient Γ . One of $m-1$ unique and repeatable lengths of the transmission line is set, and the four detector power levels recorded. These are written in one of the columns of the augmented P matrix

$$[P] = \begin{bmatrix} 1 & 1 & & 1 & 1 \\ P_{4,1} & P_{4,2} & \cdot \cdot \cdot & P_{4,m-1} & P_{4,m} \\ P_{5,1} & P_{5,2} & \cdot \cdot \cdot & P_{5,m-1} & P_{5,m} \\ P_{6,1} & P_{6,2} & \cdot \cdot \cdot & P_{6,m-1} & P_{6,m} \end{bmatrix}$$

The first subscript is the detector number, and the second denotes one of the $m-1 \geq 3$ lengths of the transmission line except in the last column. The readings in the last column are obtained with the transmission line and termination replaced by the well-matched (near-zero reflection) load. This is included to insure that the product $[P][P^t]$ is invertible. Note that the first row contains values of unity rather than $P_{3,i}$ since each column is normalized by the value obtained for $P_{3,i}$.

A second matrix $[P']$ is obtained when the sliding transmission line is reattached but the other termination with a reflection coefficient Γ' is switched in. Detector values are obtained for exactly the same transmission line lengths and put in the same columns. As above, the fourth column corresponds to measurements with the well-matched load. The only difference between $[P]$ and $[P']$ comes from the amplitude and phase of the

* Note that the meanings of b and a as used here (see Figure 2.5) are consistent with the usual convention and also with an earlier report by Cronson and Susman [6]. However, a and b were interchanged in their later report [7].

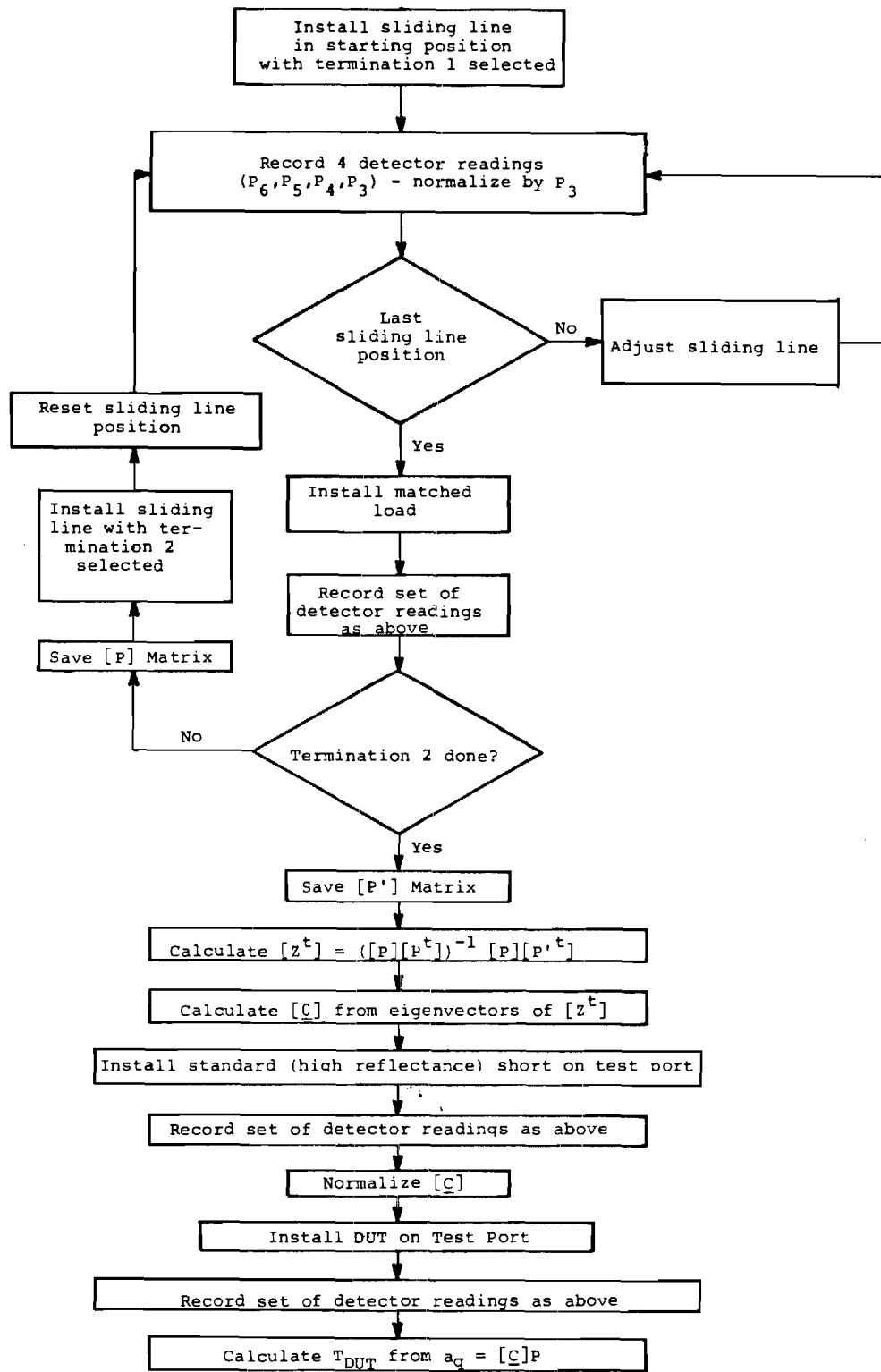


Figure 2.7 Procedure for Calibration of Six-Port [7].

reflection intrinsic to the two terminations. The only requirement is that the ratio of the reflection coefficients of the two terminations must be a complex constant independent of the sliding waveguide length.

Corresponding to the [P] and [P'] matrices are the matrices defined in the earlier discussion:

$$[B_Q] = \begin{bmatrix} |b|^2 & |b|^2 & & |b|^2 & |b|^2 \\ \Gamma_1 |b|^2 & \Gamma_2 |b|^2 & \dots & \Gamma_m |b|^2 & 0 \\ \Gamma_1^* |b|^2 & \Gamma_2^* |b|^2 & \dots & \Gamma_m^* |b|^2 & 0 \\ |\Gamma|^2 |b|^2 & |\Gamma|^2 |b|^2 & \dots & |\Gamma|^2 |b|^2 & 0 \end{bmatrix} \quad (9a)$$

$$[B'_Q] = \begin{bmatrix} |b|^2 & |b|^2 & \dots & |b|^2 & |b|^2 \\ \Gamma'_1 |b|^2 & \Gamma'_2 |b|^2 & & \Gamma'_m |b|^2 & 0 \\ \Gamma'^*_1 |b|^2 & \Gamma'^*_2 |b|^2 & & \Gamma'^*_m |b|^2 & 0 \\ |\Gamma'|^2 |b|^2 & |\Gamma'|^2 |b|^2 & \dots & |\Gamma'|^2 |b|^2 & 0 \end{bmatrix} \quad (9b)$$

In rows 2 and 3 a subscript denotes the effect on the phase of reflection by the selection of the length ℓ of the sliding transmission line (e.g. $\Gamma_1 = \Gamma \exp[-2\gamma\ell]$ where γ is the propagation constant), but rows 1 and 4 are independent of this length, as shown. The two matrices above are related by

$$[B'_Q] = [L][B_Q] \quad (10)$$

where [L] is a diagonal matrix

$$[L] = \begin{bmatrix} 1 & 0 & 0 & 0 \\ 0 & \lambda & 0 & 0 \\ 0 & 0 & \lambda^* & 0 \\ 0 & 0 & 0 & |\lambda|^2 \end{bmatrix}$$

and where $\lambda \equiv \Gamma' / \Gamma$. Equation (10), along with

$$[B_Q] = [C][P]$$

and

$$[B'_Q] = [C][P'],$$

leads to the result that

$$[L][C] = [C][P'][P^t]([P][P^t])^{-1}.$$

This equation has the form in which $[L]$ is a matrix of eigenvalues for the matrix $[Z] \equiv [P'] [P^t] ([P] [P^t])^{-1}$ and $[C]$ is the corresponding matrix of eigenvectors. The calibration matrix $[C]$ can thus be found by standard techniques for finding the eigenvectors of the matrix $[Z]$; however, it is a characteristic of such solutions that each eigenvector (i.e., each row of $[C]$) can only be determined to within a constant of proportionality. This means that the unknown reflection coefficients of test devices can be determined in a relative way, but if one compares the results obtained to that obtained for a standard high reflectivity short, the absolute scale can be transferred and the calibration matrix $[C]$ suitably normalized. Notice in the above that one of the eigenvalues in $[L]$ is known in advance, namely unity, and that the value of λ may be obtained as a bonus.

2.3.2 Analogy between QUOSM and Six-Port

Figure 2.8 shows a preferred six-port design described [7] by Cronson and Susman. The source is connected with some isolation to port 1. The DUT is connected to port 2 through the direct arm of a 22 dB directional coupler. The reference detector at port 3 on the -22 dB coupler arm monitors the power incident on the DUT. In turn, Figure 2.9 illustrates a QUOSM that is modified such that the reference detector measures the radiation incident on the DUT rather than that which leaves the source. This arrangement more closely parallels that in Figure 2.8 as will be discussed below. The reference detector is required by the conditions stated earlier to monitor all changes in the power flowing toward the test port. These changes can arise due to source fluctuations, due to a change in what is connected to the test port, and due to standing waves within the QUOSM. The latter two effects are not of the same magnitude everywhere in the QUOSM, so it is necessary to monitor directly the power going to the test port in order for the foregoing formulation to be

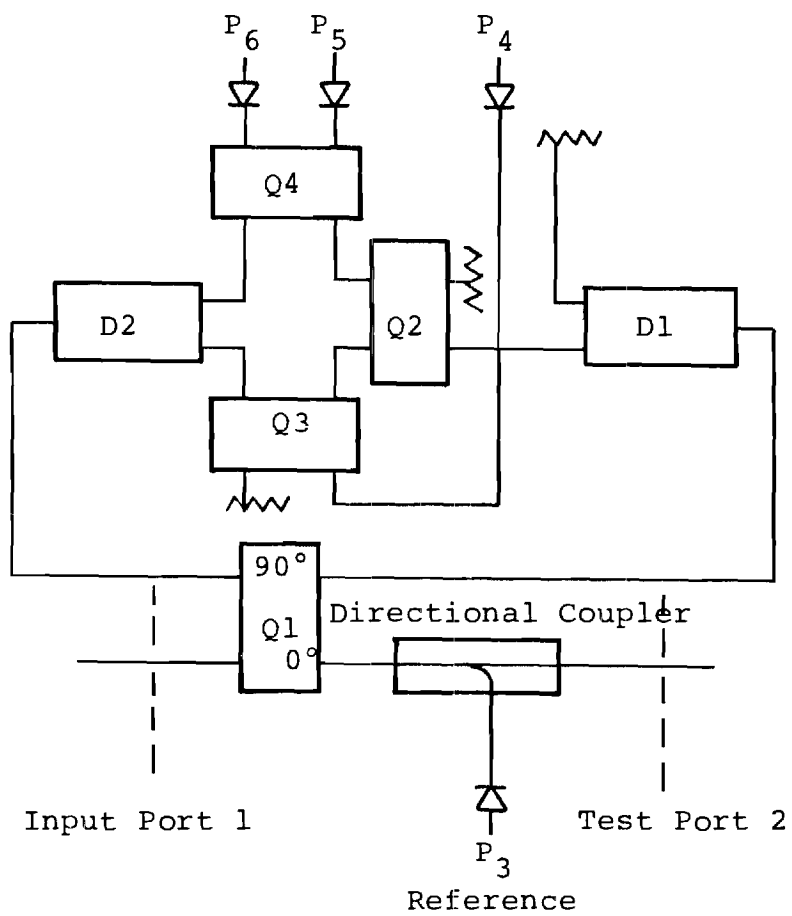


Figure 2.8 Example of a Six-port Reflectometer Circuit, after Reference [7].

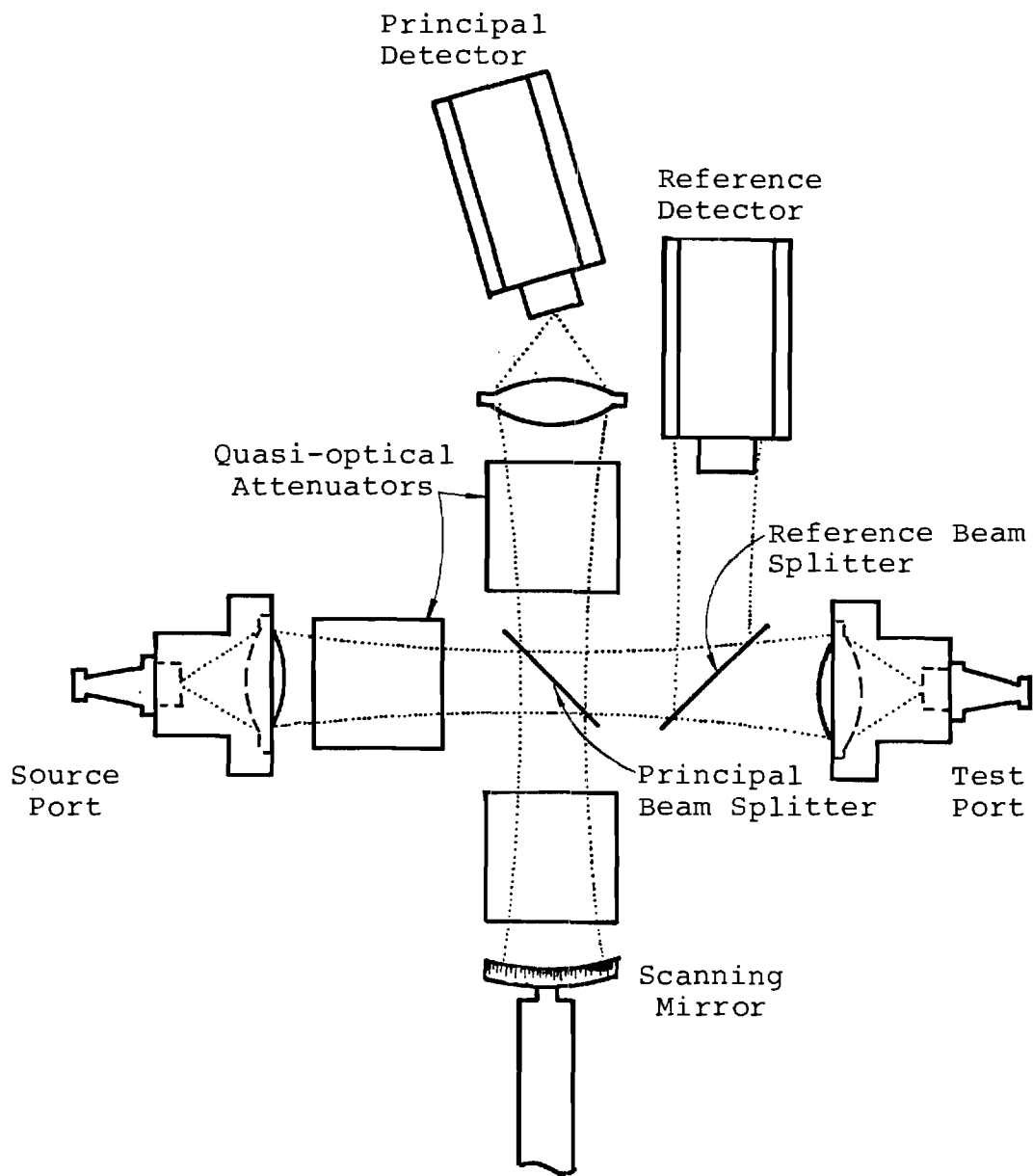


Figure 2.9 Modified QUOSM Design with Reference Detector Adjacent to Test Port.

valid. Cronson and Susman had similar arguments for the placement of the reference detector [7]. In the case of the QUOSM, instead of a directional coupler, a low-reflectivity beam splitter is used to couple power to the reference detector.

In the six-port reflectometer three ports are utilized for power measurement in addition to the reference power measurement already described. The QUOSM, in effect, utilizes time-division multiplexing to implement the power measurements made at ports 4, 5, and 6 of the six-port. In the case of the QUOSM the three powers are measured at each of three unique positions of the scanning mirror. An advantage of the QUOSM is that the mirror positions, and hence the phase shifts introduced, are computer-controlled and can be varied as the source wavelength is changed. This should allow for optimization of the phase shifts at any wavelength in the design bandwidth.

As described earlier, the self-calibration method for the six-port reflectometer requires a set of four power measurements for each of three or more unambiguous positions of a sliding transmission line with two different, terminations. For the wavelength range of the QUOSM which extends to less than one millimeter, sliding transmission lines that will give reproducible performance without undue loss are probably not practical to make, but the same effects can be achieved instead in the optical part of the QUOSM. The sliding section essentially introduces reproducible delays, and this requirement can be met in two ways illustrated in Figure 2.10. In the first, the whole lens-horn arrangement of the test port is moved along the optical axis in some fashion that insures reproducibility of positioning. One of the terminations can have a high reflectance and the other could be the same but with a 3 dB loss dielectric slab of an appropriate thickness added in front of the lens. In the second method, instead of a translation of the test port, low-loss dielectric slabs could be inserted in front of the lens to add reproducible delays. The same termination methods as in

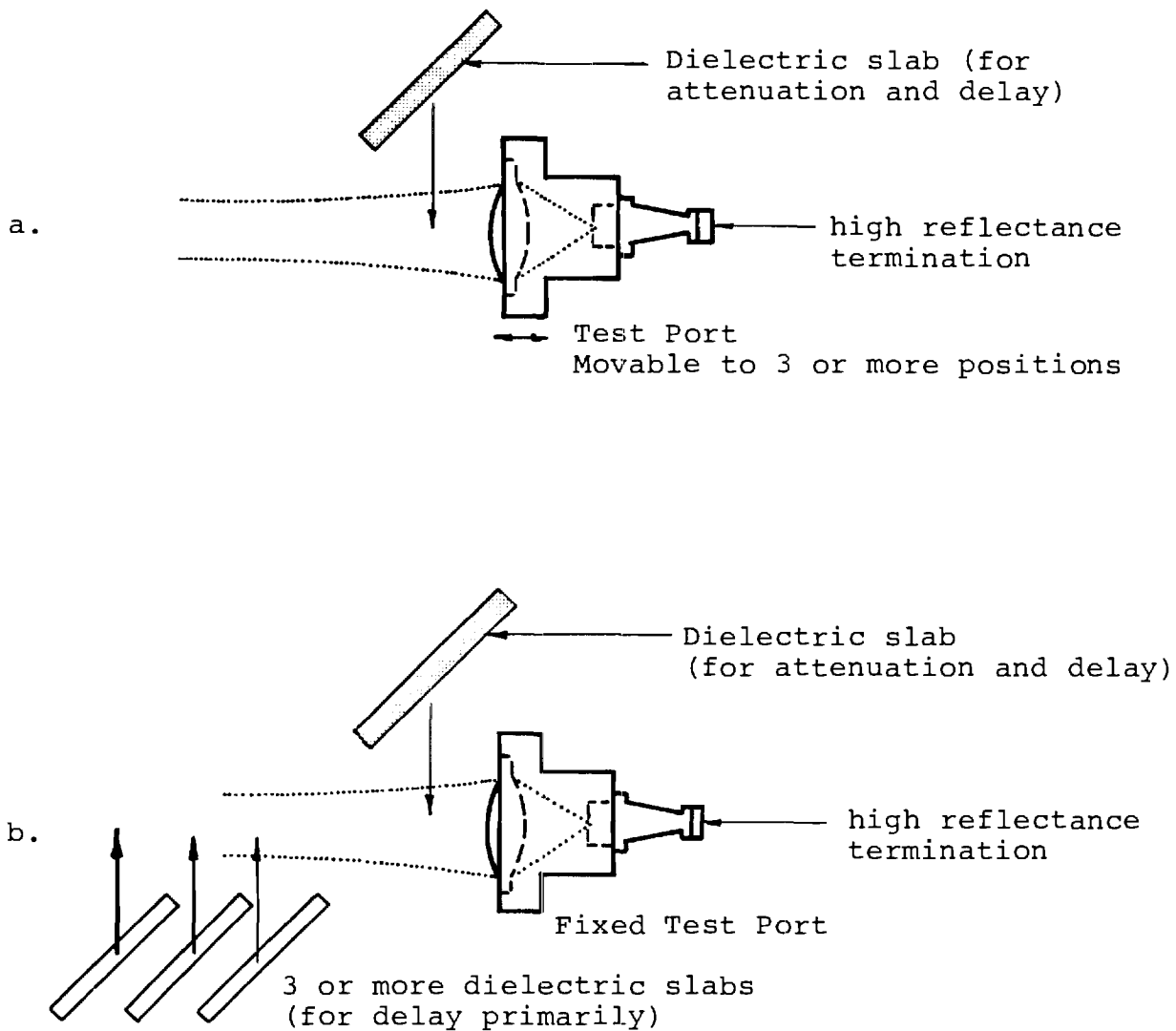


Figure 2.10 Two ways in which a sliding transmission line with two terminations can be emulated in the QUOSM. In a) the test port as a whole is moved to three or more reproducible positions. The termination is effectively modified by introducing a dielectric slab which in two passes gives ~ 3 db attenuation and 45° phase shift. In (b) the test port is fixed and the equivalent delays introduced by switching in low loss dielectric slabs of different thicknesses.

the first method could be used.

With a six-port, there is a requirement for a set of four power measurements to be made with a matched load mounted on the test-port, as discussed earlier. If the horn-lens transition in the test port of the QUOSM did not partially reflect radiation passing through it, all that would be necessary to meet the analogous requirement would be to mount a tapered load on the flange of the horn and make power measurements with the principal detector (for three mirror positions) and one with the reference detector. Such loads have been fabricated for use with the QUOSM in earlier work [3]. However, the fact that the lens and horn may be expected to reflect energy back toward the principal beam splitter, appears to mean that an additional calibration absorber is needed. This would be an absorbing pad (like that shown in Figure 1 of reference [3]) that could be inserted in the optical beam between the reference detector's beam splitter and the test port lens and could thus eliminate all reflection from the test port. Used as part of a calibration procedure analogous to that for a six-port, this would permit one to determine the complex reflectance* of the whole test port. One would then determine the complex reflectance of the port with the DUT mounted and make a second determination with a tapered load mounted. The latter would determine the amplitude and phase of the reflection from the lens-horn and could be used to remove the effect of this reflection from the results obtained when the DUT is mounted. This correction would closely parallel that described in an earlier report [1].

Since this type of correction is well-established, it was not dwelt on in the present work. Instead, as a simplification for the following discussions and for the simulations which will

* The term "reflectance" is interchangeable with "reflection coefficient", but generally refers to reflection from something other than a simple surface.

be described, the reflectance of the test port's lens-horn is taken to be zero. This significantly facilitated the simulations and focused attention on the main issues while the work was underway. In future work, the calibration step can be added, as described above, to correct for the lens-horn reflectance, which according to previous estimates [1] may be of the order of ten percent (in terms of power).

Finally, as with a six-port, an absolute reflectance and a reference for phase can be determined by the comparison of results obtained for a DUT with those for a near perfect reflector (high-reflectance short) mounted on the waveguide flange of the test port.

It has been shown above that the QUOSM either has, or can be provided with, capabilities that are analogous to those possessed by a six-port network analyzer. As a result the calibration procedure outlined for six-ports in Figure 2.7 corresponds to an analogous procedure for the QUOSM shown in Figure 2.11. In the following sections, descriptions are given of the numerical algorithms and simulations which have been prepared to test this procedure.

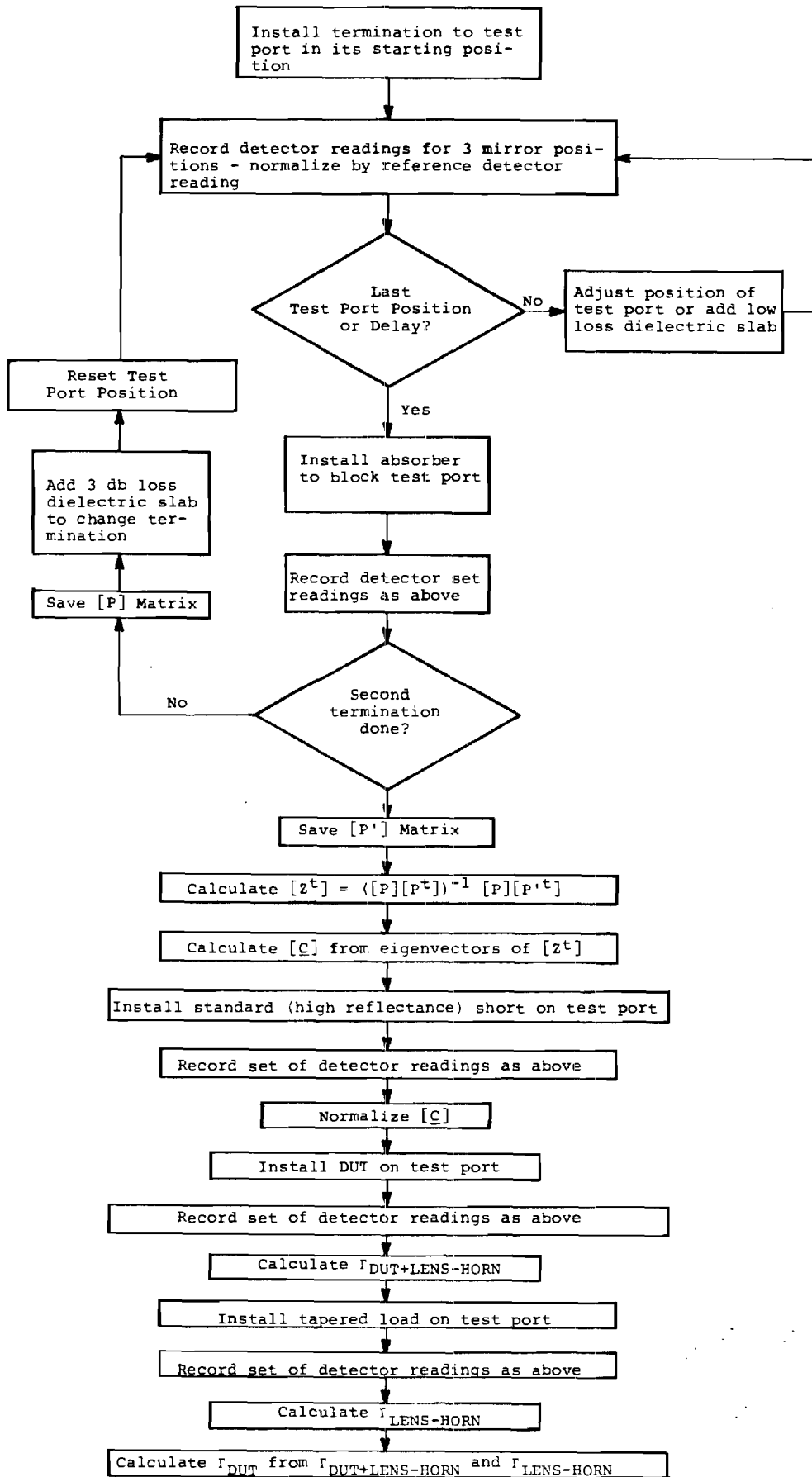


Figure 2.11 Procedure for Calibration of QUOSM

2.4 Eigenvalue/vector Analysis

As discussed above, the new calibration procedure for the QUOSM involves calculation of the eigenvalues and eigenvectors of the matrix $[Z]$, where

$$[Z] = [P'] [P^t] ([P] [P^t])^{-1}$$

and where the matrices $[P]$ and $[P']$ contain power measurements for prescribed calibration conditions. The rows of the calibration matrix $[C]$ described earlier are the left-hand form of eigenvectors of $[Z]$, since

$$[C] [Z] = [L] [C].$$

As it happens, right-hand eigenvectors are more commonly found in numerical analysis literature, and so for compatibility with standard practice, the above equation must be transformed by transposition so that the eigenvectors are of the right-hand form:

$$[Z^t] [C^t] = [C^t] [L]$$

Now the columns of the transposed calibration matrix are the right-hand eigenvectors of the matrix

$$[Z^t] = ([P] [P^t])^{-1} [P] [P'^t]$$

The eigenvalues in the diagonal matrix $[L]$ are unaffected by the above transposition.

The actual numerical procedures to derive eigenvector solutions and to calibrate the QUOSM have been developed independently of the work of Cronson and Susman. In the main, well-established numerical methods have been used which were available either from published algorithms and literature or from the library of the HP-85 computer that is included in the QUOSM as a controller and automatic data processor. The published routines selected were translated into the form of BASIC language used in the HP-85 and tested as will be described below. In general, for the present purpose of demonstrating the eigensolution approach to the calibration of a QUOSM, numerical procedures were selected which appeared to offer maximum

insensitivity to numerical ill-conditioning and to noise. Compactness of coding was given little consideration at this stage.

The first step in the eigenvector solution is the calculation of $[Z^t]$ from $[P]$ and $[P']$, and this appears at first glance to require the calculation of the inverse of $[P][P^t]$. The HP-85 computer in the QUOSM system is equipped with a ROM package of matrix routines as an extension of the BASIC language. This recognizes a one-statement command for calculating the inverse of square matrices and can be applied to finding the inverse of the 4×4 square matrix ($[P][P^t]$). This inverse can then be used to premultiply the matrix result of $[P][P^t]$. However, it is more accurate to calculate $[Z^t]$ by a method that avoids the explicit calculation of the above inverse. In general, the product of an inverse matrix $[A^{-1}]$ and another matrix $[B]$ can be expressed as the solution matrix in the familiar general problem of simultaneous linear equations whose coefficients are the elements of $[A]$:

$$\begin{aligned} [A][X] &= [B] \\ [X] &= [A^{-1}][B] \end{aligned}$$

Well-established numerical methods are available which can be used to calculate $[A^{-1}][B]$ directly and with greater accuracy than the calculation of $[A^{-1}]$ followed by multiplication by $[B]$ (see e.g., refs. [8,9]). The HP-85 package of firmware makes available a command, $X = \text{MAT SYS } (A,B)$ which implements such a solution. (According to the manufacturer, the method of UL decomposition is used [10]). Thus one may substitute $[P][P^t]$ for $[A]$ and $[P][P']^t$ for $[B]$ in the above and obtain $[Z^t]$.

The difference in results was demonstrated in a test that calculated $[X] = [A^{-1}][A]$ for various trial matrices $[A]$ containing values in the range 0 to 1, and then compared $[X]$ with $[I]$, the identity matrix. In the case where $[A^{-1}]$ was calculated explicitly and then multiplied by $[A]$ the diagonal elements of $[X]$ differed from 1 by at most 3×10^{-12} , and the off-diagonal

elements differed from 0 by at most 3.2×10^{-12} . When the system of equations was solved using the MAT SYS command the diagonal elements were found to be identically equal to 1 (for the 12 significant digits displayed). The off-diagonal elements were reduced to the order of 10^{-16} . The results of tests of this type depend to some extent on the values used to define the matrix [A], so the results described above should be taken only qualitatively as an indication of the difference between the two methods of solution.

The optimum procedure for calculation of the eigenvectors of a matrix depends in general on the nature of the matrix. According to a number of reviews which are available [e.g. 10-12], matrices are frequently poorly conditioned for eigenvector solutions and the choice of algorithm can have a significant impact on the quality of the results. In the case of interest here the matrix [Z^t] is real and unsymmetric, and in general such matrices can present special problems of ill-conditioning [11]. However, if as recommended above, one chooses calibration terminations such that $|\lambda|^2$ is approximately 0.5, the eigenvalues will be reasonably well-separated in magnitude, and in such a case, more accurate eigenvector solutions can be found [11]. (The fact that two eigenvalues λ and λ^* and the corresponding eigenvectors are complex conjugates does not affect this assessment.)

The method of solution selected for the present work is believed to be optimum or near-optimum for real, unsymmetrical matrices as regards accuracy [10,11]. In outline, the procedure involves (1) balancing the matrix using similarity transformations that nearly equalize the norms of corresponding rows and columns, (2) reducing the matrix to upper-Hessenberg form (nearly upper-triangular) by means of orthogonal,

Householder transformations^{*}, (3) further decomposing the matrix by what is known as the double-QR algorithm to obtain the eigenvalues, and finally (4) solving for the eigenvectors by inverse iteration. A FORTRAN program written by Grad and Brebner [13] and tested by several workers [14,15,16] implements the above steps and has been translated here into BASIC for use on the HP-85. An annotated listing of this program named EIGEN is given in Appendix B. Several matrices for which the eigenvalues and eigenvectors are known, including three suggested by Grad and Brebner, were used as test cases to verify that the translated version was working correctly. Agreement with expected values was obtained to at least 9 significant figures, where the computer normally displays up to 12. The test matrices are believed to have been of equal or greater difficulty by comparison with the matrices $[Z^t]$ expected to be encountered in practice, in the sense that some of the eigenvalues of the test matrices had magnitudes which were pathologically close to each other.

Two tests for the correctness of the eigenvalues have also been added to the program that apply even for matrices with unknown solutions. The first checks for the expected [17] equality between the sum of the calculated eigenvalues and the trace of the original matrix. The imaginary parts of the complex eigenvalues should cancel in the addition process to yield a number equal to the sum of the diagonal elements of the real matrix. The second test checks that the product of the eigenvalues equals the determinant of the matrix as expected [17]. Agreement under these tests has generally been found to at least 11 significant figures.

* One may note that in previous work involving the least squares method [1], orthogonal Householder transformations were also selected for similar qualities of robustness.

After the eigenvalues are calculated and verified as described above, the eigenvectors are also subjected to an additional routine test that verifies that

$$[Z^t][C^t] = [L][C^t].$$

When $[C]$ is formed by transposition, it is further tested by multiplication with the columns of power measurements in $[P]$. The matrix product $[B_Q] = [C][P]$ should indicate values consistent with the parameters used in the simulation. In particular the complex reflection parameter Γ_i

$$\Gamma_i = \frac{a_i b_i^*}{|b_i|^2}$$

for one of the sliding terminations in position i , can be found from

$$\Gamma_i = \frac{B_{Q,2,i}}{B_{Q,1,i}}$$

and compared with what was specified in the simulation.

The following sections will describe procedures that have been developed to simulate signals recorded by the detectors in the QUOSM and thus to make it possible to construct examples of the $[P]$ and $[P']$ matrices. For convenience, the programs for simulation and for the calculation of the calibration matrix are separate, and communication between them is through data files stored on cartridge tapes in the built-in facility of the HP-85 computer. The simulation program RFLCTN stores the columns of the $[P]$ and $[P']$ matrices on data files, and the program EIGEN which accesses these data then reconstructs $[P]$ and $[P']$, calculates $[Z^t]$, performs the eigenvector/value analysis, and calculates $[C^t]$ and hence $[C]$. EIGEN in turn stores $[C]$ on a file, and a final program CTIMEP can be used to calculate columns of $[B_Q]$ or $[B_Q']$ from

$$[B_Q] = [C][P]$$

$$\text{or } [B_Q'] = [C][P'].$$

Annotated listings of these programs are given in Appendices A, B, and C.

2.5 Simulation of QUOSM Signals

The purpose of the RFLCTN program is to simulate QUOSM detector signals as a function of the positions and reflectivity values assigned to various components including the source and detector. This has resulted both in a better understanding of the standing wave condition and in vital, controlled data for the development of the matrix calibration technique.

As mentioned in an earlier section, when multiple reflections occur in the QUOSM, the number of paths by which radiation can reach the detector is infinite, but for finite component reflectances, significant energy is transmitted over only a finite (though not necessarily small) number of paths. For convenience, it is possible to record first the amplitude and phase of the signals which arrive by the most direct route to any port where an output (desirable or otherwise) can occur. These ports are at the source, the principal detector, the reference detector, and the device under test. At each of these ports a certain amount of the signal is not output (or absorbed) but is instead reflected and redirected back into the QUOSM. (As a simplification in the simulation, one may without loss of generality assign zero reflectance to the reference detector.) Then all of the reflected radiation returns on a path back to the principal beam splitter where it recombines and continues back to the output ports, and so on. In each iteration more signal arrives at each output port, and the part not reflected is added vectorially to that so far accumulated. When the calculated output power on each of the ports has converged, the iterations can be halted. Appendix D discusses the fact that conservation of energy requires that the sum of the powers absorbed or output must equal the power input by the source. This was useful as a cross-check on the detailed calculations during the development of the simulation package. In Figures 2.12 to 2.15 "optical flow charts" are given which diagram the paths taken by the radiation

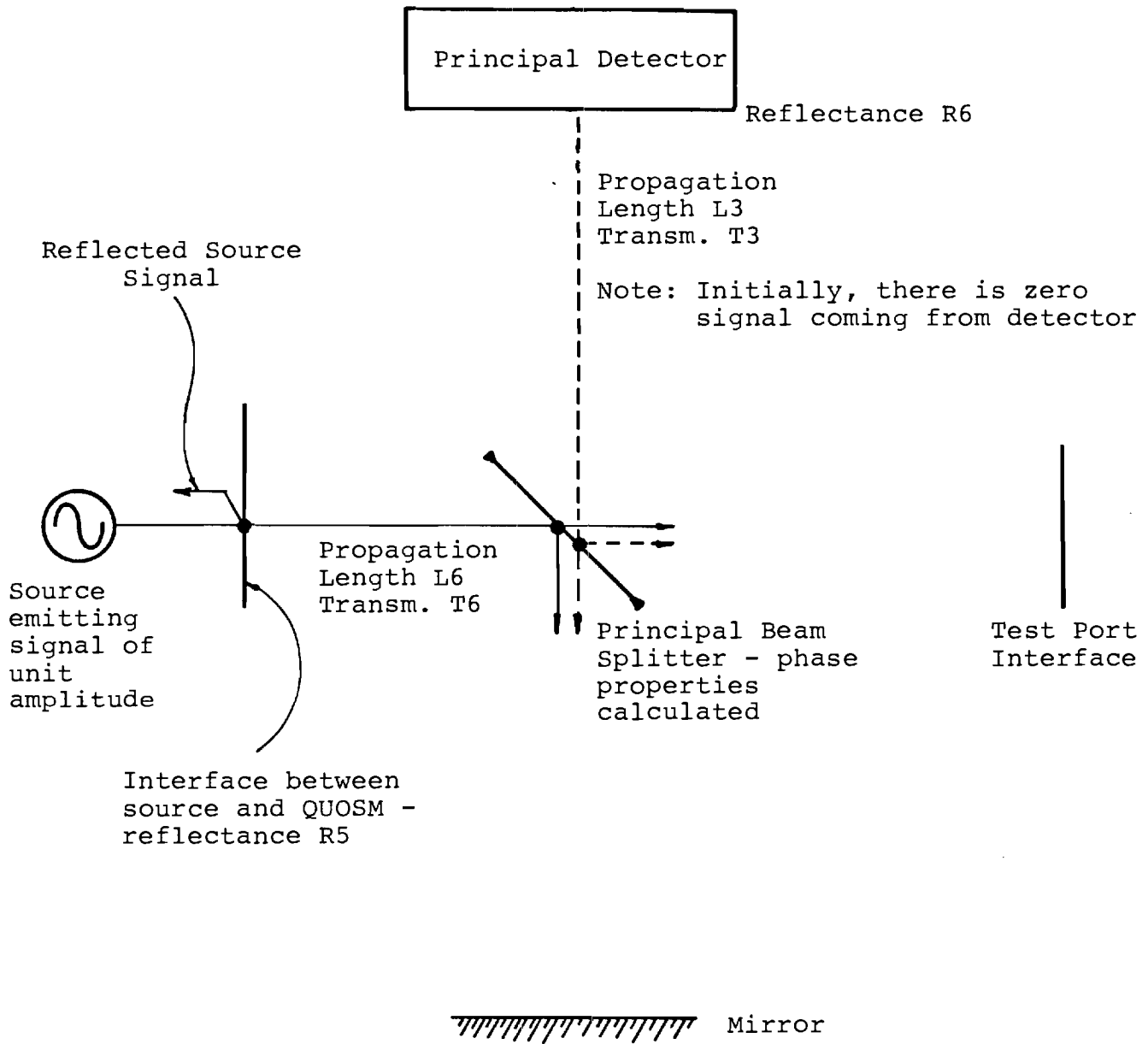


Figure 2.12 Optical Flow Chart for Initial Optical Paths from Source and Detector. Parameter labels given are those used in RFLCTN program (see Appendix A).

Principal Detector

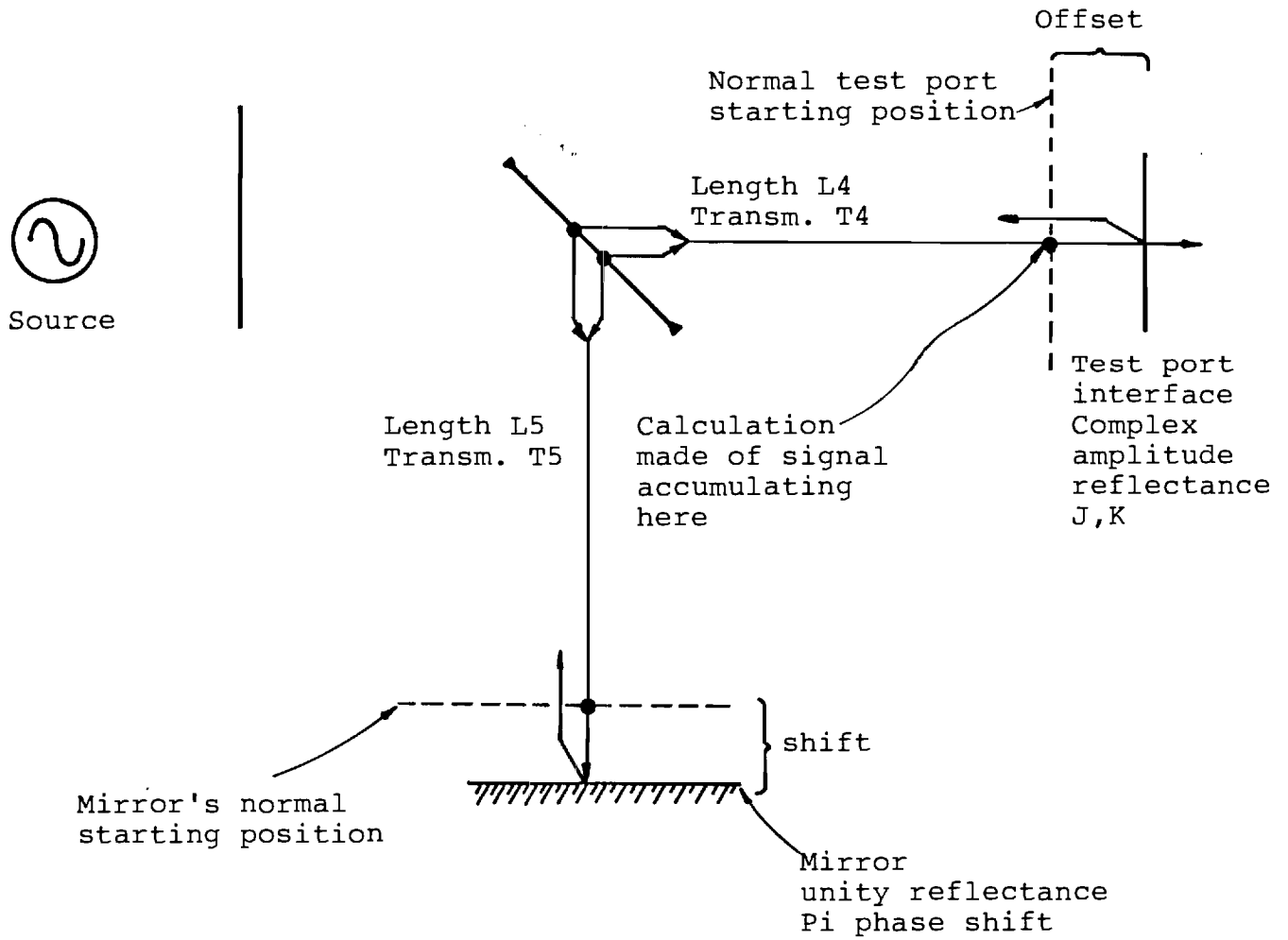


Figure 2.13 Optical Flow Chart for Optical Paths from Beam Splitter to Mirror and Test Port.

Principal Detector

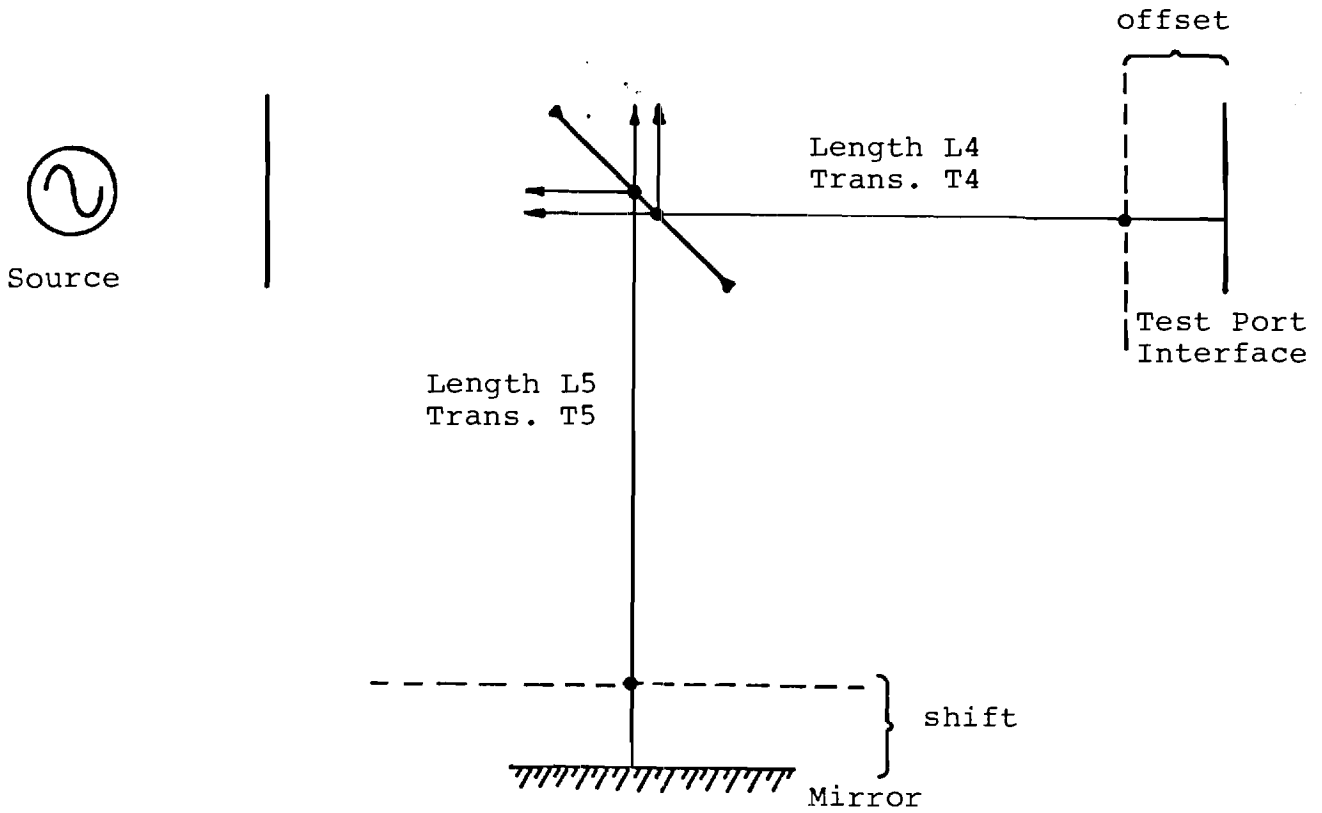


Figure 2.14 Optical flow chart for optical paths from mirror and test port back to the beam splitter.

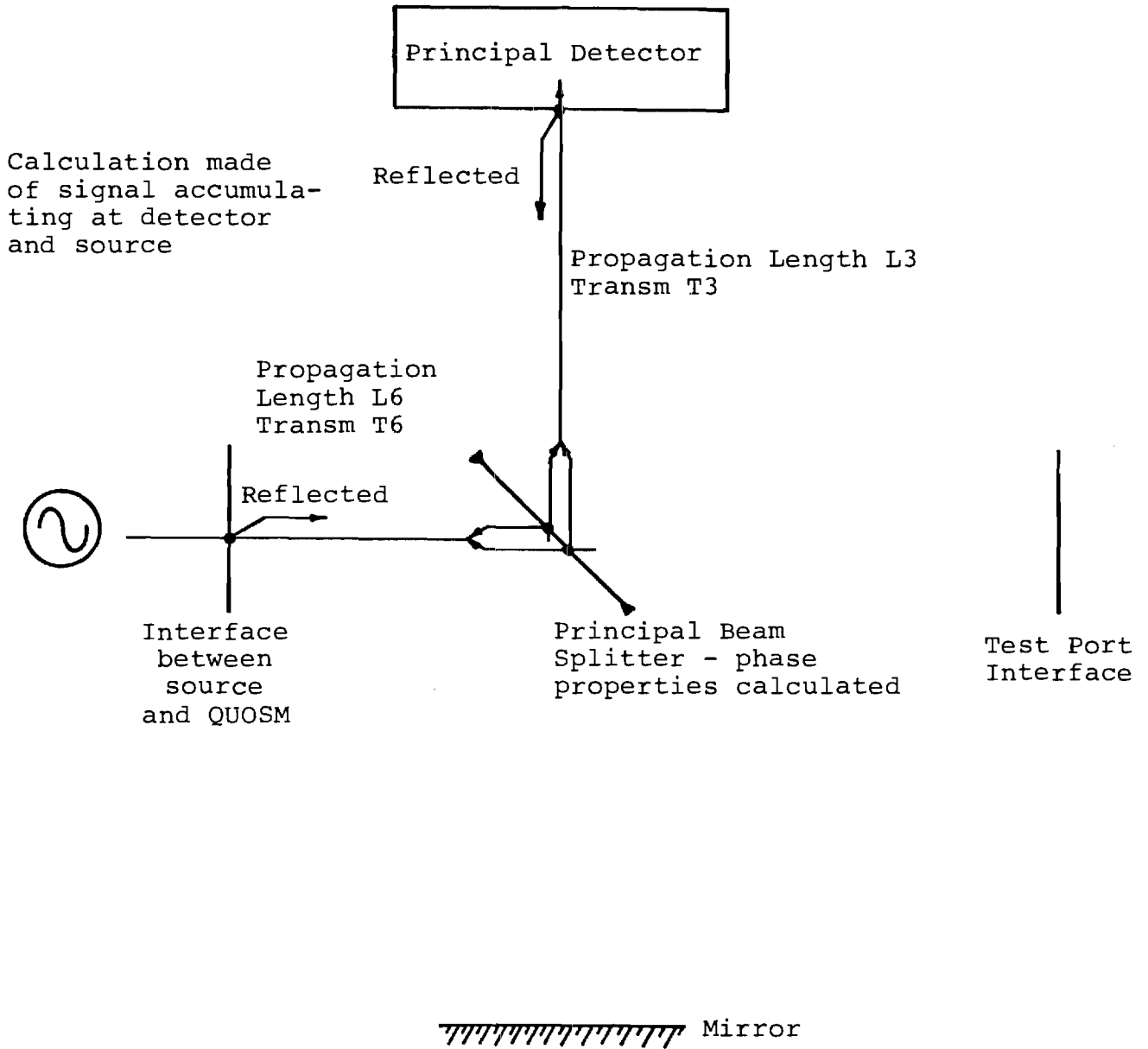


Figure 2.15 Optical flow chart for optical paths back to source and detector. Reflections at source and detector are start of next iteration.

and outline most of the details included in the calculation of the various signal amplitudes.

Figure 2.12 describes the starting conditions. Values of reflection coefficients for the source, detector, and Device Under Test (DUT) are input from the keyboard. The same is true for the source frequency and the beam splitter thickness. The indicated path lengths (L_3 , L_4 , L_5 , and L_6) are stored within the program along with path transmission values which simulate the effect of attenuators. Since BASIC programs are easily amended, these values can be readily changed. The calculation is initialized such that the source emits a signal of unit amplitude toward the QUOSM. A portion of this signal, determined by the selected source reflectivity, enters the QUOSM going toward the beam splitter. The rest is reflected toward the source at the Source/QUOSM interface. Of course no radiation is coming from the detector at this stage, and the initial detector signal is explicitly set equal to zero. This sets the conditions for the computer to begin its iterative procedure. The effects (phase change and possible amplitude change) of propagating through the path lengths L_3 and L_6 are calculated. Then the effects of the beam splitter are taken into account. The beam splitter (assumed lossless) divides the amplitude of the signal from the source into transmitted and reflected components, and calculable phase changes occur [18]. The same happens for the signal (initially zero) reflected by the detector. The four resulting signals are shown in Figure 2.12 as four short arrows originating at the beam splitter, two going toward the DUT and two toward the movable mirror.

Figure 2.13 indicates that each pair of signals propagating in the same direction are vectorially added. The effects of propagating through paths L_4 and L_5 are then calculated. The previously entered values of DUT reflection and phase shift are utilized to calculate the amplitude and phase of the signal reflected from the DUT (shown as a short arrow at the DUT). The

mirror displacement introduces an additional phase shift of the signal coming to the mirror from the beam splitter. The mirror itself is assumed to have unity reflectance and a phase shift of π radians.

Figure 2.14 illustrates the calculations performed that treat the propagation of the signals from the DUT and mirror to the beam splitter. The effects of propagating through the path lengths are once again accounted for, as are the effects of the beam splitter.

Figure 2.15 shows that the parallel beams from the beam splitter have been combined, the propagation through the paths accounted for, and the detector and source reflections applied to calculate the values for the signals from the source and detector in the next iteration.

As mentioned earlier, the signals which pass through the output ports are vectorially added and accumulated over all iterations. In the program as implemented, the power at the DUT is not formally accumulated and stored. Tests based on conservation of energy are restricted then to the case of 100 percent DUT reflectance, but such a test gives an adequate verification that the simulation is working correctly.

The complex numbers representing the signal to the main detector and to the source are converted to power readings at the end of each iteration. These power readings are compared with those of the previous iteration. When the percent difference between iterations, for both the source and the detector powers, becomes less than a selected small value, the detector power reading is normalized (i.e., divided by the power on the reference detector, as required by theoretical considerations discussed earlier).

To obtain the data necessary to form a column of [P] or [P'], the simulation program repeats the calculation of the normalized detector level for three unique mirror positions stored in the program. The fourth element of such a column is of

course unity, as it represents the reference detector signal divided by itself as discussed previously. The QUOSM has a great deal of flexibility in terms of the mirror positions used, and hence in the phase shifts, available, whereas the relative phases seen by the detectors in the six-port analyzer are normally fixed by the hardware configuration. Simple program modifications or parameter inputs are all that is required to change the mirror positions selected by the QUOSM, and hence optimization of the kind described by Engen [4] is more easily implemented, in principle, in the QUOSM.

2.6 Simulated Calibration

2.6.1 Case of Standing Waves

The calibration process described in Sections 2.3 and 2.4 has been tested with simulated data, and the the results of one such test are explained here. The source frequency was set to 94 GHz. The source and the detector were each simulated as having a power reflectance of 0.2. This is an order of magnitude larger than the value measured [3] for the detector in previous work, and is a plausible upper limit. The two fixed, but uncalibrated, terminations required for the relative calibration were assigned amplitude reflectances of 1.0 and 0.7. The phase-shift difference between the two devices was set at 45° . (The program actually asks for the value of half the phase shift). Table 2.2 shows what calibration devices are in place, the position of the scanning mirror, and the status of the position or effective shift of the test port for each element of the [P] and [P'] matrices that were calculated.

The eigenvalues of the square matrix derived from the power readings were tested on the basis that the largest eigenvalue should be unity and the smallest should be the ratio of the power reflectances of the two calibration shorts. The two intermediate eigenvalues are a complex conjugate pair found from the ratio of the amplitude reflection coefficients. The calculated eigenvalues, rounded to four decimal places, were: 1, 0.4901, $0.4951 + i 0.4951$. Thus the largest eigenvalue was correctly found to be unity. The smallest, 0.4901, was acceptably close to $0.7^2 = 0.4900$, the ratio of the power reflectances. The magnitude of the complex values is 0.7002 and the polar angle is 45° . Therefore, the calculated eigenvalues were in excellent agreement with expectation.

The calibration matrix [C] was then formed by assembling the complex eigenvectors as rows, and was tested for consistency by multiplication with each of the eight sets of power measurements.

That is, the $[B_Q]$ and $[B'_Q]$ matrices were calculated by

$$[B_Q] = [C][P]$$

and

$$[B'_Q] = [C][P'].$$

These results are compiled in Table 2.3 along with the values expected in accordance with equations (9a) and (9b) and the input parameters of the simulation. One may see that the rows of $[B_Q]$ and $[B'_Q]$ differ from expectation by a factor depending on the row. As previously explained, the rows in $[C]$ can only be found by eigenvector analysis to within a constant factor, and the magnitude of each row must be normalized by results obtained when a termination of unity reflectance is used. In this case one of the terminations used in the calibration has unity reflectance $|\Gamma| = 1$, and one may define the phase of its reflection to be zero when the DUT is unshifted. Thus, one may normalize each row of $[C]$ by the reciprocal of the values in the first column of the unnormalized $[B_Q]$; that is, the rows of $[C]$ from one through four are multiplied by -1, $1/(\.193 - 3.6 \times 10^{-5}i)$, $1/(\.193 + 3.6 \times 10^{-5}i)$, and $-1/.1664$ respectively. In Table 2.3 the normalized values for elements of $[B_Q]$ and $[B'_Q]$ were found with the normalized $[C]$ and show excellent agreement with expectation. In addition to the correctness of the relative amplitudes, the calculated phase shifts were found to be accurate to better than DUT can be found would be expected to be similar to the normalized values in the second row of $[B_Q]$ and $[B'_Q]$ as illustrated in Table 2.3. One may note, however, that instrumental noise has not as yet been introduced, and preliminary discussion of this will be given later.

2.6.2 Case of No Standing Waves

The preceding test results are representative of the case where significant standing waves are present due to the significant power reflectances of the source and detector. The case of a QUOSM without any standing waves can be simulated by

Table 2.3 Calculated Test Port Parameters B_Q and B'_Q for Case of Standing Waves

B_Q		TEST PORT POSITION			MATCHED LOAD
		1	2	3	
1	UNNORMALIZED	-1.000	-1.000	-1.000	-1.000
	NORMALIZED	1.000	1.000	1.000	1.000
	EXPECTED	1.000	1.000	1.000	1.000
a	UNNORMALIZED	$.193-3.6 \times 10^{-5}i$	$-.09635+.16736i$	$-.09664-.1670i$	$+1 \times 10^{-12}+2 \times 10^{-13}i$
	NORMALIZED	1.000	$-.4994+.8666i$	$-.5006-.8654i$	$+8 \times 10^{-12}+1 \times 10^{-12}i$
	EXPECTED	1.000	$-.5000+.8660i$	$-.5000-.8660i$	0.000
a*	UNNORMALIZED	$.193+3.6 \times 10^{-5}i$	$-.09635+.16736i$	$-.09664-.1670i$	$+1 \times 10^{-12}-2 \times 10^{-13}i$
	NORMALIZED	1.000	$-.4994-.8666i$	$-.5006+.8654i$	$+8 \times 10^{-12}-1 \times 10^{-12}i$
	EXPECTED	1.000	$-.5000-.8660i$	$-.5000+.8660i$	0.000
$ a ^2$	UNNORMALIZED	$-.1664$	$-.1664$	$-.1664$	-9×10^{-13}
	NORMALIZED	1.000	.9995	.9996	1×10^{-11}
	EXPECTED	1.000	1.000	1.000	0.000
B'_Q	UNNORMALIZED	-1.000	-1.000	-1.000	-1.000
	NORMALIZED	1.000	1.000	1.000	1.000
	EXPECTED	1.000	1.000	1.000	1.000
a'	UNNORMALIZED	$.09556+.09552i$	$-.1305+.03511i$	$.03482-.1305i$	$+1 \times 10^{-12}+2 \times 10^{-13}i$
	NORMALIZED	$.4951+.4951i$	$-.6763+.1818i$	$.1806-.6763i$	$+8 \times 10^{-12}+1 \times 10^{-12}i$
	EXPECTED	$.4950+.4950i$	$-.6761+.1812i$	$.1812-.6761i$	0.000
a'*	UNNORMALIZED	$.09556-.09552i$	$-.1305-.03511i$	$.03482+.1305i$	$+1 \times 10^{-12}-2 \times 10^{-13}i$
	NORMALIZED	$.4951-.4951i$	$-.6763-.1818i$	$.1806+.6763i$	$+8 \times 10^{-12}-1 \times 10^{-12}i$
	EXPECTED	$.4950-.4950i$	$-.6761-.1812i$	$.1812+.6761i$	0.000
$ a' ^2$	UNNORMALIZED	$-.08157$	$-.08153$	$-.08154$	-9×10^{-13}
	NORMALIZED	.4901	-.4901	-.4899	1×10^{-11}
	EXPECTED	.4900	.4900	.4900	0.000

setting these reflectances equal to zero so that radiation can follow only two paths through the interferometer.

A slight improvement in the precision of the eigenvalues was found when the standing waves were eliminated. Whereas agreement with expectation was good to three significant figures with standing waves, at least 10 significant figures of agreement were found with no standing waves. However, since three significant figures appear to be sufficient, this dependence on the standing waves is not particularly significant. Indeed, the root of this small inaccuracy may not be in the eigenvector method at all. When standing waves are introduced, the iterative simulation of QUOSM signals is truncated before the solution is exact, as mentioned earlier, and this corresponds to a residual inaccuracy of about five parts in 10^4 . It is not unreasonable to suppose that this would affect the eigenvector solution.

The eigenvectors for the case of no standing waves appeared at first glance to be substantially different than for the first case in which standing waves were present. However, the difference was only due to the need for normalization of the rows of $[C]$ and the fact that a different normalization was needed in the present case. By using the unnormalized results for the first column of $[B_Q]$ as in the previous example, one finds that the rows of $[C]$ in order, starting at the top, are multiplied by 1, $1/(.4959 + 5 \times 10^{-12}i)$, $1/(.4959 - 5 \times 10^{-12}i)$, and $-1/.2753$. Table 2.4 gives expected, unnormalized, and normalized values of the elements of both $[B_Q]$ and $[B_Q^1]$. Agreement between the expected and normalized values is again excellent and good to at least 10 significant figures.

2.6.3 All-dielectric shifted DUT calibration

The calibration procedures simulated above have been consistent with physical shifts of the whole DUT port, including its lens and horn, as the means of obtaining the required DUT

Table 2.4 Calculated Test Port Parameters B_Q and B'_Q for Case of No Standing Waves

B_Q		TEST PORT POSITION			MATCHED LOAD		
		1	2	3			
B_Q	1	UNNORMALIZED	1.000	1.000	1.000	1.000	
		NORMALIZED	1.000	1.000	1.000	1.000	
		EXPECTED	1.000	1.000	1.000	1.000	
	a	UNNORMALIZED	$.4959+5 \times 10^{-12}i$	$-.248+.4295i$	$.2480-.4295i$	$-8 \times 10^{-12}+6 \times 10^{-12}i$	$-2 \times 10^{-11}+1 \times 10^{-11}i$
		NORMALIZED	1.000	$-.5000+.8660i$	$-.5000-.8660i$	$-2 \times 10^{-11}+1 \times 10^{-11}i$	$-2 \times 10^{-11}+1 \times 10^{-11}i$
		EXPECTED	1.000	$-.5000+.8660i$	$-.5000-.8660i$	0.000	0.000
	a*	UNNORMALIZED	$.4959-5 \times 10^{-12}i$	$-.248-.4295i$	$.2480+.4295i$	$-8 \times 10^{-12}-6 \times 10^{-12}i$	$-2 \times 10^{-11}+1 \times 10^{-11}i$
		NORMALIZED	1.000	$-.5000-.8660i$	$-.5000+.8660i$	$-2 \times 10^{-11}+1 \times 10^{-11}i$	$-2 \times 10^{-11}+1 \times 10^{-11}i$
		EXPECTED	1.000	$-.5000-.8660i$	$-.5000+.8660i$	0.000	0.000
$ a ^2$	UNNORMALIZED	-.2753	-.2753	-.2753	4×10^{-12}	4×10^{-12}	
	NORMALIZED	1.000	1.000	1.000	-2×10^{-11}	-2×10^{-11}	
	EXPECTED	1.000	1.000	1.000	0.000	0.000	
B'_Q	1	UNNORMALIZED	1.000	1.000	1.000	1.000	
		NORMALIZED	1.000	1.000	1.000	1.000	
		EXPECTED	1.000	1.000	1.000	1.000	
	a'	UNNORMALIZED	$.2445+.2445i$	$-.3353+.08985i$	$.08985-.3353i$	$-8 \times 10^{-12}+6 \times 10^{-12}i$	$-8 \times 10^{-12}+6 \times 10^{-12}i$
		NORMALIZED	$.4950+.4950i$	$-.6761+.1812i$	$.1812-.6761i$	$-2 \times 10^{-11}+1 \times 10^{-11}i$	$-2 \times 10^{-11}+1 \times 10^{-11}i$
		EXPECTED	$.4950+.4950i$	$-.6761+.1812i$	$.1812-.6761i$	0.000	0.000
	a**	UNNORMALIZED	$.2455-.2455i$	$-.3353-.08985i$	$.08985+.3353i$	$-8 \times 10^{-12}-6 \times 10^{-12}i$	$-8 \times 10^{-12}-6 \times 10^{-12}i$
		NORMALIZED	$.4950-.4950i$	$-.6761-.1812i$	$.1812+.6761i$	$-2 \times 10^{-11}+1 \times 10^{-11}i$	$-2 \times 10^{-11}+1 \times 10^{-11}i$
		EXPECTED	$.4950-.4950i$	$-.6761-.1812i$	$.1812-.6761i$	0.000	0.000
	$ a' ^2$	UNNORMALIZED	-.1349	-.1349	-.1349	4×10^{-12}	4×10^{-12}
		NORMALIZED	.4900	.4900	.4900	-2×10^{-11}	-2×10^{-11}
		EXPECTED	.4900	.4900	.4900	0.000	0.000

port delays (indicated e.g. in Table 2.2). An alternative method mentioned earlier is to insert rigid dielectric plates of varying thicknesses between the beam splitter and the DUT port. This would allow the DUT port to remain rigidly mounted and yet accomplish the desired phase shifts.

This method has been simulated to get a preliminary assessment of its effectiveness in calibration. Table 2.5 gives the parameters of the simulation. One may note that some loss has been included in the dielectric plates used for phase shifts. Although low-loss dielectrics are available, inclusion of some loss gives the simulation greater generality. All the eigenvalues were found to be calculated correctly. Also, the values of the magnitude and phase of the reflection coefficients used to derive the calibration matrix were recovered correctly from the operation of multiplying the associated sets of power data by the normalized $[C]$. The largest error in the magnitude was 0.02%. The largest phase error was 0.07 degrees.

2.6.4 Noise

An arbitrary amount of noise has been added to the simulated power data of Section 2.6.1 and the calibration matrix recalculated. The peak-to-peak size of the noise was set at 10^{-4} compared with detected signals whose maximum values were of the order unity, and this is crudely consistent with previous discussions of expected detector noise [1] in the QUOSM. The noise used was obtained simply from the random number function incorporated in the BASIC language of the HP-85 computer. The results of premultiplying the "noisy" power data sets by the "noisy" calibration matrix are shown in Table 2.6 along with the noise-free and expected results for comparison. The effects of the noise may be seen in this table and are not of a surprising magnitude. Similar tests with varying noise amplitude have shown the expected increase in error as the noise level is increased.

Table 2.5 Parameters Used in Simulation in Which All Test Port Delays Achieved with Dielectric Plates

All parameters identical to those in Table 2.2 except that the dielectric plates used to introduce the test port delays reduce the apparent test port power reflectances. Accordingly the following are the calibration conditions corresponding to each element P_{ij} of the [P] matrix (Same key as in Table 2.2):

i	j	1	2	3	4
2		M1, D1, 1	M1, D2, .8	M1, D3, .64	M1, D1, 0
3		M2, D1, 1	M2, D2, .8	M2, D3, .64	M1, D1, 0
4		M3, D1, 1	M3, D2, .8	M3, D3, .64	M1, D1, 0

For the [P'] matrix:

i	j	1	2	3	4
2		M1, D4, .9	M1, D5, .72	M1, D6, .576	M1, D1, 0
3		M2, D4, .9	M2, D5, .72	M2, D6, .576	M2, D1, 0
4		M3, D4, .9	M3, D5, .72	M3, D6, .576	M3, D1, 0

Table 2.6 Calculated Test Port Parameters B_Q and B'_Q With and Without Noise

B_Q		TEST PORT POSITION			MATCHED LOAD	
		1	2	3		
B_Q	1	NOISE	1.000	1.000	1.000	.9998
		WITHOUT NOISE	1.000	1.000	1.000	1.000
		EXPECTED	1.000	1.000	1.000	1.000
	a	NOISE	$1.000+1 \times 10^{-11}i$	$-.4997+.8673i$	$-.5010-.8652i$	$-1 \times 10^{-4}-2 \times 10^{-4}i$
		WITHOUT NOISE	1.000	$-.4994+.8666i$	$-.5006-.8654i$	$-1 \times 10^{-11}+2 \times 10^{-12}i$
		EXPECTED	1.000	$-.5000+.8660i$	$-.5000-.8660i$	0.000
	a*	NOISE	$1.000-1 \times 10^{-12}i$	$-.4997-.8673i$	$-.5010+.8652i$	$-1 \times 10^{-4}+2 \times 10^{-4}i$
		WITHOUT NOISE	1.000	$-.4994-.8666i$	$-.5006+.8654i$	$-1 \times 10^{-11}-2 \times 10^{-12}i$
		EXPECTED	1.000	$-.5000-.8660i$	$-.5000+.8660i$	0.000
$ a ^2$	NOISE	1.000	1.000	.9995	-4×10^{-4}	
	WITHOUT NOISE	1.000	.9995	.9996	3×10^{-11}	
	EXPECTED	1.000	1.000	1.000	0.000	
B'_Q	1	NOISE	.9999	.9999	.9999	.9999
		WITHOUT NOISE	1.000	1.000	1.000	1.000
		EXPECTED	1.000	1.000	1.000	1.000
	a'	NOISE	$.4950+.4951i$	$-.6764+.1821i$	$.1805-.6764i$	$2 \times 10^{-4}-2 \times 10^{-4}i$
		WITHOUT NOISE	$.4951+.4951i$	$-.6763+.1818i$	$.1806-.6763i$	$-1 \times 10^{-11}+2 \times 10^{-12}i$
		EXPECTED	$.4950+.4950i$	$-.6761+.1812i$	$.1812-.6761i$	0.000
	a'*	NOISE	$.4950-.4951i$	$-.6764-.1821i$	$.1805+.6764i$	$2 \times 10^{-4}+2 \times 10^{-4}i$
		WITHOUT NOISE	$.4951-.4951i$	$-.6763-.1818i$	$.1806+.6763i$	$-1 \times 10^{-11}-2 \times 10^{-12}i$
		EXPECTED	$.4950-.4950i$	$-.6761-.1812i$	$.1812-.6761i$	0.000
	$ a' ^2$	NOISE	.4900	.4900	.4896	-7×10^{-5}
		WITHOUT NOISE	.4901	.4898	.4899	3×10^{-11}
		EXPECTED	.4900	.4900	.4900	0.000

However, the rate of increase in the error for a given increase in noise does not indicate a pathological sensitivity to noise in the power measurements. A more systematic study of the effects of different kinds of noise and error, such as was done in earlier simulations [1], will be recommended for further work involving the eigenvector method.

3.0 Reduction of Standing Waves

Another aspect of the present study has been the investigation of ways to reduce the magnitude of standing waves. In numerical methods designed to apply a correction for an undesirable phenomenon, it is often the case that accuracy is served if the size of the phenomenon can be kept reasonably small compared to the quantity of principal interest. Such was the motivation for the tests reported in this section. These occupied only a relatively small part of the effort for two reasons. First, during the course of the work, the emphasis on the numerical methods side shifted away from an extension of the phasor method, which was used earlier and which clearly is more tractable if the standing wave phenomenon is smaller. Second, in the new eigenvector method, no assumptions appear to be necessary concerning the size of the standing wave effect. As of yet, no important relationship between uncertainty and the magnitude of the standing waves is known, but a further systematic investigation of this would be prudent. Should a reduction of standing waves be required in the future, the results discussed in the following sections will be of interest. As a by-product of this study, a preliminary evaluation of pyroelectric detectors is also reported.

3.1 Experiments with the Detector

As mentioned in Section 2.1, previous attempts [3] to suppress reflections from the Golay cell detectors, by tilting them away from the optical axis of the QUOSM, failed. The apparent reason was retroreflection by the metal surrounding the detector window or by the cavity inside the detector. Alternative pyroelectric detector elements come in a variety of packages, but the most common, shown in Figure 3.1 has the pyroelectric crystal mounted in a standard transistor can.

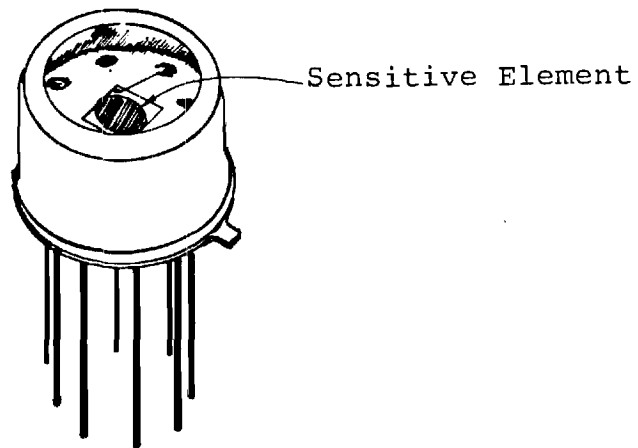


Figure 3.1 Type of Pyroelectric Detector Element Tested.

Georgia Tech-owned versions of this have been tested at a frequency of 94 GHz in the present work, and the same or slightly higher levels of standing waves were found in tests similar to those previously conducted with Golay cells. Apparently the metal can around the sensitive crystal is similarly retroreflective. Alternative forms of pyroelectric elements are commercially available in which the crystals are large discs and are not surrounded by metal. It was not in the scope of the present work to pursue this further, but such detectors may be a good choice for future systems.

What was shown in the present work is that while the pyroelectric detector has less sensitivity than a Golay cell, the signal levels available from klystron sources are high enough to offset this. Pyroelectric detectors possess the advantage of being solid-state, rugged, compact, and somewhat less expensive by comparison with Golay cells. Thus the option of using such detectors should be taken seriously for future designs. This may require some testing of several models and makes of elements, however, since they are made primarily for infrared use, and the millimeter wave performance is often poorly known by the manufacturer.

3.2 Isolation by Attenuation

It was realized that the quasi-optical attenuators [2,3] in the QUOSM could, in principle, provide a simple form of isolation. Waveguide-type isolators are neither readily available in the frequency range of the QUOSM nor well suited. Low-loss quasi-optical isolation schemes are known, for example ones involving the use of a circular polarizer [19], but they are not able to cover a wide frequency range, are not trivial to construct, and were not within the scope of the present work. Therefore, the only apparent option was to use loss as a mechanism of isolation.

Since it was found in previous work [3] that detector reflection was the primary cause of standing waves at 94 GHz, attenuation by the quasi-optical attenuator nearest the detector would be expected to reduce their magnitude. Up to 28 dB of attenuation (for a single-pass) is available from this unit [3]. For this amount the depth of modulation found in the interference pattern, when the test port was blocked by an absorber and the mirror was scanning, was only a few percent of the maximum power recorded. This may be compared with a depth of modulation of sixty percent found [3] without the attenuation. Since the klystron emits so much more power than the maximum power which the detector can handle (a factor of 10^5), such attenuation need not reduce the accuracy of the QUOSM; in other words, if the detector attenuator is not used, attenuation must be introduced at the source anyway. The problem with putting all of the required attenuation in the detector port is that this necessarily means that the power level at the test port will be high. This would be intolerable for some devices that might burn out, such as mixers for example.

Therefore one must view these results from larger perspectives. A reduction of the standing wave effects by more than an order of magnitude, while impressive, is not enough to permit one to neglect them. Secondly, the eigenvector method appears to work well enough that such drastic measures as described above are not needed, and thus it will still be possible to reduce source powers and the power to the DUT to safe levels.

4.0 Status of Hardware and Software.

In the foregoing discussion of calibration techniques, a few hardware changes or additions to the QUOSM were shown to be needed. These may be summarized as follows:

- 1) The reference detector and its beam splitter coupler must be relocated in the test port arm. The present design can readily be adapted to this configuration provided that the quasi-optical attenuator is removed from the test port arm and either omitted or moved to the source port arm. As the calibration procedure is presently understood, there is no longer a need for the attenuator in the test port arm.
- 2) A choice must be made between two alternative mechanisms of test port delays described earlier. One would require a method of translating the test port along the optical axis that preserves alignment and provides three or more reproducible positions. The other would require the selection and fabrication of some low-loss dielectric plates of appropriate thicknesses and a holder to place them reproducibly in the beam in front of the test port. Both appear to be practical but will require additional hardware to be designed and fabricated.
- 3) When during the calibration procedure the high reflectance termination is installed and the power readings for the matrix [P'] must be measured, a somewhat lossy dielectric slab must be mounted in front

of the test port. The arrangement for mounting would probably be similar to that in the second option on (2) above. For both cases the plate should be angled to suppress multiple reflections between the plate and other optical components.

- 4) Another high-loss absorber must be made that can block the test port beam. One similar to the type in the quasi-optical attenuators [3] is appropriate, although the type which incorporates epoxy-based material, rather than rubber-based, would probably be preferred as it is believed to give somewhat more absorption [3]. Attenuation values of 40db are believed possible.

None of these new requirements have been implemented. No problems of feasibility have been identified, but some further design work should be done to establish the best alternative in (2) and to work out the details for each of the items. The only new hardware items added in the present work have been two new horns made for use with WR-10 components.

All of the software is at present in an experimental state and requires considerable operator attention and involvement. The longest program EIGEN occupies 22,244 bytes out of the available 30,219 bytes in the HP-85. The running time for this program is dominated by the time for diagnostic printing of numerous intermediate calculations. Without input-output, the calibration calculations take approximately 30 seconds. As mentioned earlier, neither the program contents nor the run-time have been streamlined. Further work on this is envisioned along with efforts to structure the programs for ease of use.

5.0 Summary

There have been a number of significant accomplishments in the present work, such as the following:

1. A program has been developed that simulates the phenomenon of standing waves in the QUOSM and has provided tests of new calibration procedures.
2. A method of calibration previously developed for use with six-port network analyzers has been shown to be adaptable for use with the QUOSM. The calibration devices needed are a standard short, two standard matched loads (one quasi-optical), and two uncalibrated terminations along with a mechanism for creating reproducible delays in the test port arm of the QUOSM. Proposed implementations of each of the new requirements have been briefly described and in many cases differ from previous implementations with six-port network analyzers. Quasi-optical techniques are stressed here as they are likely to offer advantages of greater accuracy and ease of use and fabrication throughout the frequency range of the QUOSM. For example, there is relatively greater facility with the QUOSM for establishing the phase relationships between the source and reflected signals which are believed to be optimum [4, 6].
3. Numerical techniques for calculating eigenvectors have been implemented as an integral part of the calibration procedure which ultimately defines the relationship between recorded detector signals and the reflection parameters of a device under test. Simulated data have been used to show that the recommended optical and numerical procedures together provide a valid calibration, whether or not standing waves exist in the QUOSM. Very preliminary

investigations with simulated instrumental noise have found no pathological sensitivities to noise in the numerical methods employed.

4. Not of primary importance, but of some significance, have been the efforts to reduce the magnitude of standing waves. As expected the quasi-optical attenuators in the QUOSM can provide crude isolation and reductions in standing wave effects. Tests with pyroelectric detectors were significant in demonstrating that they can have adequate sensitivity, but the type tested did not reduce VSWR from the detector. Nonetheless, their smaller, more rugged construction make them desirable in future systems similar to the QUOSM.

6.0 Future Work

It is Georgia Tech's desire to continue to work on the QUOSM network analyzer in order to make necessary modifications and to carry out thorough tests involving further simulations and measurements. It is believed that this is justified by the indications of success thus far achieved and by the continuing need for network analyzers operating in the 90-340 GHz range. The need by the Army and the Army's contractors to test discrete millimeter wave components may be expected to continue for several years since millimeter wave intergrated circuits still require considerable research and development before they will have a dominant role in systems. The advantages of a quasi-optical metrology instrument are still extremely attractive; namely, ease of fabrication and use, and possibly greater accuracy since the fabrication requirements are not subject as much to compromise.

Some specific steps that would be proposed are the following:

- 1) Study the sensitivity of the QUOSM to the effects of noise and known errors through the use of more detailed simulations. This would include but not be limited to the effects of detector non-linearity as well as noise, of uncertainty in mirror position, and of imperfect calibration loads. In addition, cases of varying amounts of standing waves and varying test device parameters would be investigated. Any factors which may be postulated to improve accuracy will be tested.
- 2) Make selections among alternatives, develop detailed designs, and implement the hardware additions and changes necessary for the new calibration procedure. These items were listed in Section 4.0. In general, new hardware would be as compatible as possible with the present breadboard approach to the QUOSM; no major overhaul of the format is envisioned until a thorough test has been completed.
- 3) Write software that will efficiently accomplish measurements and calibration and that can be readily operated by the staff of the TMDE Support Group.
- 4) Conduct fairly extensive measurements of test devices to be agreed with the sponsor. In addition, tests can be devised to elucidate typical amounts of reflections from flange connections. Flange reflections are recognized as a greater problem for systems operating in the short millimeter wavelength range, and demonstration of such effects would be a useful beginning with the QUOSM.

When a single QUOSM has been demonstrated to work as a reliable reflectometer, it is envisioned that a dual-QUOSM system can be designed, analogous to dual six-port systems, that will permit devices to be tested both for their reflection and transmission properties. The simulation and numerical analysis tools developed in the present program can contribute to the planning and design of such a system.

7.0 References

1. R. A. Bohlander, A. McSweeney, and R. G. Shackelford, "Quasi-Optical Scanning Multiport (QUOSM) Network Analyzer," Interim Report No. 1, GT/Project A-2751, Contract DAAH01-80-C-1634, U.S. Army Missile Command (13 April 1981).
2. R. A. Bohlander, A. McSweeney, J. M. Newton, V. T. Brady, and R. G. Shackelford, "Quasi-Optical Scanning Multiport (QUOSM) Network Analyzer," Interim Report No. 2, GT/Project A-2751, Contract DAAH01-80-C-1634, U.S. Army Missile Command (23 September 1981).
3. R. A. Bohlander, A. McSweeney, V. T. Brady, O. A. Simpson, and R. G. Shackelford, "Quasi-Optical Scanning Multiport (QUOSM) Network Analyzer," Final Report, GT/Project A-2751, Contract No. DAAH01-80-C-1634, U.S. Army Missile Command (26 April 1982).
4. G. F. Engen, "The Six-Port Reflectometer: An Alternative Network Analyzer," IEEE Trans. Microwave Theory and Techniques, MTT-25, 1075-80 (1977).
5. See for example, S. Y. Liao, Microwave Devices and Circuits, Englewood Cliffs, New Jersey: Prentice-Hall, Inc. (1980).
6. H. M. Cronson and L. Susman, "Automated Six-Port Microwave Calibration System," Final Technical Report SCRC-CR-77-32, Contract No. DAAH01-75-C-1112, U.S. Army Missile Command (April 1977).
7. H. M. Cronson and L. Susman, "Dual Six-Port Microwave Calibration System," Interim Report SCRC-CR-78-12, Contract No. DAAH01-77-C-0693, U.S. Army Missile Command (March 1978).
8. S. D. Conte and C. deBoor, Elementary Numerical Analysis: An Algorithmic Approach, New York: McGraw-Hill Book Co. pp.166-167 (1980).
9. Hewlett-Packard, "HP-85 Matrix ROM Manual," Manual No. 00085-90144, p. 33 (1980).
10. J. H. Wilkinson and C. Reinsch, Linear Algebra, Berlin: Springer Verlag, pp. 191-201 (1971).
11. J. H. Wilkinson, "Calculation of Eigensystems of Matrices," in Numerical Analysis, an Introduction, J. Walsh ed., Washington, D.C.: Thompson Book Co., pp. 27-61 (1967).
12. J. H. Wilkinson, The Algebraic Eigenvalue Problem, Oxford: Clarendon Press (1965).
13. J. Grad and M. A. Brebner, "Eigenvalues and Eigenvectors of a Real General Matrix," Algorithm 343, Comm. ACM 11, 820-26 (Dec. 1968).

14. H. D. Knoble, "Certification of Algorithm 343 [F1] Eigenvalues and Eigenvectors of a Real General Matrix," Comm. ACM 13, 122-4 (Feb. 1970).
15. W. Knight and W. Mersereau "Certification of Algorithm 343 [F1] Eigenvalues and Eigenvectors of a Real General Matrix" Collected Algorithms from CACM, 343-P8-R1 (1970).
16. H. Niessner, "Remark on Algorithm 343 [F2], Collected Algorithms from CACM, 343-P9-R1 (1971).
17. B. Noble, Applied Linear Algebra, Englewood Cliffs, New Jersey: Prentice-Hall, Inc., p. 280 (1969).
18. G. W. Chantry, Submillimetre Spectroscopy, London: Academic Press, pp. 317-319 (1971).
19. R. W. McMillan, R. A. Bohlander, D. S. Ladd, R. E. Forsythe, A. McSweeney, J. M. Newton, O. A. Simpson, M. J. Sinclair, and J. C. Butterworth, "Near Millimeter Wave Radar Technology," Vol. 1, Interim Technical Report Phase III, GT/Project A-2445, Contract No. DAAK70-79-C-0108, U.S. Army Mobility Equipment and Development Command, Night Vision and Electro-Optics Laboratory (11 October 1982).

Appendix A. Software to Simulate QUOSM Signals Including the
Effects of Standing Waves

An annotated copy of the program RFLTCN, described in the
text follows. It occupies 9,690 bytes of memory.

PROGRAM NAME: RFLCTN

```

100 REM This program calculates
110 REM the signal at the principal detector of the
120 REM Quasi-Optical Scanning
130 REM Multipoint network analyzer
140 REM lyzer
150 REM it takes into account
160 REM any number of reflections through the
170 REM system.
180 REM
190 OPTION BASE 1
200 DIM R(41),S(41),X(41),T(41)
210 DIM D(4)
220 D(4)=1
225 DATA 0.60,120
230 CLEAR @ PRINT
240 N9=3 ! # DATA PTS. <42
250 PRINT "# MIRROR POSITIONS: "
    :N9
260 CLEAR @ PRINT
270 DISP "Insert CASSETTE for data."
280 DISP "It must be set to RECORD."
290 DISP
300 DISP "Type CREATE filename--\N
    :8*#"
305 DISP "where N is Number coll.
    :e.g.12"
310 DISP "and # is # of mirror positions."
320 DISP "Press CONT when ready."
    :
330 PAUSE
340 CLEAR @ PRINT
350 DISP "Enter FILE NAME:"
360 DISP "( 1-6 characters )"
370 INPUT F#
380 PRINT "File name: ",F#
390 L6=200 ! (mm) SOURCE to B.S.
400 T6=1 ! SQR amp xmtn SOURCE
410 L3=200 ! (mm) DET. to B.S.
420 T3=1 ! SQR amp xmtn DET.
430 L4=200 ! (mm) B.S. to DUT
440 T4=1 ! SQR amp xmtn DUT
450 L5=200 ! (mm) B.S. to MIRROR
460 T5=1 ! SQR amp xmtn MIRROR
470 CLEAR @ PRINT
480 PRINT @ PRINT @ PRINT
490 DISP "Enter SOURCE"
500 DISP "POWER reflectivity:"
510 DISP "( 0 < R < 1 )"
520 INPUT R5
530 S9=1-R5 ! SOURCE PWR xmtn
540 PRINT "SOURCE Pwr reflectivity:"
    :
550 PRINT R5
560 L=-SQR(R5) @ M=0
570 CLEAR @ PRINT
580 DISP "Enter DETECTOR"

```

Preset shifts of mirror in degrees
(i.e., 1 wavelength=360°)
Set number of mirror positions

Load tape to receive data

Create data file

Set distances between optical
components LX
Set the one-way amplitude transmission
factor between optical
components TX

Enter power reflectance of source

Enter power reflectance of detector

```

590 DISP "POWER reflectivity:"
600 DISP "( 0 < R < 1 )"
610 INPUT R6
620 D9=1-R6 ! DET. PWR XMTN
630 PRINT "DET. power reflectivi
ty:"
640 PRINT R6
650 A=-SQR(R6) @ B=0
660 CLEAR @ PRINT
670 DISP "Enter value for FREQ.(
GHz):"
680 DISP "(e.g. 90-340 GHz)"
690 INPUT F
700 PRINT "FREQ.=":F:"GHz"
710 L1=300/F
720 PRINT "Wavelength=":L1:"mm"
730 DEF FNF(L) = 2*PI*FP(L/L1)
740 F6=FNF(L6)
750 G6=T6*COB(F6) @ H6=-T6*SIN(F
6)
760 F3=FNF(L3)
770 G3=T3*COB(F3) @ H3=-T3*SIN(F
3)
780 F4=FNF(L4)
790 G4=T4*COB(F4) @ H4=-T4*SIN(F
4)
800 F5=FNF(L5)
810 G5=T5*COB(F5) @ H5=-T5*SIN(F
5)
820 CLEAR @ PRINT
830 DISP "Enter value for beamspl
itter"
840 DISP "THICKNESS (mils)"
850 DISP "(25.4 micron = 1 mil)"
860 INPUT T
870 PRINT "Beamsplitter thicknes
s:"
880 PRINT T:" mils"
890 CLEAR @ PRINT
900 GOSUB 2570 ! Calc.B.S. R&T
910 CLEAR @ PRINT
920 DISP "Enter complex number R
air"
930 DISP "in POLAR form (R,ANGLE
in DEG)"
940 DISP "for DUT reflect. coeff
"
950 DISP "(e.g. 1.0,0)"
960 INPUT G,H
970 PRINT "Polar DUT reflect.coe
ff.:"
980 PRINT G,H
990 H=H*PI/180
1000 RAD
1010 J=G*COB(H) @ K=G*SIN(H)
1020 PRINT "Rect. DUT reflect.co
eff.:"
1030 PRINT J,K
1040 CLEAR @ PRINT
1050 DISP "Enter DUT OFFSET (deg
)"

```

Enter Frequency (GHz)

Calculate Wavelength in mm

Convert each distance between optical components to FX radians. Then compute the factor (GX,HX) = TX exp(-i FX) by which a signal phasor changes in traveling between the optical components.

Enter beam splitter thickness

Calculate beam splitter complex reflection and transmission amplitude factors.

Enter magnitude of DUT amplitude reflectance and the angle by which the wave is delayed on reflection.

Enter half the delay (in degrees) caused by off-setting the test port from its initial position.

```

1060 INPUT F7
1070 PRINT "DUT OFFSET:":(F7)"deg
"
1080 F7=F7*PI/180
1090 G7=COS(F7) @ H7=-SIN(F7)
1100 CLEAR @ PRINT
1110 DISP "Enter MIRROR offset (
deg):"
1120 INPUT M0
1130 PRINT "MIRROR OFFSET:":(M0)"
deg."
1140 M0=2*M0*PI/180
1145 RESTORE
1150 FOR I=1 TO N9
1160 READ S
1170 I1=1 @ CLEAR
1190 ! MIRROR PHASE
1200 S=2*S*PI/180+PI+M0
1210 N=COS(S)
1220 O=SIN(S)
1230 D0=0 @ S0=0
1240 U0=0 @ U1=0
1250 CLEAR
1260 REM From SOURCE
1270 V=1*SQR(S9) @ W=0
1280 REM From DETECTOR
1290 X=0 @ Y=0
1300 M0=1*SQR(R5/S9) @ W0=0
1310 X0=0 @ Y0=0
1320 ! SOURCE-BS phase:
1330 P=V @ Q=W
1340 V=P*G6-Q*H6 @ W=P*H6+Q*G6
1350 ! DET.-BS phase:
1360 P=X @ Q=Y
1370 X=P*G3-Q*H3 @ Y=P*H3+Q*G3
1380 DISP I, I1
1390 REM From BEAMSPLITTER:
1400 GOSUB 3000 ! *B.S. R & T
1410 ! From B.S. to DUT:
1420 P=V1+X1 @ Q=W1+Y1
1430 ! Phase shift, BS TO DUT
1440 V=P*G4-Q*H4 @ W=P*H4+Q*G4
1450 ! Accumulated vector @ DUT
1460 U0=U0+V @ U1=U1+W
1470 ! Power at DUT.
1480 P9=U0^2+U1^2
1490 ! Prop. thru DUT OFFSET
1500 P=V*G7-W*H7 @ Q=V*H7+W*G7
1510 ! Signal reflected by DUT:
1520 V=P*J-Q*K @ W=P*K+Q*J
1530 ! Prop. thru DUT OFFSET
1540 P=V*G7-W*H7 @ Q=V*H7+W*G7
1550 ! Phase shift, DUT to BS:
1560 V=P*G4-Q*H4 @ W=P*H4+Q*G4
1570 ! From BS to MIRROR:
1580 P=V2+X2 @ Q=W2+Y2
1590 ! Phase shift, BS to MIRROR
1600 X=P*G5-Q*H5 @ Y=P*H5+Q*G5
1610 ! Reflect from MIRROR:
1620 P=X*N-Y*O @ Q=X*O+Y*N

```

Convert to radians-F7
Calculate exp(-iF7)

Enter any change desired in the mirror starting position, and convert to radians.
Read shift of mirror position.

Calculate delay S in radians caused by shift in mirror position and by reflection from mirror

Initialize

Initial signal from source Amplitude V:REAL
W:IMAG

Initial signal from detector Amplitude X:REAL
Y:IMAG

Initial signal reflected back into source
Initial signal reflected back into detector
START OF ITERATIVE PROCEDURE

Calculate change in signal propagating from source and detector to B.S.

Transmission through and reflection from B.S.

Combination of signals going to DUT

Signal accumulated that impinges on DUT.

DUT power calculated. (Used as REF. Detector Signal)

Propagation through DUT offset

Calculate effects of DUT reflection

Propagation back through DUT offset

Propagation back to Beam Splitter

Combination of signals going to mirror

Propagation to normal mirror starting position

Combined effect of reflection from mirror and mirror shift.

```

1630 ! Phase shift, MIRROR to BS
1640 X=P*G5-Q*H5 @ Y=P*H5+Q*G5
1650 REM From BEAMSPLITTER:
1660 GOSUB 3000 ! *B.S. R & T
1670 REM To SOURCE:
1680 P=V1+X1 @ Q=W1+Y1
1690 ! Phase shift, BS to SOURCE
1700 V=P*G6-Q*H6 @ W=P*H6+Q*G6
1710 REM To DETECTOR:
1720 P=V2+X2 @ Q=W2+Y2
1730 ! Phase shift, BS to DET.
1740 X=P*G3-Q*H3 @ Y=P*H3+Q*G3
1750 W0=W0+W @ W0=W0+W
1760 X0=X0+X @ Y0=Y0+Y
1770 P=W0^2+W0^2 ! Pwr to SOURCE
1780 P=S9*P
1790 Q=X0^2+Y0^2 ! Pwr to DET.
1800 Q=D9*Q
1810 D2=Q @ S2=P ! Save PWR val
1820 P=V @ Q=W
1830 ! From SOURCE:
1840 V=P*L-Q*M @ W=Q*L+P*M
1850 P=X @ Q=Y
1860 ! From DETECTOR:
1870 X=P*A-Q*B @ Y=Q*A+P*B
1880 I1=I1+1
1890 IF D2<>0 THEN 1920
1900 IF D0<>0 THEN 1920
1910 GOTO 1950
1920 E=ABS(D2-D0)/((D2+D0)/2)
1930 IF E<.0005 THEN 1950
1940 D0=D2 @ S0=S2 @ GOTO 1330
1950 IF S2<>0 THEN 1980
1960 IF S0<>0 THEN 1980
1970 GOTO 2010
1980 E=ABS(S2-S0)/((S2+S0)/2)
1990 IF E<.0005 THEN 2010
2000 GOTO 1940
2010 D(I)=D2 @ S(I)=S2 ! D&S Pwr
2020 T(I)=D2+S2 ! DET+SOURCE Pwr
2030 R(I)=P9
2040 NEXT I
2050 GOTO 2090
2060 PRINT
2070 PRINT "DET+SOURCE power:"
2080 GOSUB 3060 ! Plot TOTAL Pwr
2090 FOR I=1 TO N9 @ T(I)=D(I)/R
(I)
2100 NEXT I
2110 PRINT
2120 PRINT " NORM DETECTOR power
:"
2130 GOSUB 3060 ! Plot DET Pwr.
2140 CLEAR @ PRINT
2150 DISP "Instal CASSETTE for d
ata."
2160 DISP
2170 DISP "Enter RECORD NUMBER:"
2180 DISP "(0-8, 0=do NOT save)"
2190 INPUT R9

```

Return propagation to B.S.

Transmission through and reflection from B.S.

Combination of signals going to source- followed by propagation

Combination of signals going to detector- followed by propagation

Accumulation of signal returning to source and to detector

Calculation of powers

Save power values for convergence test

Calculate complex amplitudes reflected by source and detector.

Increment iteration counter

Convergence tests

If not converged, do next iteration

Further convergence tests

Save detector and power back to source

Save sum of these

Save power impinging on DUT.

Plot total power normalized by DUT power

Plot normalized detector power

The [P] and [P'] matrices are stored in the same file. The [P] matrix occupies records 1-m of the file, and [P'], records m+1 through 2m (where m defined in Section 2.3.1)

```

2200 PRINT "RECORD # ";R9
2210 IF R9=0 THEN 2300
2220 FOR I=1 TO N9
2230 D(I)=D(I)/R(I)
2240 PRINT I;D(I)
2250 NEXT I
2255 PRINT 4;D(4)
2260 ASSIGN# 1 TO F#
2270 PRINT# 1,R9 ; D()
2280 ASSIGN# 1 TO *
2290 GOTO 2400
2300 FOR I=1 TO N9 @ T(I)=S(I)
2310 NEXT I
2320 PRINT
2330 PRINT "SOURCE power."
2340 GOSUB 3060 ! Plot SOURCE
2350 FOR I=1 TO N9 @ T(I)=R(I)
2360 NEXT I
2370 PRINT
2380 PRINT "DUT power:"
2390 GOSUB 3060 ! Plot DUT
2400 CLEAR @ PRINT
2410 DISP "New MIRROR offset? 1=
YES"
2420 INPUT C
2430 IF C=1 THEN 1100 ! END
2440 CLEAR
2450 DISP "New DUT? 1=YES"
2460 INPUT C
2470 IF C=1 THEN 910
2480 CLEAR
2490 DISP "New FREQUENCY? 1=YES"
2500 INPUT C
2510 IF C=1 THEN 660
2520 CLEAR
2530 DISP "New DETECTOR? 1=YES"
2540 INPUT C
2550 IF C=1 THEN 570
2560 GOTO 470 ! New SOURCE
2570 REM Subroutine to calculate
2580 REM complex beamsplitter
2590 REM reflection & xmtn
2600 REM amplitude coefficients
2610 RAD
2620 N1=1.0003
2630 N2=1.7
2640 U=PI/4
2650 C1=COS(ASN(SIN(U)*N1/N2))
2660 REM Wavenumber (mils-1)
2670 N3=10*2.54/(1000*L1)
2680 D2=4*PI*N2*T*N3*C1
2690 C0=COS(U)
2700 R4=(N1*C0-N2*C1)/(N1*C0+N2*
C1)
2710 C2=COS(D2)
2720 S3=SIN(D2/2)*(1+R4^2)
2730 C3=COS(D2/2)*(1-R4^2)
2740 Z1=2*R4^2*(1-C2)
2750 Z2=1-2*R4^2*C2+R4^4
2760 Z6=-SIN(D2)*(1-R4^2)

```

Record normalized detector signals

Plot power returned to source

Plot power impinging on DUT

This section prepares the operator to use RFLCTN again and change only one or a few of the parameters.

The usual thing with the new calibration procedure is to set a new DUT offset and/or new DUT reflection parameters and calculate a new column of the [P] or [P'] matrices.

Subroutine to calculate beam splitter complex transmission and reflection coefficients. See text for reference.

```

2770 Z7=(1-C2)*(1+R4^2)
2780 Z3=ATN2(Z6,Z7)
2790 Z4=(1-R4^2)^2
2800 Z8=R4^2*SIN(D2)
2810 Z9=1-R4^2*C2
2820 Z5=ATN2(Z8,Z9)
2830 R1=-SQR(Z1/Z2)*COS(Z3)
2840 R2=-SQR(Z1/Z2)*SIN(Z3)
2850 T1=SQR(Z4/Z2)*COS(D2/2+Z5)
2860 T2=SQR(Z4/Z2)*SIN(D2/2+Z5)
2870 A3=PI-ATN2(C3,S3)
2880 A4=ATN2(S3,C3)
2890 PRINT "Complex refl. coeff.
:"
2900 PRINT R1,R2
2910 PRINT "Complex xmtn. coeff.
:"
2920 PRINT T1,T2
2930 PRINT "Reflectivity:"
2940 PRINT R1^2+R2^2
2950 PRINT "Transmissivity:"
2960 PRINT T1^2+T2^2
2970 PRINT "REFL.PHASE= ";A3;" R
ADIANS"
2980 PRINT "TRANS.PHASE= ";A4;"
RADIANS"
2990 RETURN ! To approx. 830
3000 REM From beamsplitter.
3010 V1=T1*W-T2*W @ W1=T1*W+T2*W
3020 V2=R1*W-R2*W @ W2=R1*W+R2*W
3030 X1=R1*X-R2*Y @ Y1=R1*Y+R2*X
3040 X2=T1*X-T2*Y @ Y2=T1*Y+T2*X
3050 RETURN
3060 ! This subroutine PLOTS
3070 ! data in array T(I)
3080 PEN 1 @ GCLEAR
3090 SCALE 0,400,0,1.2
3100 XAXIS 0,45,0,400
3110 YAXIS 0, 1,0,1
3120 XAXIS 1,2,45,0,400
3130 YAXIS 400, 1,0,1
3140 MOVE 0,T(1)
3150 FOR I=1 TO N9
3160 DRAW 360/N9*(I-1),T(I)
3170 NEXT I
3180 BEEP @ PRINT
3190 PAUSE
3200 RETURN
3210 CLEAR @ PRINT
3220 DISP "THE END"
3230 PRINT "THE END"
3240 END
4546 PLIST 1160,1190

```

Return to 900

Subroutine that applies B.S. complex transmission and reflection factors to signals impinging on it.

Return

Subroutine for graph plots on screen

Pause to copy to paper; if desired press "COPY" key, then press "CONTINUE".

Appendix B. Software to Calculate Eigenvalues and Eigenvectors
for Calibrating the QUOSM

An annotated copy of the program EIGEN, described in the text, follows. It occupies 22,244 bytes of memory and has a run time of about thirty seconds apart from all input/output operations.

PROGRAM NAME: EIGEN

```
100 OPTION BASE 1
110 INTEGER IS
120 DIM A(4,4),B(4,4),D(4),E(4)
130 DIM F(4),H(4,4),I(4),J(4)
140 DIM L(100),P(4,4),Q(4),R(4)
150 DIM S(4),T(4,4),V(4,4)
160 DIM W(4),X(4,4),Y(4,4),Z(4,4)
170 CLEAR @ PRINT
180 BEEP
190 DISP "Insert DATA cartridge."
200 DISP
210 DISP "Enter data FILE NAME:"
220 INPUT F$
230 PRINT "File name:":F$
240 ASSIGN# 1 TO F$
250 FOR J=1 TO 4
260 READ# 1,J ; D()
270 FOR I=1 TO 4
280 P(I,J)=D(I)
290 NEXT I
300 NEXT J
310 FOR J=5 TO 8
320 K=J-4
330 READ# 1,J ; D()
335 FOR I=1 TO 4
340 B(I,K)=D(I)
350 NEXT I
380 NEXT J
390 ASSIGN# 1 TO *
400 CLEAR @ PRINT
410 PRINT "Matrix P:" @ PRINT
420 FOR J=1 TO 4
430 FOR I=1 TO 4
440 PRINT I;J:P(I,J)
450 NEXT I
460 PRINT
470 NEXT J
480 PRINT @ PRINT
490 PRINT "Matrix P':"
500 PRINT
510 FOR J=1 TO 4
520 FOR I=1 TO 4
530 PRINT I;J:B(I,J)
540 NEXT I
550 PRINT
560 NEXT J
570 CLEAR @ PRINT
580 DISP "CALCULATING"
590 MAT T=TRN(P) ! P transpose
600 MAT Y=P*T ! P*Pt
605 D1=DET(Y)
610 MAT X=B*T ! P'*Pt
611 MAT Y=TRN(Y)
612 MAT X=TRN(X)
613 PRINT @ PRINT "(PPt)*(PPt)in
v" @ PRINT
614 MAT P=Y
615 MAT H=SYS(Y,P)
```

Enter name of file containing matrices [P]
and [P']

Read matrices column by column

Print matrix [P] column by column

Print matrix [P'] column by column

```

616 MAT H=TRN(H) ! H=(PPt)*(PPt)
    inv
617 MAT PRINT USING "MD.E,X" ; H
618 PRINT
630 MAT A=SYS(Y,X) ! TRANS(P'Pt)
    *(PPt)inv
660 MAT Z=A
662 PRINT
663 PRINT "Matrix A:"
664 PRINT
666 MAT PRINT USING "MD.DDE,2X"
    ; A
668 PRINT
670 D2=DET(A)
680 PRINT "D1=";D1
681 T=0
682 FOR I=1 TO 4
683 T=T+A(I,I)
684 NEXT I
685 PRINT "TRACE A:";T
690 PRINT "DET A:";D2
700 T=39
710 N=4
720 GOSUB 890
730 CLEAR @ PRINT
740 PRINT "STATUS INFO:"
750 MAT PRINT COL 0/
760 CLEAR @ PRINT
770 PRINT "REAL EigenVALUES:"
780 MAT PRINT R/
790 CLEAR @ PRINT
800 PRINT "IMAG. EigenVALUES:"
810 MAT PRINT I/
811 CLEAR @ PRINT
812 R=0 @ C=0
813 FOR I=1 TO N
814 R=R+R(I) @ C=C+I(I)
815 NEXT I
816 PRINT "SUM of eigenVALUES:"
817 PRINT R;"i";C
818 CLEAR @ PRINT
819 R=1 @ C=0
820 FOR I=1 TO N @ A=R @ B=C
821 R=A*R(I)-B*I(I)
822 C=A*I(I)+B*R(I)
823 NEXT I
824 PRINT "PROD. of eigenVALUES:"
    "
825 PRINT R;"i";C
826 CLEAR @ PRINT
830 PRINT "REAL part of vectors:"
    "
840 MAT PRINT COL W/
850 CLEAR @ PRINT
860 PRINT "IMAG. part of vectors:"
    "
870 MAT PRINT COL H/
880 GOTO 8010

```

Calculation of matrix $[z^t]$

Print it

Print determinant of $[P][P^t]$ to show it is not singular
 Print trace and determinant of $[z^t]$ for later comparison with sum of its eigenvalues, and with eigenvectors.

Go to Eigensolution subroutine written by Grad and Brebner with modifications suggested by Niessner. (See text for references).

Print eigenvalues

Print sum of eigenvalues

Print product of eigenvalues

Print eigenvectors

Skip over EIGENP and continue program at statement 8010.

```

890 REM SUBROUTINE EIGENP
900 IF N>1 THEN 970
910 R(1)=A(1,1)
920 I(1)=0
930 V(1,1)=1
940 H(1,1)=0
950 Q(1)=2
960 RETURN ! FROM SUBROUTINE EIGENP
970 GOSUB 2260 ! CALL SCALE FROM EIGENP
980 REM COMPUTE EIGENVALUES OF NORMALIZED MATRIX
990 E3=EXP(-T*LOG(2))
1000 GOSUB 2740 ! CALL HESOR
1010 ! POSSIBLE DECOMP OF UPPER HESS MATRIX INTO SUBMATRICES OF LOWER ORDER IS INDICATED IN
1020 ! ARRAY L( ). DECOMP. OCCURS WHEN SOME SUBDIAG. ELEMENTS ARE IN MODULUS <E0.
1030 ! THIS DIMINISHES EIGENVECTOR WORK
1040 J=N
1050 I=1
1060 L(1)=1
1070 IF J=1 THEN 1150
1080 IF ABS(S(J-1))>E0 THEN 1110
1090 I=I+1
1100 L(I)=0
1110 J=J-1
1120 L(I)=L(I)+1
1130 IF J<>1 THEN 1080
1140 REM EIGENVECTOR PROBLEM
1150 K4=1
1160 K0=0
1170 L4=L(1)
1180 M=N
1190 FOR I4=1 TO N
1200 I0=N-I4+1
1210 IF I4<=L4 THEN 1250
1220 K4=K4+1
1230 M=N-L4
1240 L4=L4+L(K4)
1250 IF Q(I0)=0 THEN 1440
1260 IF I(I0)<>0 THEN 1390
1270 ! TRANSFER UPPER-HESS MAT OF ORDER M FROM ARRAYS H AND S INTO A
1280 FOR K1=1 TO M
1290 FOR L1=K1 TO M
1300 A(K1,L1)=H(K1,L1)
1310 NEXT L1
1320 IF K1=1 THEN 1340
1330 A(K1,K1-1)=S(K1-1)
1340 NEXT K1
1350 ! COMPUTATION OF REAL EIGENVECTOR I0 OF UPPER-HESS MATRIX CORRESP. TO EIGENVALUE R(I0)
1360 GOSUB 4860 ! CALL REALVE
1370 GOTO 1440
1380 ! COMPUTATION OF COMPLEX EIGENVECTOR I0 OF UPPER-HESS CORRESP. TO COMPLEX EIGENVALUE W(I0)
1390 IF K0<>0 THEN 1430
1400 K0=1
1410 GOSUB 5960 ! CALL COMPVE
1420 GOTO 1440
1430 K0=0
1440 NEXT I4
1450 ! RECONSTRUCTION OF MATRIX USED IN REDUCTION OF MATRIX A TO UPPER-HESS FORM BY HOUSEHOLDER
1460 ! METHOD
1470 MAT A=IDN
1480 IF N<=2 THEN 1640
1490 M=N-2
1500 FOR K=1 TO M
1510 L=K+1
1520 FOR J=2 TO N
1530 D1=0
1540 FOR I=L TO N
1550 D2=H(I,K)
1560 D1=D1+D2*A(J,I)
1570 NEXT I
1580 FOR I=L TO N
1590 A(J,I)=A(J,I)-H(I,K)*D1
1600 NEXT I
1610 NEXT J
1620 NEXT K
1630 ! COMPUTATION OF EIGENVECTORS OF ORIGINAL NON-SCALED MATRIX
1640 K0=1
1650 FOR I=1 TO N
1660 I8=Q(I)-1
1670 IF I8<0 THEN 2240
1680 L=0
1690 IF I(I)=0 THEN 1740
1700 L=1
1710 IF K0=0 THEN 1740
1720 K0=0
1730 GOTO 2240
1740 IF I8<0 THEN 2240
1750 IF I8>0 THEN 1780
1760 IF L=0 THEN 2000
1770 IF L<>0 THEN 2190
1780 FOR J=1 TO N
1790 D1=0 @ D2=0
1800 FOR K=1 TO N
1810 D3=A(J,K)
1820 D1=D1+D3*V(K,I)
1830 IF L=0 THEN 1850
1840 D2=D2+D3*V(K,I-1)
1850 NEXT K
1860 W(J)=D1/F(J)
1870 IF L=0 THEN 1890

```

```

1880 S(J)=D2/F(J)
1890 NEXT J
1900 ! NORMALIZATION OF EIGENVECTORS AND COMPUTATION OF ORIGINAL NONNORM MATRIX
1910 IF L=1 THEN 2020
1920 D1=0
1930 FOR M=1 TO N
1940 D1=D1+W(M)^2
1950 NEXT M
1960 D1=SQR(D1)
1970 FOR M=1 TO N
1980 H(M,I)=0 @ V(M,I)=W(M)/D1
1990 NEXT M
2000 R(I)=R(I)*E2
2010 GOTO 2240
2020 R=0
2030 FOR J=1 TO N
2040 R1=W(J)^2+S(J)^2
2050 IF R>R1 THEN 2080
2060 R=R1
2070 L=J
2080 NEXT J
2090 D3=W(L)
2100 R1=S(L)
2110 FOR J=1 TO N
2120 D1=W(J)
2130 D2=S(J)
2140 V(J,I)=(D1*D3+D2*R1)/R
2150 H(J,I)=(D2*D3-D1*R1)/R
2160 V(J,I-1)=V(J,I)
2170 H(J,I-1)=-H(J,I)
2180 NEXT J
2190 K0=1
2200 R(I)=R(I)*E2
2210 R(I-1)=R(I)
2220 I(I)=I(I)*E2
2230 I(I-1)=-I(I)
2240 NEXT I
2250 RETURN ! FROM SUBROUTINE EIGENF
2260 MAT H=A ! SUBROUTINE SCALE
2270 MAT F=(1)
2280 B1=.75
2290 B2=1.33
2300 I1=0
2310 C1=0
2320 FOR I=1 TO N
2330 C2=0
2340 C3=0
2350 FOR J=1 TO N
2360 IF I=J THEN 2390
2370 C2=C2+ABS(A(J,I))
2380 C3=C3+ABS(A(I,J))
2390 NEXT J
2400 IF C2=0 THEN 2450
2410 IF C3=0 THEN 2450
2420 Q=C2/C3
2430 IF Q<B1 THEN 2470
2440 IF Q>B2 THEN 2470

```

```

2450 C1=C1+1
2460 GOTO 2540
2470 F1=SQR(Q)
2480 FOR J=1 TO N
2490 IF I=J THEN 2520
2500 A(I,J)=A(I,J)*F1
2510 A(J,I)=A(J,I)/F1
2520 NEXT J
2530 F(I)=F(I)*F1
2540 NEXT I
2550 I1=I1+1
2560 IF I1>30 THEN 2700
2570 IF C1<N THEN 2310
2580 F2=0
2590 FOR I=1 TO N
2600 FOR J=1 TO N
2610 IF I=J THEN 2630
2620 A(I,J)=H(I,J)*F(I)/F(J)
2630 Q=A(I,J)
2640 F2=F2+Q*Q
2650 NEXT J
2660 NEXT I
2670 MAT A=(1/F2)*A
2680 E2=F2
2690 RETURN ! FROM SUBROUTINE SCALE
2700 MAT A=H
2710 MAT F=(1)
2720 E2=1
2730 RETURN ! FROM SUBROUTINE SCALE
2740 ! SUBROUTINE HESQR
2750 IF N>2 THEN 2790
2760 IF N<2 THEN 3360
2770 S(1)=A(2,1)
2780 GOTO 3360
2790 M=N-2
2800 FOR K=1 TO M
2810 L=K+1
2820 S0=0
2830 FOR I=L TO N
2840 H(I,K)=A(I,K)
2850 S0=S0+ABS(A(I,K))
2860 NEXT I
2870 IF S0<>ABS(A(K+1,K)) THEN 2910
2880 S(K)=A(K+1,K)
2890 H(K+1,K)=0
2900 GOTO 3360
2910 S2=0
2920 FOR I=L TO N
2930 S1=A(I,K)
2940 S1=S1/S0
2950 A(I,K)=S1
2960 S2=S2+S1*S1
2970 NEXT I
2980 S1=SQR(S2)
2990 IF A(L,K)<0 THEN 3010
3000 S1=-S1
3010 S2=S2-S1*A(L,K)

```

```

3020 A(L,K)=A(L,K)-S1
3030 H(L,K)=H(L,K)-S1*S0
3040 S(K)=S1*S0
3050 X=S0*SQR(S2)
3060 FOR I=L TO N
3070 H(I,K)=H(I,K)/X
3080 S(I)=A(I,K)/S2
3090 NEXT I
3100 ! PREMULTIPLICATION BY MATR
IX PR
3110 FOR J=L TO N
3120 S1=0
3130 FOR I=L TO N
3140 S1=S1+A(I,K)*A(I,J)
3150 NEXT I
3160 FOR I=L TO N
3170 A(I,J)=A(I,J)-S(I)*S1
3180 NEXT I
3190 NEXT J
3200 ! POST MULTIPLICATION BY MA
TRIX PR
3210 FOR J=1 TO N
3220 S1=0
3230 FOR I=L TO N
3240 S1=S1+A(J,I)*A(I,K)
3250 NEXT I
3260 FOR I=L TO N
3270 A(J,I)=A(J,I)-S(I)*S1
3280 NEXT I
3290 NEXT J
3300 NEXT K
3310 FOR K=1 TO M
3320 A(K+1,K)=S(K)
3330 NEXT K
3340 ! TRANSFER UPPER HALF OF MA
TRIX A TO ARRAY H AND CALCUL
ATION OF SMALL NO. E0
3350 S(N-1)=A(N,N-1)
3360 E0=0
3370 FOR K=1 TO N
3380 Q(K)=0
3390 IF K<>N THEN E0=E0+S(K)^2
3400 FOR I=K TO N
3410 H(K,I)=A(K,I)
3420 E0=E0+A(K,I)^2
3430 NEXT I
3440 NEXT K
3450 E0=E3*SQR(E0)
3460 ! QR ITERATIVE PROCESS. UPP
ER-HESS MATRIX H IS REDUCED
TO UPPER MODIFIED TRIANGUL
AR
3470 ! DETERMINATION OF SHIFT OF
ORIGIN FOR THE FIRST STEP
OF QR ITERATIVE PROCESS
3480 S3=A(N,N-1)
3490 IF N<=2 THEN S3=0
3500 IF A(N,N)<>0 THEN S3=0
3510 IF A(N-1,N)<>0 THEN S3=0
3520 IF A(N-1,N-1)<>0 THEN S3=0
3530 M=N
3540 N0=0
3550 M0=N*10
3560 ! TESTING IF UPPER HALF HES
S MATRIX =0. IF SO, QR PROC
ESS UNNECESSARY
3570 FOR I=2 TO N
3580 FOR K=I TO N
3590 IF A(I-1,K)<>0 THEN 3690
3600 NEXT K
3610 NEXT I
3620 FOR I=1 TO N
3630 Q(I)=1
3640 R(I)=A(I,I)
3650 I(K)=0
3660 NEXT I
3670 RETURN ! FROM SUBROUTINE HE
SOR
3680 ! START MAIN LOOP OF QR PRO
CESS IN HESQR
3690 K=M-1
3700 M1=K
3710 I=K
3720 ! FIND ANY DECOMPOSITIONS O
F THE MATRIX
3730 REM GOTO 4300 IF LAST SUBMA
T OF DECOMP OF ORDER 1
3740 REM GOTO 4360 IF LAST SUBMA
T OF DECOMP OF ORDER 2
3750 IF K=0 THEN 4580
3760 IF K<0 THEN RETURN
3770 IF ABS(A(M,K))<=E0 THEN 458
0
3780 IF M=2 THEN 4640
3790 I=I-1
3800 IF ABS(A(K,I))<=E0 THEN 383
0
3810 K=I
3820 IF K>1 THEN 3790
3830 IF K=M1 THEN 4640
3840 ! TRANSFORMATION OF MATRIX
OF ORDER >2
3850 S0=A(M,M)+A(M1,M1)+S3
3860 S1=A(M,M)*A(M1,M1)-A(M,M1)*
A(M1,M)+.25*S3*S3
3870 A(K+2,K)=0
3880 ! CALCULATE X1,Y1,Z1 FOR SU
BMATRIX OBTAINED BY DECOMP
3890 X=A(K,K)*(A(K,K)-S0)+A(K,K+
1)*A(K+1,K)+S1
3900 Y=A(K+1,K)*(A(K,K)+A(K+1,K+
1)-S0)
3910 R=ABS(X)+ABS(Y)
3920 IF R/E0-E0/E3>0 THEN 3960
3930 IF S3-A(M,M-1)=0 THEN 3960
3940 S3=A(M,M-1)
3950 GOTO 3830
3960 Z=A(K+2,K+1)*A(K+1,K)
3970 S3=0
3980 N0=N0+1

```

```

3990 ! LOOP FOR ONE STEP OF QR P
      ROCESS
4000 FOR I=K TO M1
4010 IF I=K THEN 4080
4020 ! CALCULATE XR,YR,ZR
4030 X=A(I,I-1)
4040 Y=A(I+1,I-1)
4050 Z=0
4060 IF I+2>M THEN 4080
4070 Z=A(I+2,I-1)
4080 S2=ABS(X)+ABS(Y)+ABS(Z)
4090 IF S2=0 THEN 4130
4100 X=X/S2
4110 Y=Y/S2
4120 Z=Z/S2
4130 S0=SQR(X*X+Y*Y+Z*Z)
4140 IF X<0 THEN 4160
4150 S0=-S0
4160 IF I=K THEN 4180
4170 A(I,I-1)=S0*S2
4180 IF S2<>0 THEN 4200
4190 IF I+3>M THEN 4540 ELSE 451
      0
4200 S1=1-X/S0
4210 S0=X-S0
4220 X=Y/S0
4230 Y=Z/S0
4240 ! PREMULTIPLICATION BY MATR
      IX PR
4250 FOR J=I TO M
4260 S0=A(I,J)+A(I+1,J)*X
4270 IF I+2>M THEN 4290
4280 S0=S0+A(I+2,J)*Y
4290 S0=S0*S1
4300 A(I,J)=A(I,J)-S0
4310 A(I+1,J)=A(I+1,J)-S0*X
4320 IF I+2>M THEN 4340
4330 A(I+2,J)=A(I+2,J)-S0*Y
4340 NEXT J
4350 ! POST MULTIPLICATION BY MA
      TRIX PR
4360 L=I+2
4370 IF I<M1 THEN 4390
4380 L=M
4390 FOR J=K TO L
4400 S0=A(J,I)+A(J,I+1)*X
4410 IF I+2>M THEN 4430
4420 S0=S0+A(J,I+2)*Y
4430 S0=S0*S1
4440 A(J,I)=A(J,I)-S0
4450 A(J,I+1)=A(J,I+1)-S0*X
4460 IF I+2>M THEN 4480
4470 A(J,I+2)=A(J,I+2)-S0*Y
4480 NEXT J
4490 IF I+3>M THEN 4540
4500 S0=-A(I+3,I+2)*Y*S1
4510 A(I+3,I)=S0
4520 A(I+3,I+1)=S0*X
4530 A(I+3,I+2)=S0*Y+A(I+3,I+2)
4540 NEXT I

```

```

4550 IF N0>M0 THEN 4840
4560 GOTO 3690
4570 ! COMPUTE THE LAST EIGENVAL
      UE
4580 R(M)=A(M,M)
4590 I(M)=0
4600 Q(M)=1
4610 M=K
4620 GOTO 3690
4630 ! COMPUTE EIGENVALUES OF LA
      ST 2X2 MATRIX OBTAINED BY D
      ECOMPOSITION
4640 R=.5*(A(K,K)+A(M,M))
4650 S0=.5*(A(M,M)-A(K,K))
4660 S0=S0*S0+A(K,M)*A(M,K)
4670 Q(K)=1
4680 Q(M)=1
4690 IF S0<0 THEN 4770
4700 T0=SQR(S0)
4710 R(K)=R-T0
4720 R(M)=R+T0
4730 I(K)=0
4740 I(M)=0
4750 M=M-2
4760 GOTO 3690
4770 T0=SQR(-S0)
4780 R(K)=R
4790 I(K)=T0
4800 R(M)=R
4810 I(M)=-T0
4820 M=M-2
4830 GOTO 3690
4840 RETURN ! FROM SUBROUTINE HE
      SQ
4850 ! END OF SUBROUTINE HESQR
4860 ! SUBROUTINE REALVE
4870 W(1,I0)=1
4880 IF M=1 THEN 5890
4890 E1=R(I0)
4900 IF I0=M THEN 4990
4910 K=I0+1
4920 R=0
4930 FOR I=K TO M
4940 IF E1<>R(I) THEN 4970
4950 IF I(I)<>0 THEN 4970
4960 R=R+3
4970 NEXT I
4980 E1=E1+R*E3
4990 FOR K=1 TO M
5000 A(K,K)=A(K,K)-E1
5010 NEXT K
5020 ! GAUSSIAN ELIMINATION OF U
      PPER-HESS MATRIX A. ALL ROW
      CHANGES ARE INDICATED IN T
      HE ARRAY J
5030 ! ALL MULTIPLIERS ARE SAVED
      AS SUBDIAGONAL ELEMENTS OF
      A.
5040 K=M-1
5050 FOR I=1 TO K

```

```

5060 L=I+1
5070 J(I)=0
5080 IF A(I+1,I) <> 0 THEN 5120
5090 IF A(I,I) <> 0 THEN 5240
5100 A(I,I)=E0
5110 GOTO 5240
5120 IF ABS(A(I,I)) >= ABS(A(I+1,I)) THEN 5190
5130 J(I)=1
5140 FOR J=I TO M
5150 R=A(I,J)
5160 A(I,J)=A(I+1,J)
5170 A(I+1,J)=R
5180 NEXT J
5190 R=-A(I+1,I)/A(I,I)
5200 A(I+1,I)=R
5210 FOR J=L TO M
5220 A(I+1,J)=A(I+1,J)+R*A(I,J)
5230 NEXT J
5240 NEXT I
5250 IF A(M,M) <> 0 THEN 5280
5260 A(M,M)=E0
5270 ! VECTOR (1,1,...,1) IS STORED IN RIGHT HAND COLUMN VECTOR
5280 FOR I=1 TO M
5290 IF I > M THEN W(I)=0 ELSE W(I)=1
5300 NEXT I
5310 ! INVERSE ITERATION IS PERFORMED ON MATRIX UNTIL INFINITE NORM ON RIGHT HAND VECTOR > BOUND
5320 ! = .01/(N*E3)
5330 B3=.01/(N*E3)
5340 N0=0
5350 I1=1
5360 ! BACK SUBSTITUTION
5370 R=0
5380 FOR I=1 TO M
5390 J=M-I+1
5400 S0=W(J)
5410 IF J=M THEN 5470
5420 L=J+1
5430 FOR K=L TO M
5440 S1=W(K)
5450 S0=S0-S1*A(J,K)
5460 NEXT K
5470 W(J)=S0/A(J,J)
5480 T0=ABS(W(J))
5490 IF R >= T0 THEN 5510
5500 R=T0
5510 NEXT I
5520 ! COMPUTATION OF RIGHT HAND SIDE VECTOR FOR NEW ITERATION STEP
5530 FOR I=1 TO M
5540 W(I)=W(I)/R
5550 NEXT I
5560 ! TEST FOR CONVERGENCE--SEE SOURCE
5570 R1=0
5580 FOR I=1 TO M
5590 T0=0
5600 FOR J=I TO M
5610 T0=T0+A(I,J)*W(J)
5620 NEXT J
5630 T0=ABS(T0)
5640 IF R1 >= T0 THEN 5660
5650 R1=T0
5660 NEXT I
5670 IF I1=1 THEN 5690
5680 IF P0 <= R1 THEN 5890
5690 FOR I=1 TO M
5700 W(I,I0)=W(I)
5710 NEXT I
5720 P0=R1
5730 IF N0=1 THEN 5890
5740 IF I1 > 6 THEN 5900
5750 I1=I1+1
5760 IF R < B3 THEN 5790
5770 N0=1
5780 ! GAUSSIAN ELIMINATION OF RIGHT HAND SIDE VECTOR
5790 K=M-1
5800 FOR I=1 TO K
5810 R=W(I+1)
5820 IF J(I)=0 THEN 5860
5830 W(I+1)=W(I)+W(I+1)*A(I+1,I)
5840 W(I)=R
5850 GOTO 5870
5860 W(I+1)=W(I+1)+W(I)*A(I+1,I)
5870 NEXT I
5880 GOTO 5370
5890 Q(I0)=2
5900 IF M=N THEN 5950
5910 J=M+1
5920 FOR I=J TO N
5930 W(I,I0)=0
5940 NEXT I
5950 RETURN ! FROM REALVE
5960 ! SUBROUTINE COMPVE
5970 F4=R(I0)
5980 E4=I(I0)
5990 ! MODIFICATION OF EIGENVALUE IF MORE EIGENVALUES ARE EQUAL
6000 IF I0=M THEN 6120
6010 K=I0+1
6020 R=0
6030 FOR I=K TO M
6040 IF F4 <> R(I) THEN 6070
6050 IF ABS(E4) <> ABS(I(I)) THEN 6070
6060 R=R+3
6070 NEXT I
6080 R=R*E3
6090 F4=F4+R
6100 E4=E4+R
6110 ! MATRIX ((H-F4*I)*(H-F4*I)+(E4*E4*I)

```

```

6120 R=F4^2+E4^2
6130 S0=2*F4
6140 L=M-1
6150 FOR I=1 TO M
6160 FOR J=1 TO M
6170 D=0
6180 A(J,I)=0
6190 FOR K=I TO J
6200 D=D+H(I,K)*H(K,J)
6210 NEXT K
6220 A(I,J)=D-S0*H(I,J)
6230 NEXT J
6240 A(I,I)=A(I,I)+R
6250 NEXT I
6260 FOR I=1 TO L
6270 R=S(I)
6280 A(I+1,I)=-S0*R
6290 I2=I+1
6300 FOR J=1 TO I2
6310 A(J,I)=A(J,I)+R*H(J,I+1)
6320 NEXT J
6330 IF I=1 THEN 6350
6340 A(I+1,I-1)=R*S(I-1)
6350 FOR J=I TO M
6360 A(I+1,J)=A(I+1,J)+R*H(I,J)
6370 NEXT J
6380 NEXT I
6390 ! GAUSSIAN ELIMINATION OF M
MATRIX ((H-F4*I)*(H-F4*I)+(E
4^2)*I) IN ARRAY A.
6400 ! ROW INTERCHANGES THAT OCC
UR, INDICATED IN ARRAY J.
6410 ! ALL MULTIPLIERS USED ARE
STORED IN FIRST AND SECOND
DIAGONAL OF A
6420 K=M-1
6430 FOR I=1 TO K
6440 I2=I+1
6450 I3=I+2
6460 J(I)=0
6470 IF I=K THEN 6490
6480 IF A(I+2,I) <> 0 THEN 6530
6490 IF A(I+1,I) <> 0 THEN 6530
6500 IF A(I,I) <> 0 THEN 6760
6510 A(I,I)=E0
6520 GOTO 6760
6530 IF I=K THEN 6590
6540 IF ABS(A(I+1,I)) >= ABS(A(I+2
,I)) THEN 6590
6550 IF ABS(A(I,I)) >= ABS(A(I+2,I
)) THEN 6690
6560 L=I+2
6570 J(I)=2
6580 GOTO 6620
6590 IF ABS(A(I,I)) >= ABS(A(I+1,I
)) THEN 6670
6600 L=I+1
6610 J(I)=1
6620 FOR J=1 TO M
6630 R=A(I,J)
6640 A(I,J)=A(L,J)
6650 A(L,J)=R
6660 NEXT J
6670 IF I <> K THEN 6690
6680 I3=I2
6690 FOR L=I2 TO I3
6700 R=-A(L,I)/A(I,I)
6710 A(L,I)=R
6720 FOR J=I2 TO M
6730 A(L,J)=A(L,J)+R*A(I,J)
6740 NEXT J
6750 NEXT L
6760 NEXT I
6770 IF A(M,M) <> 0 THEN 6810
6780 A(M,M)=E0
6790 ! VECTOR (1,1,...,1) STORED
IN RIGHT-HAND SIDE VECTORS
V(I,I0)&V(I,I0-1) REPRESEN
TING
6800 ! COMPLEX RIGHT-HAND SIDE V
ECTORS
6810 FOR I=1 TO N
6820 IF I > M THEN 6860
6830 V(I,I0)=1
6840 V(I,I0-1)=1
6850 GOTO 6880
6860 V(I,I0)=0
6870 V(I,I0-1)=0
6880 NEXT I
6890 ! INVERSE ITERATION PERFORM
ED ON THE MATRIX UNTIL INFI
NITE NORM OF RIGHT-HAND SID
E VECTOR
6900 ! IS GREATER THAN BOUND=.01
/(N*E3)
6910 B3=.01/(N*E3)
6920 N0=0
6930 I1=1
6940 FOR I=1 TO M
6950 W(I)=H(I,I)-F4
6960 NEXT I
6970 ! SEQUENCE OF COMPLEX VECTO
RS Z(S)=P(S)+I*Q(S) & W(S+1
)=V(S+1)+I*U(S+1) GIVEN BY
RELATIONS
6980 REM (A-(F4-I*E4)*I)*W(S+1)=
Z(S) & Z(S+1)=W(S+1)/MAX(W
S+1))
6990 ! THE FINAL W(S) TAKEN AS C
OMPUTED EIGENVECTOR
7000 ! COMPUTATION OF RIGHT-HAND
SIDE VECTOR (A-F4*I)*P(S)-
E4*Q(S). A IS UPPER-HESS MA
TRIX.
7010 FOR I=1 TO M
7020 D=W(I)*V(I,I0)
7030 IF I=1 THEN 7050
7040 D=D+S(I-1)*V(I-1,I0)
7050 L=I+1
7060 IF L > M THEN 7100

```

```

8010 CLEAR @ PRINT
8020 IMAGE MD.DDDE,2X,"I",SD.DDD
      E
8030 MAT A=Z
8040 FOR I=1 TO N
8050 PRINT "EigenVALUE #",I,":"
8060 PRINT USING 8020 ; R(I),I(
      )
8070 PRINT
8080 PRINT "EigenVECTOR:"
8090 PRINT
8100 FOR J=1 TO N
8110 PRINT USING 8020 ; W(J,I),H
      (J,I)
8120 NEXT J
8130 PRINT
8140 PRINT "[A]v(I):"
8150 FOR J=1 TO N
8160 R=0 @ C=0
8170 FOR K=1 TO N
8180 R=R+A(J,K)*W(K,I)
8190 C=C+A(J,K)*H(K,I)
8200 NEXT K
8210 PRINT USING 8020 ; R,C
8220 F(I)=R @ Q(I)=C
8230 NEXT J
8240 PRINT
8250 PRINT "L(I)*v(I):"
8260 FOR K=1 TO N
8270 D(I)=R(I)*W(K,I)-I(I)*H(K,I
      )
8280 E(I)=R(I)*H(K,I)+I(I)*W(K,I
      )
8290 PRINT USING 8020 ; D(I),E(I
      )
8300 NEXT K
8310 PRINT
8320 FOR J=1 TO N
8330 M=R(J)*R(J)+I(J)*I(J)
8340 IF ABS(F(J)-D(J))>.001*M TH
      EN 8370
8350 IF ABS(Q(J)-E(J))>.001*M TH
      EN 8370
8360 GOTO 8380
8370 PRINT "Error at EigenVALUE
      #";I
8380 NEXT I
8390 CLEAR @ PRINT @ BEEP
8400 DISP "Insert CASSETTE for V
      ECTORS."
8410 DISP "It must be set to REC
      ORD."
8420 DISP
8430 DISP "Type: CREATE 'name--'
      ,2*N,8*N"
8440 DISP "where N is order of m
      atrix,e.g.4"
8450 DISP "Press CONT when ready
      "
8460 PAUSE

```

For each eigenvalue

and the corresponding eigenvector

Check that the basic equation defining the eigenvalue/vector problem is true: compare matrix times eigenvector

with eigenvalue times eigenvector

If not nearly equal, indicate an error.

Load cassette to dump eigenvector to a file.

```

8470 CLEAR @ PRINT
8480 DISP "Enter FILE NAME:"
8490 DISP "( 1-6 characters )"
8500 INPUT F#
8510 PRINT "VECTOR File Name:":F
    #
8520 CLEAR @ PRINT
8530 ASSIGN# 2 TO F#
8540 FOR J=1 TO N
8550 FOR I=1 TO N
8560 D(I)=V(I,J)
8570 NEXT I
8580 PRINT# 2,J ; D()
8590 NEXT J
8600 FOR J=N+1 TO 2*N
8610 FOR I=1 TO N
8620 D(I)=H(I,J-N)
8630 NEXT I
8640 PRINT# 2,J ; D()
8650 NEXT J
8660 ASSIGN# 2 TO *
8670 BEEP @ PRINT @ PRINT "END"
8680 DISP "END"
8690 END

```

Save column eigenvector (real part)
on a file record

Save column eigenvector (imaginary part)
on a file record.

Stop.

Appendix C. Software to Calculate Termination Parameters

An annotated copy of the program CTIMEP described in the text, follows. It occupies 2,946 bytes of memory.

PROGRAM NAME: CTIMEP

```
110 OPTION BASE 1
116 DEG
120 DIM D(4),V(4,4),H(4,4),Q(4),
    P(4,8)
125 DIM C(4,8),R(4,8)
130 DISP "Insert 'VCTRod' cartri
    dae."
140 DISP
150 DISP "Enter FILE NAME:"
160 INPUT F#
170 PRINT "VCTR file name: ";F#
180 ASSIGN# 1 TO F#
190 FOR J=1 TO 4
200 READ# 1,J ; D()
210 FOR I=1 TO 4
220 V(I,J)=D(I)
230 NEXT I
240 NEXT J
250 FOR J=5 TO 8
260 READ# 1,J ; D()
270 FOR I=1 TO 4
280 H(I,J-4)=D(I)
290 NEXT I
300 NEXT J
305 ASSIGN# 1 TO *
310 CLEAR @ PRINT
315 IMAGE MD.DDDE,2X,"1",SD.DDDE
320 PRINT "EigenVECTORS:"
330 PRINT
340 FOR J=1 TO 4
350 PRINT "EigenVECTOR #";J
360 PRINT
370 FOR I=1 TO 4
380 PRINT USING 315 ; V(I,J),H(I
    ,J)
390 NEXT I
395 PRINT
400 NEXT J
402 MAT V=TRN(V)
404 MAT H=TRN(H)
410 PRINT @ CLEAR @ BEEP
420 DISP "Insert 'POWadd' cartri
    dae."
430 DISP
440 DISP "Enter FILE NAME:"
450 INPUT F#
460 PRINT "POWER file name: ";F#
470 ASSIGN# 1 TO F#
475 FOR RS=1 TO 8
480 READ# 1,RS ; Q()
500 PRINT "POWER vector:"
510 PRINT
520 FOR I=1 TO 4
530 PRINT Q(I)
535 P(I,RS)=Q(I)
540 NEXT I
545 NEXT RS
548 ASSIGN# 1 TO *
550 CLEAR @ PRINT
560 PRINT "[C]*[P]:"
```

Read in file containing calibration matrix $[C^t]$ column by column

Real part

Imaginary part

Print out Eigenvectors

Transpose $[C^t]$ to $[C]$

Read in file containing the matrices $[P]$ and $[P']$ column by column. Store internally in a 4x8 augmented matrix

Print each column

```

570 MAT R=V*P
580 MAT C=H*P
590 FOR J=1 TO 8
600 PRINT
610 FOR I=1 TO 4
630 PRINT USING 315 ; R(I,J),C(I
,J)
635 NEXT I
640 NEXT J
700 FOR I=1 TO 4
710 D=R(I,1)^2+C(I,1)^2
720 FOR J=1 TO 4
730 V=(R(I,1)*V(I,J)+C(I,1)*H(I
,J))/D
740 H=(R(I,1)*H(I,J)-C(I,1)*V(I
,J))/D
741 V(I,J)=V
742 H(I,J)=H
745 NEXT J
747 NEXT I
750 CLEAR @ PRINT
760 PRINT "NORMALIZED [C]*[P]:"
765 MAT R=V*P
766 MAT C=H*P
770 FOR J=1 TO 8
780 PRINT
790 FOR I=1 TO 4
800 PRINT USING 315 ; R(I,J),C(I
,J)
810 NEXT I
820 NEXT J
830 PRINT @ PRINT "MAG & PHASE:"
840 FOR J=1 TO 8
850 PRINT
860 FOR I=1 TO 4
870 D=R(I,J)^2+C(I,J)^2
880 A=ATN2(C(I,J),R(I,J))
890 PRINT USING 900 ; SQRT(D);A
900 IMAGE MD.DDDE,3X,SDDD.DD
910 NEXT I
920 NEXT J
930 PRINT "END"
9998 RAD
9999 END

```

Form matrices for real and imaginary parts of $[C]*[P \ \& \ P']$ where $[P \ \& \ P']$ is the augmented matrix.

Print results

Normalize $[C]$ by the method described in the text.

Print normalized complex results of $[C] * [P \ \& \ P']$ in cartesian form

Express normalized complex results in polar form.

Appendix D. Energy Conservation in the QUOSM

There are no particularly significant occurrences of absorption within the QUOSM, except when the quasi-optical attenuators are used. In the simulations actually made absorption was neglected. In this case and in the steady state, the source power entering the QUOSM must equal the sum of the powers leaving all of the QUOSM ports. The authors have occasionally noted discussions of Michelson interferometers in which it is argued that the power coming out of a particular port can exceed the input power for a particular path difference so long as the average over all path differences agrees with energy conservation. This is clearly nonsense since one could leave the instrument set at a particular path difference and get more power out than is put in. As described in the text, the simulation program written for the QUOSM was provided with the facility to check for energy conservation, and this was helpful in the identification and elimination of several errors during the development of the program.

One particularly interesting requirement in the simulation was exposed in this way; namely, that all partial reflections must be modeled with a certain degree of realism or else energy conservation will appear to fail. Partial reflection (and transmissions) occur at the beam splitters and at the interfaces between the QUOSM and the source and detector, and the key properties are the phase changes introduced at these surfaces. Chantry recognized this fact [see p.67 ref.18] and stated that what is required is for a π phase change to occur somewhere in the system. A more complete statement is given by the Stoke's relations [D1, D2] for a non-absorbing interface between non-absorbing media; namely, if t and r are the complex amplitude transmission and reflection coefficients for incidence on one side of the interface and t' and r' , for the other side, then

$$t t'^* = 1 - r r'^*$$

$$r' = -r$$

Provided these conditions are met, the expected energy conservation should occur in the system.

In the simulation program described elsewhere, the phase behavior of the Mylar film beam splitter was modeled in detail, following reference [18]. However, it is more difficult to specify and describe the source and detector interfaces in similar detail, and so a simplification has been made, one which satisfies the above Stokes' relations. In both cases, all phase shifts at the interface are set equal to zero with this exception: the waves travelling from the principal beam splitter toward the source or detector ports are shifted by π at the interface when they are reflected. Although such details are important in the matter of energy conservation, they have a trivial effect on the standing wave patterns, and thus there is no loss of generality in such an oversimplification. In the simulations of the QUOSM which have been described, the operator controls the remaining significant parameters of the detector and source interfaces, their power reflectance values, and thereby establishes the magnitude of the standing wave effects.

References for Appendix D

- D1. G.G. Stokes, Mathematical and Physical Papers, Vol. II, New York: Johnson Reprint Corp., pp. 89-103 (1966).
- D2. E.Hecht and A. Zajac, Optics, Reading, Massachusetts: Addison-Wesley Publishing Co., p.91ff (1974).
- 18. See reference list with main text.

FINAL REPORT
GT/PROJECT A-3233

**QUASI-OPTICAL SCANNING MULTIPOINT (QUOSM)
NETWORK ANALYZER:
SOLUTIONS TO THE PROBLEM OF STANDING WAVES**

By

R. A. Bohlander
A. McSweeney
V. T. Brady
R. G. Shackelford

Prepared for

U.S. ARMY MISSILE COMMAND
TMDE SUPPORT GROUP
REDSTONE ARSENAL, ALABAMA 35898

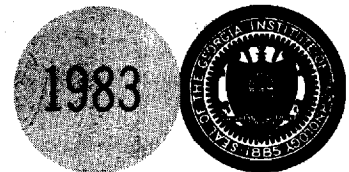
Under

Contract No. DAAH01-81-D-A003
Delivery Order No. 51

April 1983

GEORGIA INSTITUTE OF TECHNOLOGY

A Unit of the University System of Georgia
Engineering Experiment Station
Atlanta, Georgia 30332



QUasi-Optical Scanning Multiport (QUOSM)
Network Analyzer: Solutions to the
Problem of Standing Waves

R.A.Bohlander, A.McSweeney,
V.T.Brady, and R.G.Shackelford

FINAL REPORT

Contract No. DAAH01-81-D-A003
Delivery Order Number 51
(A-3233)

Prepared by
Engineering Experiment Station
Georgia Institute of Technology
Atlanta, Georgia 30332

Prepared for
U.S. Army Missile Command
TMDE Support Group
Redstone Arsenal, Alabama 35898

April 8, 1983

REPORT DOCUMENTATION PAGE		READ INSTRUCTIONS BEFORE COMPLETING FORM
1. REPORT NUMBER A-3233	2. GOVT ACCESSION NO.	3. RECIPIENT'S CATALOG NUMBER
4. TITLE (and Subtitle) Quasi-optical Scanning Multiport (QUOSM) Network Analyzer: Solutions to the Problem of Standing Waves		5. TYPE OF REPORT & PERIOD COVERED FINAL REPORT 21 Apr. 82 - 30 Nov. 82
		6. PERFORMING ORG. REPORT NUMBER A-3233
7. AUTHOR(s) R. A. Bohlander, A. McSweeney, V. T. Brady, and R. G. Shackelford		8. CONTRACT OR GRANT NUMBER(s) DAAH01-81-D-A003 Delivery Order No. 51
9. PERFORMING ORGANIZATION NAME AND ADDRESS Georgia Institute of Technology EES/EML/MMD Atlanta, Georgia 30332		10. PROGRAM ELEMENT, PROJECT, TASK AREA & WORK UNIT NUMBERS
11. CONTROLLING OFFICE NAME AND ADDRESS U.S. Army Missile Command TMDE Support Group Redstone Arsenal, Alabama 35898		12. REPORT DATE 8 Apr. 83
		13. NUMBER OF PAGES 92
14. MONITORING AGENCY NAME & ADDRESS (if different from Controlling Office)		15. SECURITY CLASS. (of this report) UNCLASSIFIED
		15a. DECLASSIFICATION/DOWNGRADING SCHEDULE
16. DISTRIBUTION STATEMENT (of this Report)		
17. DISTRIBUTION STATEMENT (of the abstract entered in Block 20, if different from Report)		
18. SUPPLEMENTARY NOTES		
19. KEY WORDS (Continue on reverse side if necessary and identify by block number) Network Analyzers Reflectometer Millimeter Wave Quasi-Optical Six-Ports		
20. ABSTRACT (Continue on reverse side if necessary and identify by block number) Advanced calibration and data analysis techniques have been developed to compensate for the effect of standing waves in a new type of millimeter wave reflectometer. This instrument, the Quasi-Optical Scanning Multiport, was developed under a previous contract to be an alternative to guided wave Six Port Network Analyzers and one which offers much greater facility at the high frequency end of the millimeter wave spectrum. The present work describes a calibration		

procedure adapted from use with six-ports that involves an eigen-vector analysis of detector readings with various calibration devices installed. The calibration devices required are a wave-guide load and short, a quasi-optical absorbing load, and a quasi-optical means of delaying signals to and from the test port. A computer simulation has been implemented to demonstrate that the technique works. Tests of pyroelectric detectors have also been made. Recommendations for future work are made.

Table of Contents

	<u>PAGE</u>
1.0 Introduction.....	1
1.1 Statement of Objectives.....	2
2.0 Correction for Standing Waves in Calibration Procedure.....	4
2.1 Introduction.....	4
2.2 Extension of the Phasor Representation to Include Standing Waves.....	10
2.3 Method Adapted from the Analysis of Six-Ports.....	16
2.4 Eigenvalue/vector Analysis.....	34
2.5 Simulation of QUOSM Signals.....	39
2.6 Simulated Calibration.....	47
3.0 Reduction of Standing Waves.....	57
3.1 Experiments with the Detector.....	57
3.2 Isolation by Attenuation.....	59
4.0 Status of Hardware and Software.....	61
5.0 Summary.....	63
6.0 Future Work.....	64
7.0 References.....	67
 Appendices	
A. Software to Simulate QUOSM Signals Including the Effects of Standing Waves.....	69
B. Software to Calculate Eigenvalues and Eigenvectors for Calibrating the QUOSM.....	76
C. Software to Calculate Termination Parameters.....	88
D. Energy Conservation in the QUOSM.....	91

LIST OF FIGURES

<u>FIGURE</u>		<u>PAGE</u>
2.1	Original QUOSM Design.....	5
2.2	Quasi-Optical Scanning Multiport (QUOSM) Network Analyzer.....	6
2.3	Vector Diagram of QUOSM Signals Without Standing Waves.....	8
2.4	Phasor Sum for Standing Wave Case.....	14
2.5	Six-Port Network.....	17
2.6	Calibration Device Required by Eigenvector Method.	22
2.7	Procedure for Calibration of Six-Port.....	24
2.8	Example of a Six-Port Reflectometer Circuit.....	27
2.9	Modified QUOSM Design.....	28
2.10	Emulation of Sliding Transmission Line for QUOSM..	30
2.11	Procedure for Calibration of QUOSM.....	33
2.12	Initial Optical Paths from Source and Detector....	40
2.13	Optical Paths from Beam Splitter to Mirror and Test Port.....	41
2.14	Optical Paths from Mirror and Test Port back to the Beam Splitter.....	42
2.15	Optical Paths back to Source and Detector.....	43
3.1	Type of Pyroelectric Detector Element Tested.....	58

LIST OF TABLES

<u>TABLE</u>		<u>PAGE</u>
2.1	List of Signal Paths.....	12
2.2	Parameters Used in Simulation of Standing Waves....	48
2.3	Test Port Parameters for Case of Standing Waves....	50
2.4	Test Port Parameters for Case of No Standing Waves.	52
2.5	Parameters for Test Port Delays Achieved with Dielectric Plates.....	54
2.6	Test Port Parameters With and Without Noise.....	55

1.0 Introduction

Under contract DAAH01-81-D-A003 delivery order number 51, the Engineering Experiment Station of Georgia Tech (GT/EES) has performed further work on a millimeter wave network analyzer based on quasi-optical rather than guided-wave techniques. An analyzer called a QUasi-Optical Scanning Multiport (QUOSM) was developed under a previous contract (DAAH01-80-C-1634), and the focus of the current work reported here is the development of advanced calibration and data analysis techniques. These address problems with internal standing waves that were found during the previous contract activities. Present results indicate that the problems have been largely overcome and that the QUOSM shows considerable promise. Further work on indicated hardware modifications and on obtaining new data will be recommended.

Automatic network analyzers based on guided-wave six-port circuits had been implemented down to millimeter wavelengths when work on a quasi-optical alternative was initiated under the previous contract. The QUOSM was designed to circumvent the difficulty of constructing guided-wave components, and the increased power losses in them at frequencies higher than 100 GHz. In addition, the four major advantages of automatic network analyzers have been preserved in the design of the QUOSM: (1) Both amplitude and relative phase information for power crossing the test interface are measured utilizing simple power detectors instead of more complex heterodyne systems. (2) Imperfections in the measurement system are found by calibration and are corrected numerically in treating the data. (3) The "circuit" is well-suited to automatic network analysis because it requires little, if any, tuning or modification for each interface to be tested. (4) The "circuit" covers a relatively wide frequency band when calibrated at each test frequency within the band. The working range of the QUOSM is intended to be 90 to 340 GHz with no changes in components within this range except for the need to

change the couplers to the source and to the test device when waveguide sizes change.

Work in the previous contract was divided into three phases:

1) The initial phase [1] culminated in a preliminary design of the QUOSM and included a study of its expected performance based on computer simulations.

2) The second phase of the work [2] consisted of the detailed design, procurement, and fabrication of the components.

3) The system was assembled, aligned, and tested in the third phase [3]. A computer program was written to perform the data acquisition and analysis based on the previous computer simulations.

During the course of testing the QUOSM performance, internal standing waves were discovered that were of such magnitude that the calibration and analysis procedures would have to be revised substantially in order to take them into account. On the basis of measurements made at that time, reasonable steps to reduce the magnitude of the standing wave phenomenon were suggested, but it was judged unlikely that the problem could be essentially eliminated in that way. Thus, consistent with the trend of most modern work on automatic network analyzers, the stress in the present work was on adjustments to the calibration and analysis procedures as a solution to the standing wave problem.

1.1 Statement of Objectives

In summary, the objectives under the present contract (DAAH01-81-D-A003 delivery order 51) were the following:

1. To develop a calibration procedure and an algorithm that corrects for standing wave effects in deriving the reflection properties of a device under test (DUT).
2. To reduce standing wave effects in the QUOSM since this may improve the accuracy afforded by the correction procedures.

3. To provide two horns that add the capability to test WR-10 devices with the QUOSM.
4. To demonstrate the use of the QUOSM on some trial test devices and to demonstrate the effect of flange reflections.

The first three objectives have been met, but the level of effort required to meet the first objective was greater than foreseen, and thus the fourth objective could not be met within the time and funds available. Recommendations for further work will be made in this report.

2.0 Correction for Standing Waves in Calibration Procedure

2.1 Introduction

The QUOSM was originally designed to be similar to the Michelson or Twyman-Green types of optical interferometers. These are generally described as "two-beam" interferometers from the fact that the principal beam splitter divides the beam from the source into two parts which are later recombined at the detector where some degree of interference between the two beams may be seen. The similarity between the QUOSM and these interferometers may be seen in Figure 2.1 in which the principal components are shown in relation to the path of the radiation.

A photograph of the actual system is given in Figure 2.2 and a brief review of the design will be given here. The reader is referred to previous reports [1-3] for more detailed descriptions and explanations. Radiation from a source such as a klystron is launched into the interferometer by the source horn. This in turn feeds a lens which forms a beam that has a Gaussian profile and a minimum lateral width on the principal beam splitter. The beam first falls on another beam splitter, however, that directs a small fraction of the power to a reference detector which was designed to provide a leveling signal to compensate for source fluctuations. Then the signal is split into two beams by the principal beamsplitter, one beam falling on a mirror which can be moved in precisely measured increments along the beam, thereby introducing delay, and another falling on a lens and horn pair which are identical to the source port and which serve as the test device and calibration port. Radiation reflected by a test device as well as that reflected by the movable mirror are recombined then at the principal beam splitter and continue on to a lens which focuses the radiation on the principal detector. The movable mirror and the test port components are designed and positioned such that there is complete symmetry of the Gaussian beam around its intersection with the principal beam splitter.

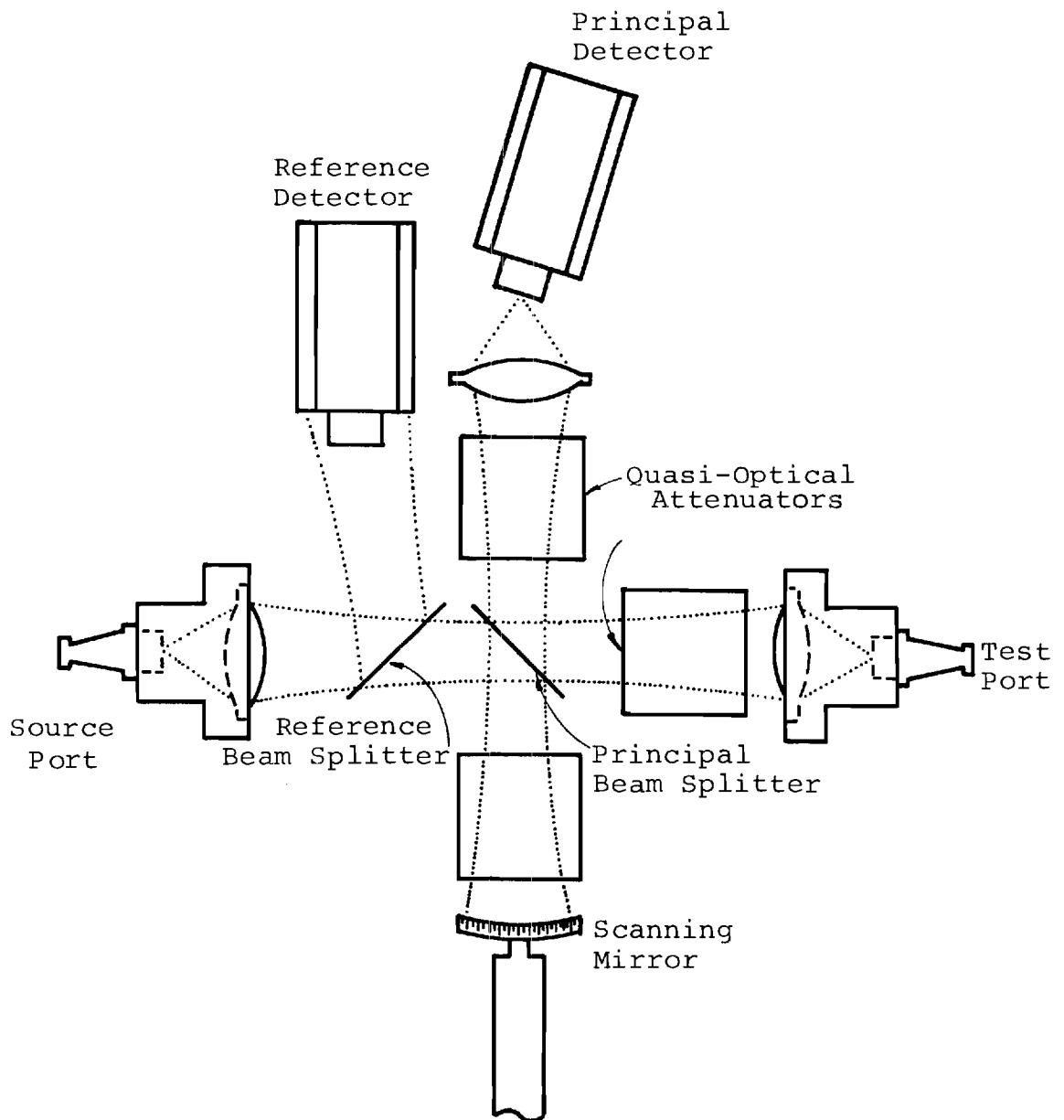
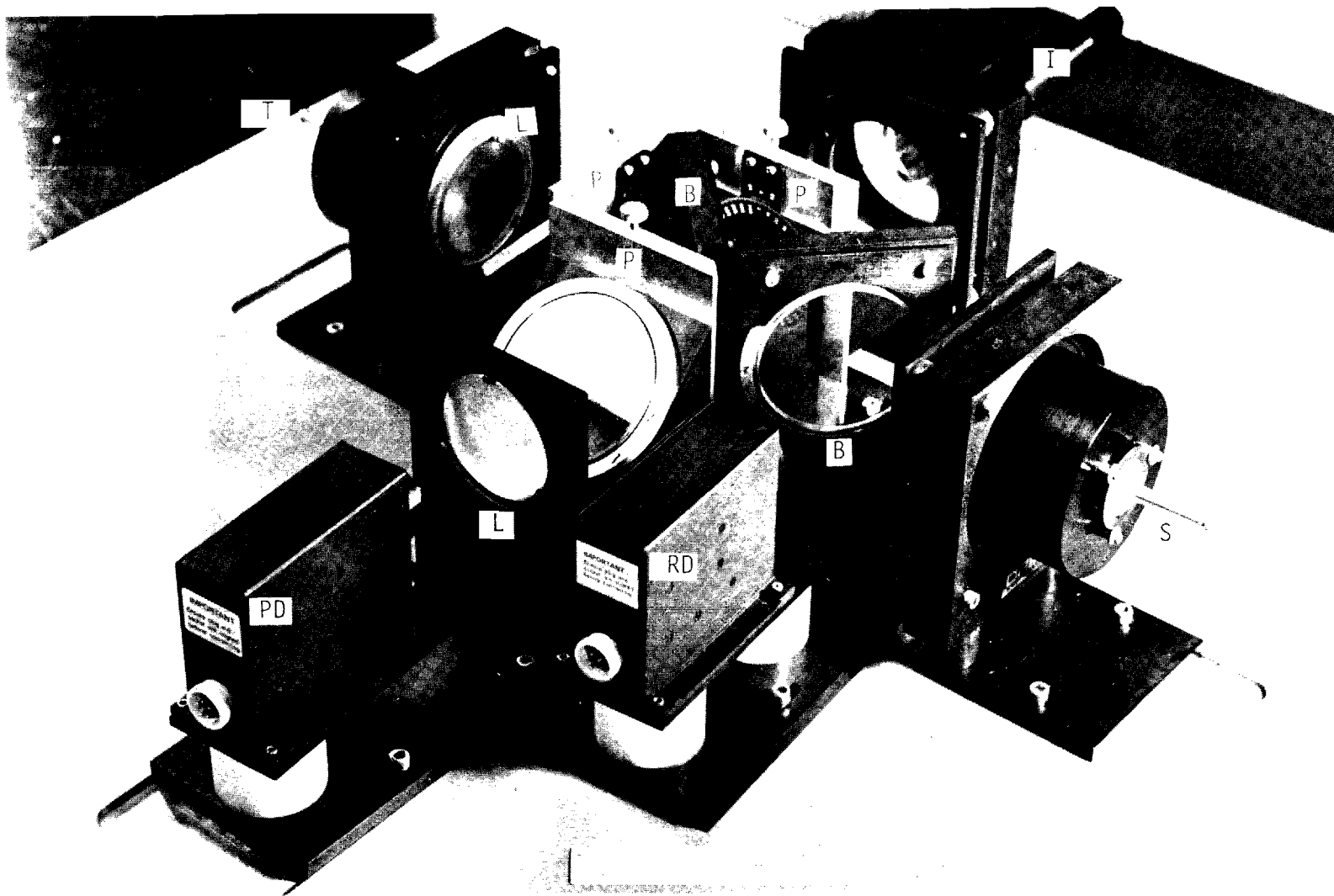


Figure 2.1 Original QUOSM Design.



9

Fig. 2.2 Quasi-Optical Scanning Multiport (QUOSM) Network Analyzer.
B = Beamsplitter, I = Inchworm, L = Lens
P = Polarizing beamsplitter, PD = Primary Detector,
RD = Reference Detector, S = Source horn, T = Test port

One may notice also that the beam passes through quasi-optical signal attenuators in the mirror, test port, and principal detector arms of the system and these are provided for such signal level adjustments as may be necessary and for some isolation capability, as will be discussed later. Both detectors are of the Golay cell type with 5mm diameter apertures fitted with crystal quartz windows and appropriate optical filters. As configured, they are sensitive to the entire frequency range 90 to 340 GHz required in the use of the QUOSM.

In a previous theoretical model of QUOSM performance [1], the signal arriving at the detector was assumed to be formed by the combination of three signals; namely, that reflected by the scanning mirror, that reflected by the lens-horn transition of the test port, and that reflected by the test device itself. The amplitudes and phases of these signals may be represented by phasor-type vectors, and the combined signal, as a vector sum as shown in Figure 2.3. The dashed line shows the loci of the tips of the detector phasor when the scanning mirror location is moved along the optical beam. This can be used to show that the resulting detector signal power will vary sinusoidally with linear motion of the scanning mirror, and have a period equal to half the source wavelength. Previous analysis showed how to find the phase of the signal reflected by the test port and the relative amplitudes of the signals from the test port and from the scanning mirror [1]. A least squares method was used to fit sinusoidal functions and to obtain the desired parameters. A null reflector (tapered load) was devised for a calibration at the test port that allows one to measure the reflection from the test port horn and lens and thus to separate this signal component from reflections by test devices themselves. The second calibration device is a near perfect reflector that is used as a standard for reflectivity and as a reference for phase.

An essential assumption for the above model to be correct is that the signals falling on the detector are completely absorbed,

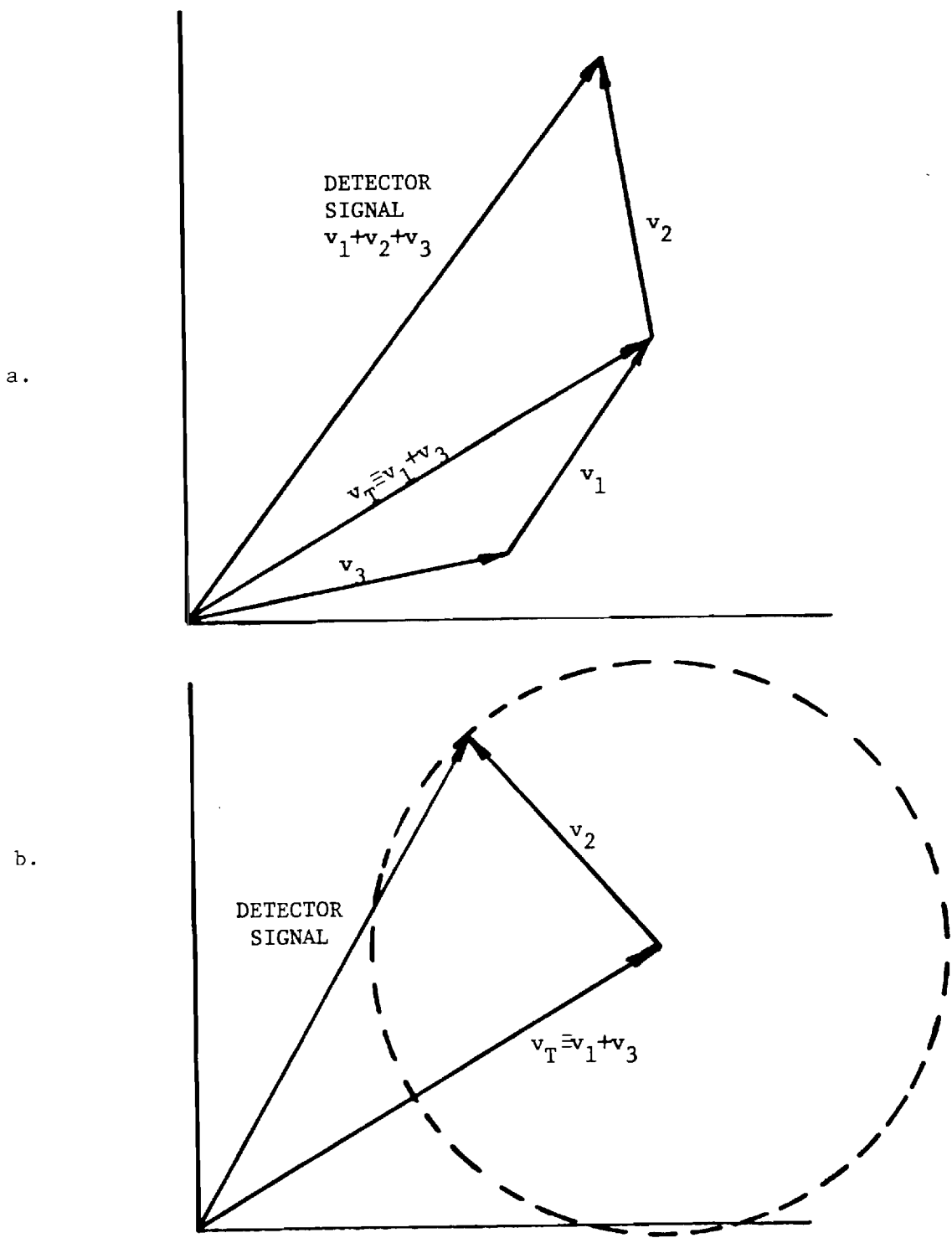


Figure 2.3a. Vector diagram of signals reaching the principal detector in QUOSM. Each vector represents a field strength so that the power reaching the detector is the square of the length of the vector marked "detector signal." The direction of each vector indicates signal phase. v_1 comes from the test port, v_2 from the scanning mirror and v_3 from the horn-lens at the test port. 2:35. The dashed line shows where the tip of vector v_2 lies for all possible positions of the scanning mirror. The tip of the vector representing the detector signal also lies on this circle.

or at least that any residual signal scattered or reflected by the detector does not reenter the interferometric portion of the QUOSM. Since some of the signals reflected by the test port and by the scanning mirror are also returned to the source port, there is a similar requirement that signals scattered by the source port not reenter the interferometric portion of the system. If these conditions are not met, electromagnetic energy is partly trapped between the ends of the four arms of the QUOSM (i.e., in the beams bounded by the source port, the test port, the scanning mirror, and the detector), and in this cavity-like system, standing waves are formed. In the final report of the previous contract activity [3], it was shown that reflections at the detector port were larger than expected and in particular that a tilt of the detector did not suppress the reflections as expected. Apparently, the metal surrounding the detector element acted somewhat like a retro-reflector in its reflection properties. It was demonstrated [3] that this did indeed produce standing waves; for, with the test port blocked by an absorber, one could still observe interference fringes when the scanning mirror was moved.

One approach to solving this problem, in principle, is to devise more thorough ways to suppress the standing waves. Consideration was given to various mechanisms but this was not chosen as the primary line of attack in the present work for several reasons. First, reliance for accuracy on the perfection of components in a network analyzer has been found to be unsatisfactory in general [4] and is contrary to current trends in metrology. Secondly, the problem is not necessarily isolated in just one component. Not only would an improved detector configuration be required, but it is also likely that something would need to be done to reduce back reflections from the lenses. Such a reduction over a wide frequency range, although tractable, is not a negligible undertaking. Moreover, although it could be argued in the particular case studied previously [3] that the

reflections from the detector port were more important than those from the source port, this would not necessarily be true for all frequencies. The beam splitter properties at frequencies other than 94 GHz could be such as to give more weight to the effects of the source port. Measurements of the reflectance of the source port have not been made, so this possible source of standing waves cannot be totally discounted. Since there were these difficulties and complications, the primary effort in the present contract was instead the investigation of ways to allow for the effects of standing waves through mathematical procedures in the analysis of the data and through revisions in the calibration procedures.

The following sections discuss the efficacy of two alternative analytical methods, one of which turned out to be successful. Later, some brief experiments are described that were aimed at whether the standing waves could be reduced in magnitude.

2.2 Extension of the Phasor Representation to Include Standing Waves

Once standing waves are introduced into the interferometric section of the QUOSM, the number of paths which radiation can follow and reach the detector becomes infinite. If the reflectance of the source port and detector port are both sufficiently low, one may argue that radiation which is reflected more than once by either one of these ports (or a combination of them) is too weak to be significant. Unfortunately it has been found that this approximation is not a good one given what are now believed to be reasonable values of the detector or source port reflectances. From modeling efforts which will be described later, it was found that a few multiple reflections generally were significant. Further close examinations of the detector signal obtained when the test port was blocked and the scanning

mirror moved, have suggested that multiple reflections were occurring. Since this is the case, it has been concluded that a meaningful phasor description of the signals in the QUOSM is completely unmanageable as a basis for calibration and analysis.

The reader may if he wishes skip the remainder of this section and proceed to Section 2.3 where a viable alternative is discussed. In the remainder of this section, a phasor description is discussed for the case in which the low detector and low source reflectance approximation mentioned above holds. This serves to show that even this first-order standing wave case is much more complicated than one would like since the number of paths by which radiation can reach the detector is considerably more than two, as shown by the list in Table 2.1.

Each signal path can be represented by a phasor that shows the amplitude and relative phase of the signal that reaches the detector; and then, as before, the net detector signal may be found from the squared modulus of the vector sum of the phasors. Intuitively, some simplification can be made by grouping the phasors as indicated in Table 2.1 and by forming the vector sum of the phasors in each group. There are two ideas behind this: (1) Clearly the paths like S-M-D-T-D and S-T-D-M-D are indistinguishable in terms of detector signal, and the sum is just twice the phasor for one of them. (2) Phasors that come from paths that differ only by whether the source (S) or the detector (D) acts as a partial reflector in the middle can be added without loss of generality. This second point is somewhat subtle. The radiation reflected by the detector and the source merges again when the two beams intersect at the beam splitter, and the final result is the same as if there had been one partial reflector with an effective complex reflectance which is a fixed linear combination of the complex reflectances of the source port and the detector port. This linear combination does not depend on the mirror position nor on the nature of the reflection at the test port, and thus at a given frequency it is constant and may

Table 2.1 List of Signal Paths Connecting the Source to the Detector in the QUOSM

Key

- S Source
- D Detector
- T Test Port
- M Scanning Mirror

Zero-Order Paths

S-M-D (means that radiation goes from the source to the mirror to the detector)

S-T-D

First-Order Paths Contributing to Standing Waves

S-M-D-M-D two reflections by the mirror

S-M-S-M-D

S-M-D-T-D one reflection each by the

S-M-S-T-D mirror and the test port

S-T-D-M-D

S-T-S-M-D

S-T-D-T-D two reflections by the

S-T-S-T-D test port

in principle be found by calibration. Therefore, in the case of first-order standing waves, one may represent the detector signal by forming the vector sum of five phasors, two which come from the zero-order paths, and three which come from the first-order groups in Table 2.1.

Even with these simplifications, the picture derived from the phasor sum is quite complicated, as is illustrated in Figure 2.4. The fixed vectors are those which involve only reflections by the test port. The remaining phasors involve reflections from the scanning mirror and will rotate when the mirror moves. The sum of vectors W_3 and W_4 rotates around the foot of W_3 , and the loci of the tips of the sum are on a dashed circle as shown. Finally the tip of signal W_5 moves on an epicycle shown as a dash-dot line in the figure. The squared modulus of the vector sum representing the detector signal can be decomposed into a sum of a constant plus two sinusoidal variations with mirror position, one with a period of half of a wavelength and one with a period of a quarter of a wavelength. This picture is further complicated by the fact that each signal component reflected by the test port, like those represented by W_1 , W_2 , and W_4 , is in reality the vector sum of a signal reflected by the test port horn-lens and one reflected by the test device.

The general method used previously [1] (for the case in which the QUOSM was assumed to have no standing waves) was to use a calibration load in place of the test device to reduce the number of vectors and make it possible to solve for the remaining ones by the least squares method. Then one was able to exchange the load for the test device and use the knowledge gained to solve for the magnitude and phase of the remaining vectors by further application of the least squares method. Since there are many more vectors in the diagram in Figure 2.4 than in Figure 2.3, it is fairly apparent that more calibration steps and devices would be needed to be able to decompose the detector signal into all the component vectors. A large absorber that could be placed

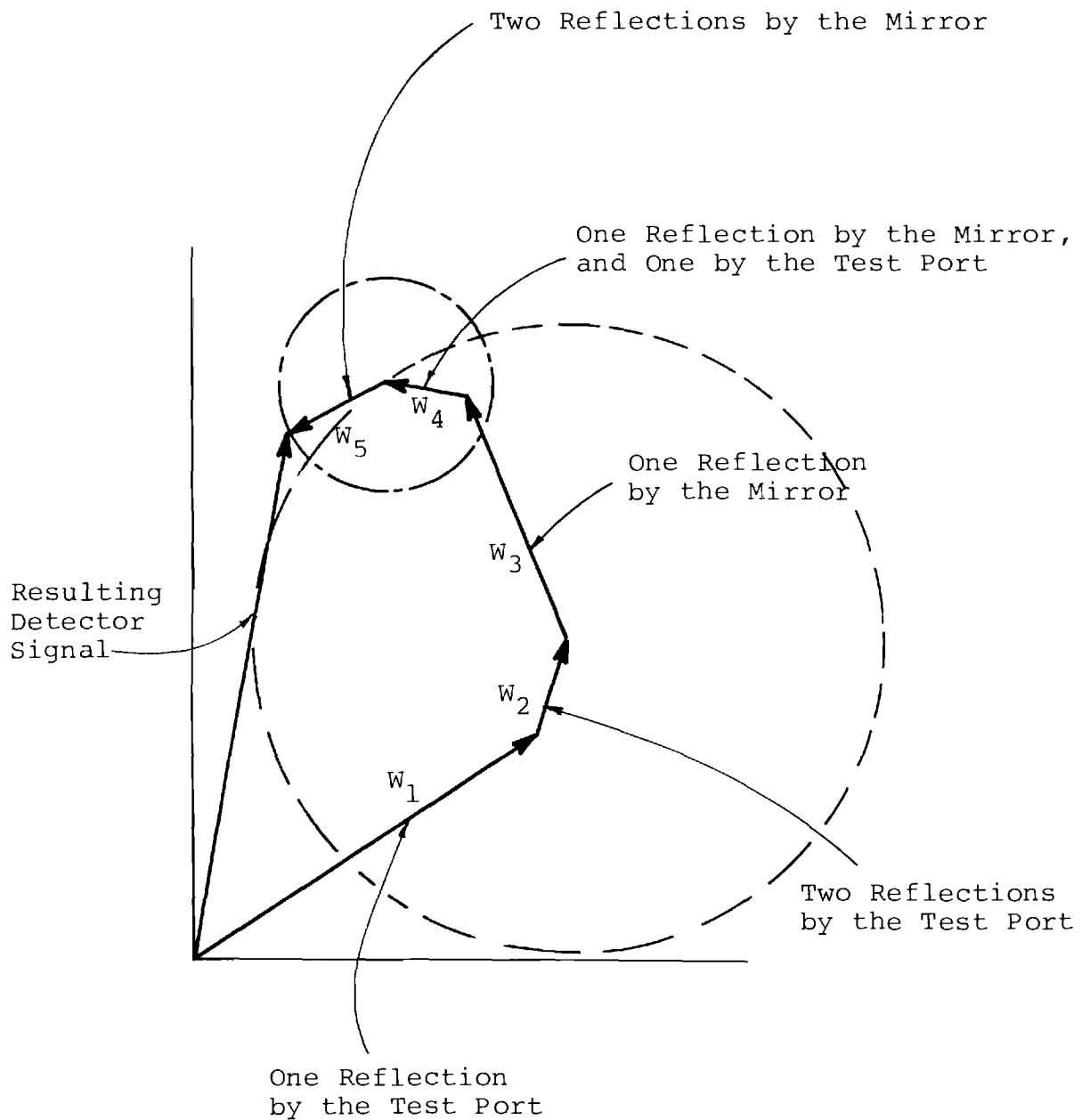


Figure 2.4 Phasor Sum for the Detector Signal in the First-order Standing Wave Case.

alternately in front of the test port and then in front of the scanning mirror would be helpful. However, absorbers alone will not be completely sufficient, since for example, no absorber can remove just one of a pair of signals like W_1 and W_2 , and some other type of calibration device would be needed.

Work on this phasor approach was halted at this point due to the evidence, discussed earlier, that more than one reflection from the detector or source port is likely to be significant. One can readily see from the foregoing discussion that the phasor analysis would be untractable in this case. An alternative method is much better suited, as it turns out, and is described in the following sections.

2.3 Method Adapted from the Analysis of Six-Ports

2.3.1 Review of Findings for Six-Ports

Present-day calibration and data reduction schemes used with six-port reflectometers are based on the concept of the scattering matrix [S]. A significant advantage of this approach compared with phasor analysis of multiport devices is that multiple reflections, and hence standing waves, are more easily handled. The complex S parameters in the matrix [S] relate traveling waves moving away from each port in terms of linear combinations of traveling waves incident upon every port [5], and multiple reflections are implicitly included in these linear combinations. One of the most effective schemes of analysis is that of Cronson and Susman [6,7] who developed an eigenvector analysis derived from scattering matrices for calibrating the single six-port reflectometer.

In the study reported on here, a closer analogy has been drawn between the QUOSM and the six-port reflectometer. From this it may be shown how the analytical tools developed by Cronson and Susman can be adapted to the calibration and reduction of data from a QUOSM regardless of whether or not there are standing waves present. This will be substantiated by simulations described later.

Before consideration is given to the analogy between the six-port reflectometer and the QUOSM, the work of Cronson and Susman on mathematical analyses of six-port reflectometers will be reviewed. Figure 2.5 represents a six-port network with source port (port 1), test port (port 2), and power measurement ports (ports 3-6). Note that port 3 monitors the power incident on the DUT at the test port. It is well known [8] that the wave amplitude incident on each of the four output power meters can be written as a linear combination of the complex scattering variables a and b at the test or measurement port. The complex

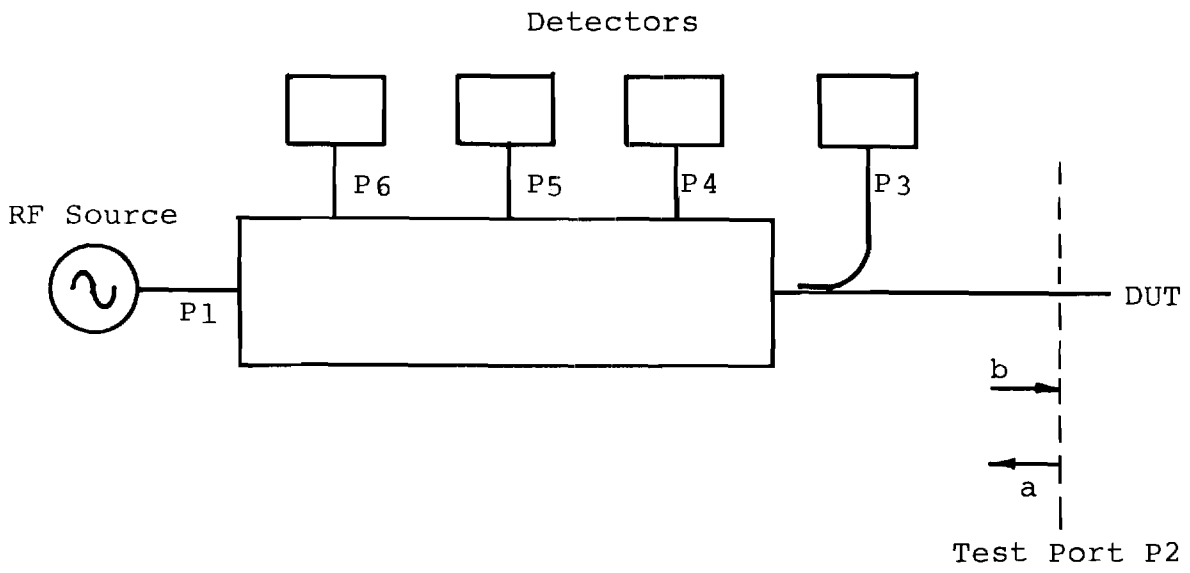


Figure 2.5 Six-port Network.

reflection coefficient at port 2 is defined as:

$$\Gamma = a/b \quad (1)$$

Thus, one may show that an unknown reflection coefficient can be found from four power measurements through the use of a matrix equation which will be given below. The output power at port i , P_i , is a linear combination of four complex quadratic variables: $|b|^2$, ab^* , a^*b , and $|a|^2$. The sets of four power readings and quadratic variables may be expressed as column matrices $[p]$ and $[b_q]$

$$[p] = \begin{bmatrix} p_3 \\ p_4 \\ p_5 \\ p_6 \end{bmatrix} \quad [b_q] = \begin{bmatrix} |b|^2 \\ ab^* \\ a^*b \\ |a|^2 \end{bmatrix}$$

and the matrix equation relating the two may be written as*

$$[p] = [C^{-1}] [b_q] \quad (2)$$

where $[C^{-1}]$ is a 4 by 4 complex matrix of proportionality constants. If $[C^{-1}]$ is invertible the above equation is written in its more useful form:

$$[b_q] = [C] [p]. \quad (3)$$

Thus, once $[C]$ is calculated in the calibration process, an unknown reflection coefficient of a test device

$$\Gamma = a/b = ab^*/|b|^2 \quad (4)$$

can be calculated from the result of multiplying the constant calibration matrix $[C]$ by a set of four power measurements taken with the test device connected to the six-port.

A brief review of the procedure [7] for calibration with known standards follows. Suppose one has a set of m standard reflectors for which the complex values Γ_i are known. Then the column matrices $[b_q]_i$ can be calculated a priori in terms of $|b|^2_i$, the column matrices $[p]_i$ can be measured, and each are

* Throughout the report brackets around a letter will denote a matrix. If the letter symbol is underlined the matrix is square.

related by equation (3). Since the calibration matrix $[C]$ is constant for all the standards, an augmented matrix equation can be constructed:

$$[B_Q] = [C] [P], \quad (5)$$

where

$$[B_Q] = \begin{bmatrix} |b|_1^2 & \cdot & \cdot & \cdot & |b|_m^2 \\ ab_1^* & & & & ab_m^* \\ a^*b_1 & & & & a^*b_m \\ |a|_1^2 & \cdot & \cdot & \cdot & |a|_m^2 \end{bmatrix}$$

$$[P] = \begin{bmatrix} P_{31} & \cdot & \cdot & \cdot & P_{3m} \\ P_{41} & & & & P_{4m} \\ P_{51} & & & & P_{5m} \\ P_{61} & \cdot & \cdot & \cdot & P_{6m} \end{bmatrix}$$

It is helpful for later discussion to note that a $4 \times m$ matrix $[B_Q]$ can be decomposed into the product of an $m \times m$ diagonal matrix whose diagonal elements are the power levels incident on each standard load

$$[B_Q] = \begin{bmatrix} |b|_1^2 & 0 & 0 & \dots & 0 \\ 0 & |b|_2^2 & 0 & & 0 \\ 0 & 0 & & & \\ 0 & 0 & 0 & \dots & |b|_m^2 \end{bmatrix}$$

and a $4 \times m$ matrix $[\Gamma]$ of known reflection coefficients

$$[\Gamma] = \begin{bmatrix} 1 & 1 & \dots & 1 \\ \Gamma_1 & \Gamma_2 & & \Gamma_m \\ \Gamma_1^* & \Gamma_2^* & & \Gamma_m^* \\ |\Gamma_1|^2 & |\Gamma_2|^2 & \dots & |\Gamma_m|^2 \end{bmatrix}$$

Then from equation (5),

$$[B_Q] = [\Gamma][B_Q] = [C][P]. \quad (6)$$

When one only needs to find out the ratio $\Gamma = a/b$ for a test device, it is unnecessary to know the absolute value of the

calibration matrix. Rather it is sufficient to know each element of $[C]$ to within a fixed (but unknown) constant of proportionality. In this case, the calibration matrix is sufficiently determined by equation (6) provided that the following conditions are met:

1. the calibration loads, $[\Gamma_i]$, are known,
2. the power, $|b|^2$, incident on the test port is either kept constant or the relative size of the powers $|b_1|^2$, $|b_2|^2$, ... are known, and
3. at least four columns of $[P]$ are linearly independent.

Condition 3 is required so that $[P][P^t]$ can be inverted in the solution for the calibration matrix $[C]$:

$$[C] = ([B_Q] [P^t])([P] [P^t])^{-1}. \quad (9)$$

If fewer than four of the columns of matrix $[P]$ are linearly independent, then the rank of $[P][P^t]$ is less than its order (four) and the matrix is singular or not invertible. Provided that the above conditions are satisfied, Equation (9) can be utilized to calculate the elements of the calibration matrix $[C]$ from the known values of $[B_Q]$ and the measured values of $[P]$. This matrix is constant for a given wavelength, but must be recalculated for substantially different wavelengths.

In practice, the second condition is most easily met by dedicating one of the four detectors (say the one on port 3) to monitoring the power flowing toward the test port. The coupler for this detector is best located near the test port as shown in Figure 2.5 so that the detector is highly isolated from the reflected signal. If both the $[B_Q]$ matrix and the matrix of power readings $[P]$ are multiplied (i.e., normalized) by the matrix

$$[P^{-1}_0] = \begin{bmatrix} 1/P_{3,1} & 0 & \cdot & \cdot & \cdot & \cdot & 0 \\ 0 & 1/P_{3,2} & & & & & 0 \\ 0 & 0 & & & & & 0 \\ \vdots & \vdots & & & & & \\ 0 & 0 & \cdot & \cdot & \cdot & \cdot & 1/P_{3,m} \end{bmatrix}$$

then condition (2) above is fulfilled. Rather than complicate the notation further, it will be understood in the remainder of this report that this normalization will always be done.

Condition 1 on the other hand is difficult to achieve in practice. As the test wavelength is decreased into the low-millimeter range it becomes increasingly difficult to characterize standards accurately enough for the above procedure to be effective. A self-calibration method has been implemented by Cronson and Susman [7] to alleviate this difficulty. Strictly speaking, a self-calibration method would not require any known standards, just calibration devices that are repeatable. In their method, the repeatable calibration devices are a pair of terminations (diagrammed in Figure 2.6) that can be connected to the test port by a sliding transmission line. For best results, the two terminations differ in the signal they reflect by 3 dB and in the phase of the reflection by about 45° [6]. Several repeatable lengths of the sliding transmission line are used, and the two terminations are connected to the sliding section by a switch so that repeatable exchanges can be made. The self-calibration method of Cronson and Susman is almost ideal in that only two other calibration devices are needed which are standards in the usual meaning of the term. These are standards for opposite ends of the reflection scale; namely, a matched load for near-zero reflection and a known short of high reflection. Thus, the number of standards required has been reduced from four or more to only two. The key point in this advance was the realization on the part of Cronson and Susman that the relationship between the power measurements made and the calibration matrix could be formulated as an eigenvector problem.

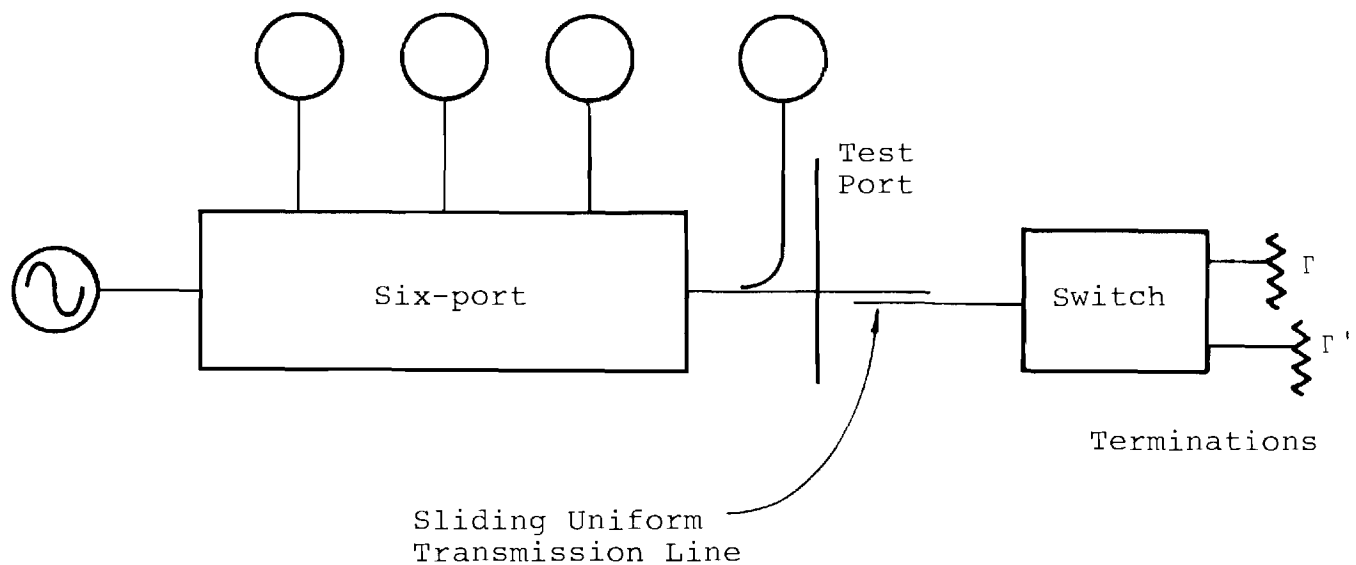


Figure 2.6 A Calibration Device Required by the Eigenvector Method. It comprises two terminations of reflectance, Γ and Γ' , which can be selected by the switch and a sliding transmission line that makes it possible to vary the line length to the termination in a reproducible way.

The following is a review of the self-calibration method for the six-port reflectometer as given by Cronson and Susman [7].* A flow chart of the method is given in Figure 2.7. First, the sliding waveguide section is attached to the test port and one of the terminations selected with a reflection coefficient Γ . One of $m-1$ unique and repeatable lengths of the transmission line is set, and the four detector power levels recorded. These are written in one of the columns of the augmented P matrix

$$[P] = \begin{bmatrix} 1 & 1 & & 1 & 1 \\ P_{4,1} & P_{4,2} & \cdot \cdot \cdot & P_{4,m-1} & P_{4,m} \\ P_{5,1} & P_{5,2} & \cdot \cdot \cdot & P_{5,m-1} & P_{5,m} \\ P_{6,1} & P_{6,2} & \cdot \cdot \cdot & P_{6,m-1} & P_{6,m} \end{bmatrix}$$

The first subscript is the detector number, and the second denotes one of the $m-1 \geq 3$ lengths of the transmission line except in the last column. The readings in the last column are obtained with the transmission line and termination replaced by the well-matched (near-zero reflection) load. This is included to insure that the product $[P][P^t]$ is invertible. Note that the first row contains values of unity rather than $P_{3,i}$ since each column is normalized by the value obtained for $P_{3,i}$.

A second matrix $[P']$ is obtained when the sliding transmission line is reattached but the other termination with a reflection coefficient Γ' is switched in. Detector values are obtained for exactly the same transmission line lengths and put in the same columns. As above, the fourth column corresponds to measurements with the well-matched load. The only difference between $[P]$ and $[P']$ comes from the amplitude and phase of the

* Note that the meanings of b and a as used here (see Figure 2.5) are consistent with the usual convention and also with an earlier report by Cronson and Susman [6]. However, a and b were interchanged in their later report [7].

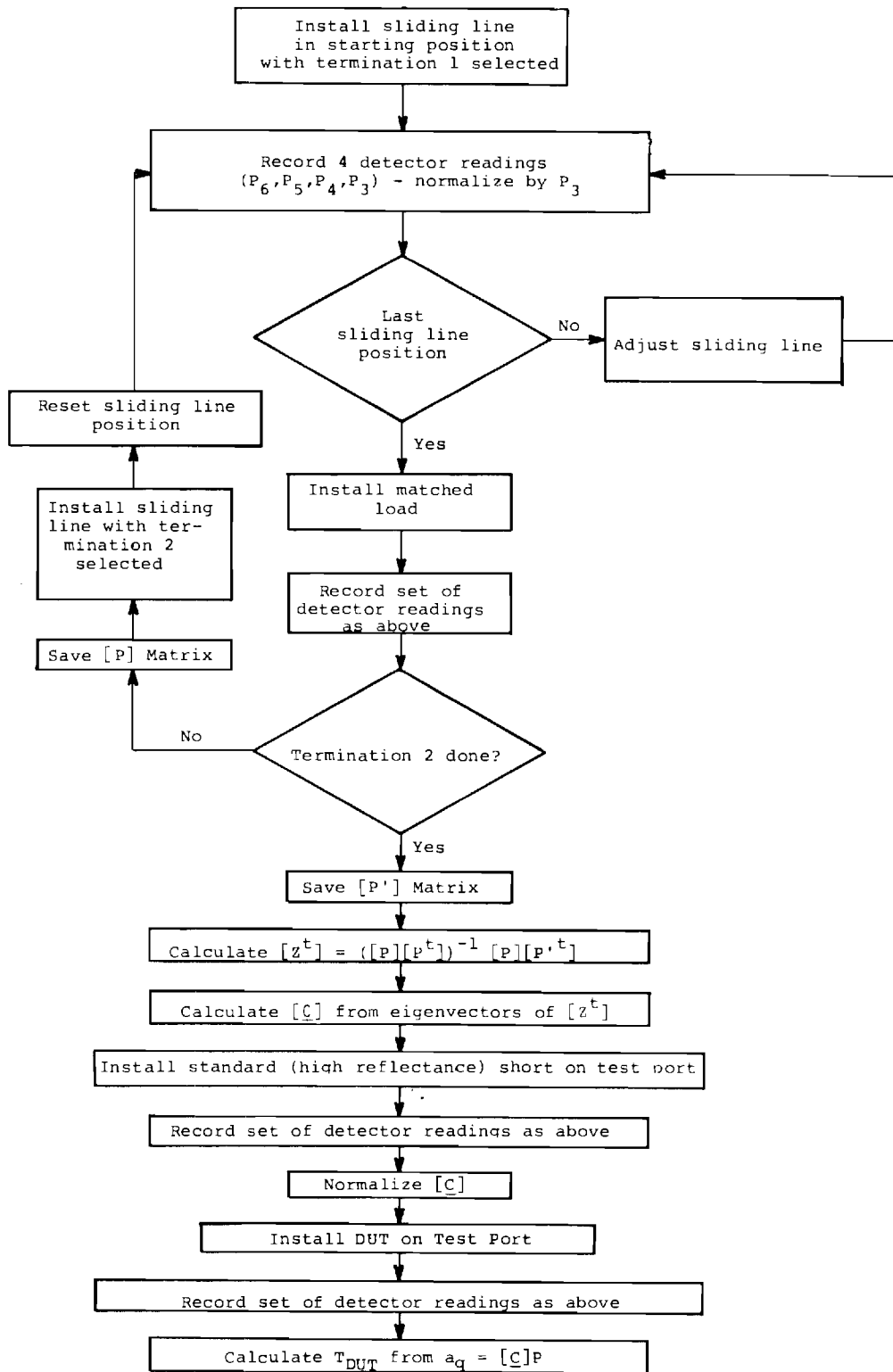


Figure 2.7 Procedure for Calibration of Six-Port [7].

reflection intrinsic to the two terminations. The only requirement is that the ratio of the reflection coefficients of the two terminations must be a complex constant independent of the sliding waveguide length.

Corresponding to the [P] and [P'] matrices are the matrices defined in the earlier discussion:

$$[B_Q] = \begin{bmatrix} |b|^2 & |b|^2 & & |b|^2 & |b|^2 \\ \Gamma_1 |b|^2 & \Gamma_2 |b|^2 & \dots & \Gamma_m |b|^2 & 0 \\ \Gamma_1^* |b|^2 & \Gamma_2^* |b|^2 & \dots & \Gamma_m^* |b|^2 & 0 \\ |\Gamma|^2 |b|^2 & |\Gamma|^2 |b|^2 & \dots & |\Gamma|^2 |b|^2 & 0 \end{bmatrix} \quad (9a)$$

$$[B_Q'] = \begin{bmatrix} |b|^2 & |b|^2 & \dots & |b|^2 & |b|^2 \\ \Gamma_1' |b|^2 & \Gamma_2' |b|^2 & & \Gamma_m' |b|^2 & 0 \\ \Gamma_1'^* |b|^2 & \Gamma_2'^* |b|^2 & & \Gamma_m'^* |b|^2 & 0 \\ |\Gamma'|^2 |b|^2 & |\Gamma'|^2 |b|^2 & \dots & |\Gamma'|^2 |b|^2 & 0 \end{bmatrix} \quad (9b)$$

In rows 2 and 3 a subscript denotes the effect on the phase of reflection by the selection of the length ℓ of the sliding transmission line (e.g. $\Gamma_1 = \Gamma \exp[-2\gamma\ell]$ where γ is the propagation constant), but rows 1 and 4 are independent of this length, as shown. The two matrices above are related by

$$[B_Q'] = [L][B_Q] \quad (10)$$

where [L] is a diagonal matrix

$$[L] = \begin{bmatrix} 1 & 0 & 0 & 0 \\ 0 & \lambda & 0 & 0 \\ 0 & 0 & \lambda^* & 0 \\ 0 & 0 & 0 & |\lambda|^2 \end{bmatrix}$$

and where $\lambda \equiv \Gamma' / \Gamma$. Equation (10), along with

$$[B_Q] = [C][P]$$

and

$$[B_Q'] = [C][P'],$$

leads to the result that

$$[L][C] = [C][P'] [P^t] ([P][P^t])^{-1}.$$

This equation has the form in which $[L]$ is a matrix of eigenvalues for the matrix $[Z] \equiv [P'] [P^t] ([P] [P^t])^{-1}$ and $[C]$ is the corresponding matrix of eigenvectors. The calibration matrix $[C]$ can thus be found by standard techniques for finding the eigenvectors of the matrix $[Z]$; however, it is a characteristic of such solutions that each eigenvector (i.e., each row of $[C]$) can only be determined to within a constant of proportionality. This means that the unknown reflection coefficients of test devices can be determined in a relative way, but if one compares the results obtained to that obtained for a standard high reflectivity short, the absolute scale can be transferred and the calibration matrix $[C]$ suitably normalized. Notice in the above that one of the eigenvalues in $[L]$ is known in advance, namely unity, and that the value of λ may be obtained as a bonus.

2.3.2 Analogy between QUOSM and Six-Port

Figure 2.8 shows a preferred six-port design described [7] by Cronson and Susman. The source is connected with some isolation to port 1. The DUT is connected to port 2 through the direct arm of a 22 dB directional coupler. The reference detector at port 3 on the -22 dB coupler arm monitors the power incident on the DUT. In turn, Figure 2.9 illustrates a QUOSM that is modified such that the reference detector measures the radiation incident on the DUT rather than that which leaves the source. This arrangement more closely parallels that in Figure 2.8 as will be discussed below. The reference detector is required by the conditions stated earlier to monitor all changes in the power flowing toward the test port. These changes can arise due to source fluctuations, due to a change in what is connected to the test port, and due to standing waves within the QUOSM. The latter two effects are not of the same magnitude everywhere in the QUOSM, so it is necessary to monitor directly the power going to the test port in order for the foregoing formulation to be

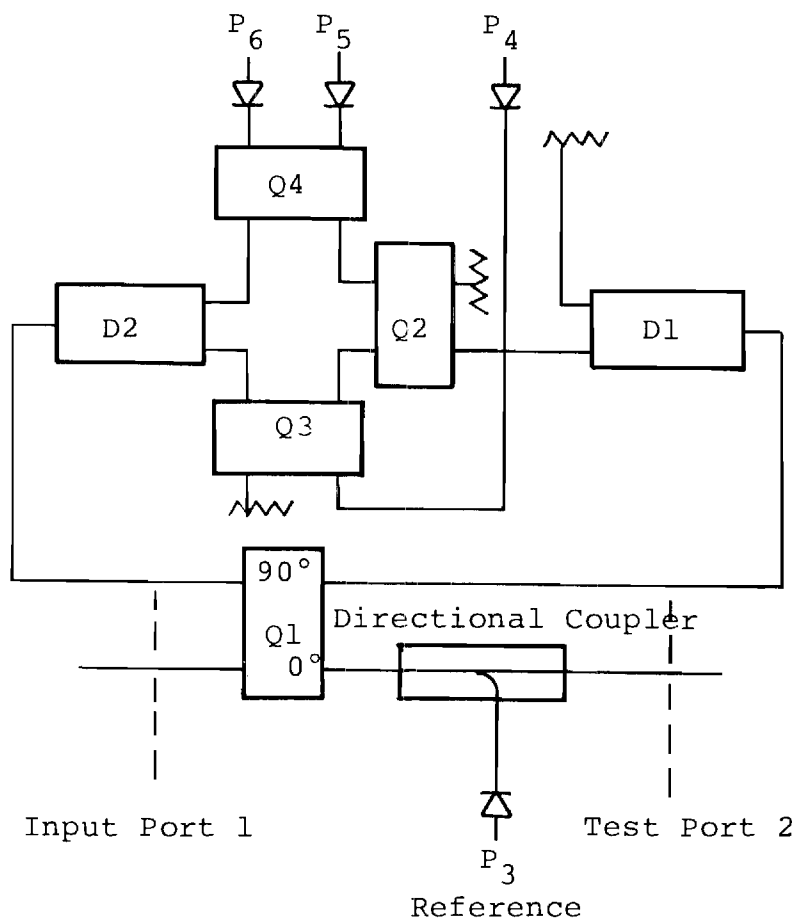


Figure 2.8 Example of a Six-port Reflectometer Circuit, after Reference [7].

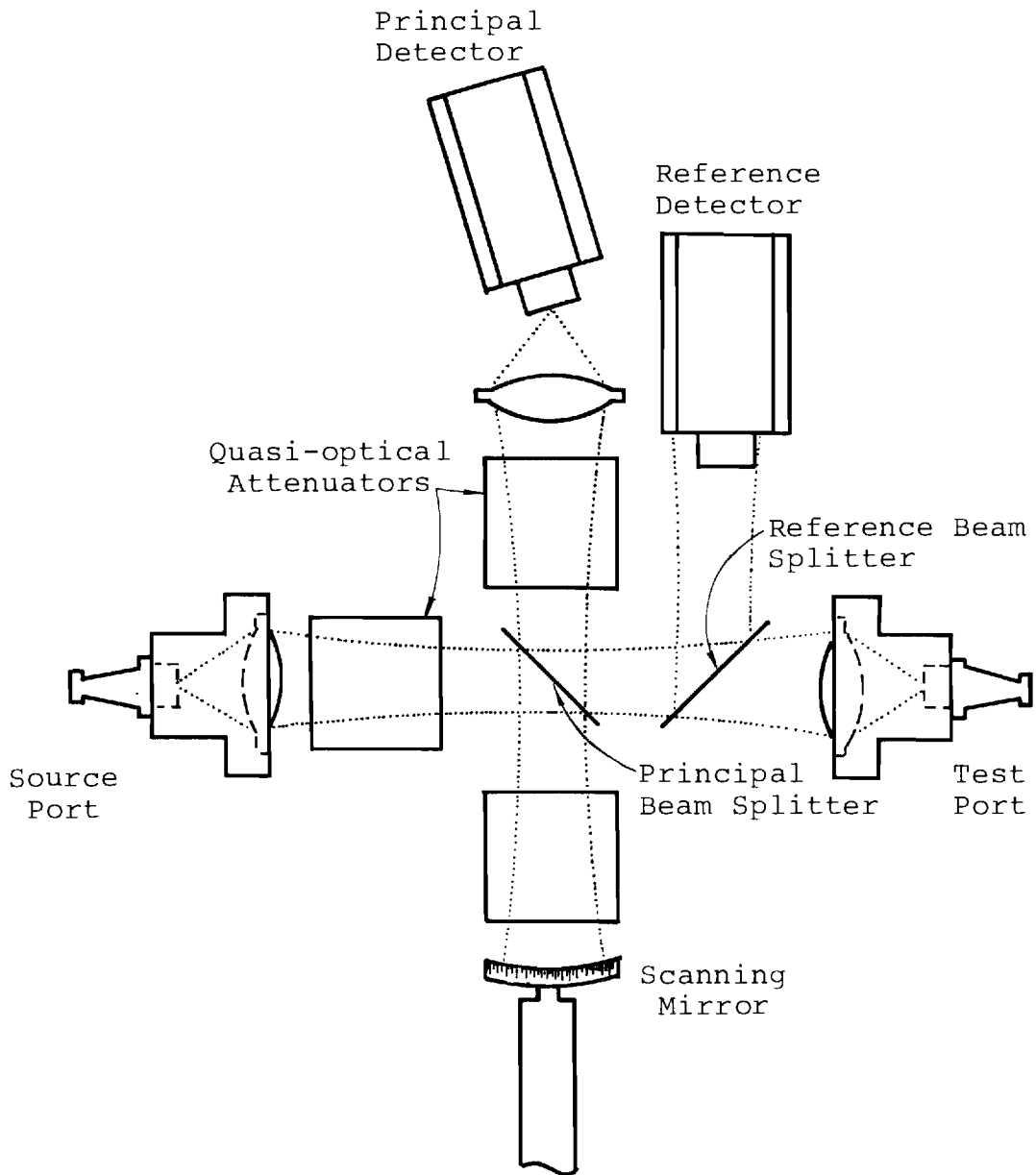


Figure 2.9 Modified QUOSM Design with Reference Detector Adjacent to Test Port.

valid. Cronson and Susman had similar arguments for the placement of the reference detector [7]. In the case of the QUOSM, instead of a directional coupler, a low-reflectivity beam splitter is used to couple power to the reference detector.

In the six-port reflectometer three ports are utilized for power measurement in addition to the reference power measurement already described. The QUOSM, in effect, utilizes time-division multiplexing to implement the power measurements made at ports 4, 5, and 6 of the six-port. In the case of the QUOSM the three powers are measured at each of three unique positions of the scanning mirror. An advantage of the QUOSM is that the mirror positions, and hence the phase shifts introduced, are computer-controlled and can be varied as the source wavelength is changed. This should allow for optimization of the phase shifts at any wavelength in the design bandwidth.

As described earlier, the self-calibration method for the six-port reflectometer requires a set of four power measurements for each of three or more unambiguous positions of a sliding transmission line with two different, terminations. For the wavelength range of the QUOSM which extends to less than one millimeter, sliding transmission lines that will give reproducible performance without undue loss are probably not practical to make, but the same effects can be achieved instead in the optical part of the QUOSM. The sliding section essentially introduces reproducible delays, and this requirement can be met in two ways illustrated in Figure 2.10. In the first, the whole lens-horn arrangement of the test port is moved along the optical axis in some fashion that insures reproducibility of positioning. One of the terminations can have a high reflectance and the other could be the same but with a 3 dB loss dielectric slab of an appropriate thickness added in front of the lens. In the second method, instead of a translation of the test port, low-loss dielectric slabs could be inserted in front of the lens to add reproducible delays. The same termination methods as in

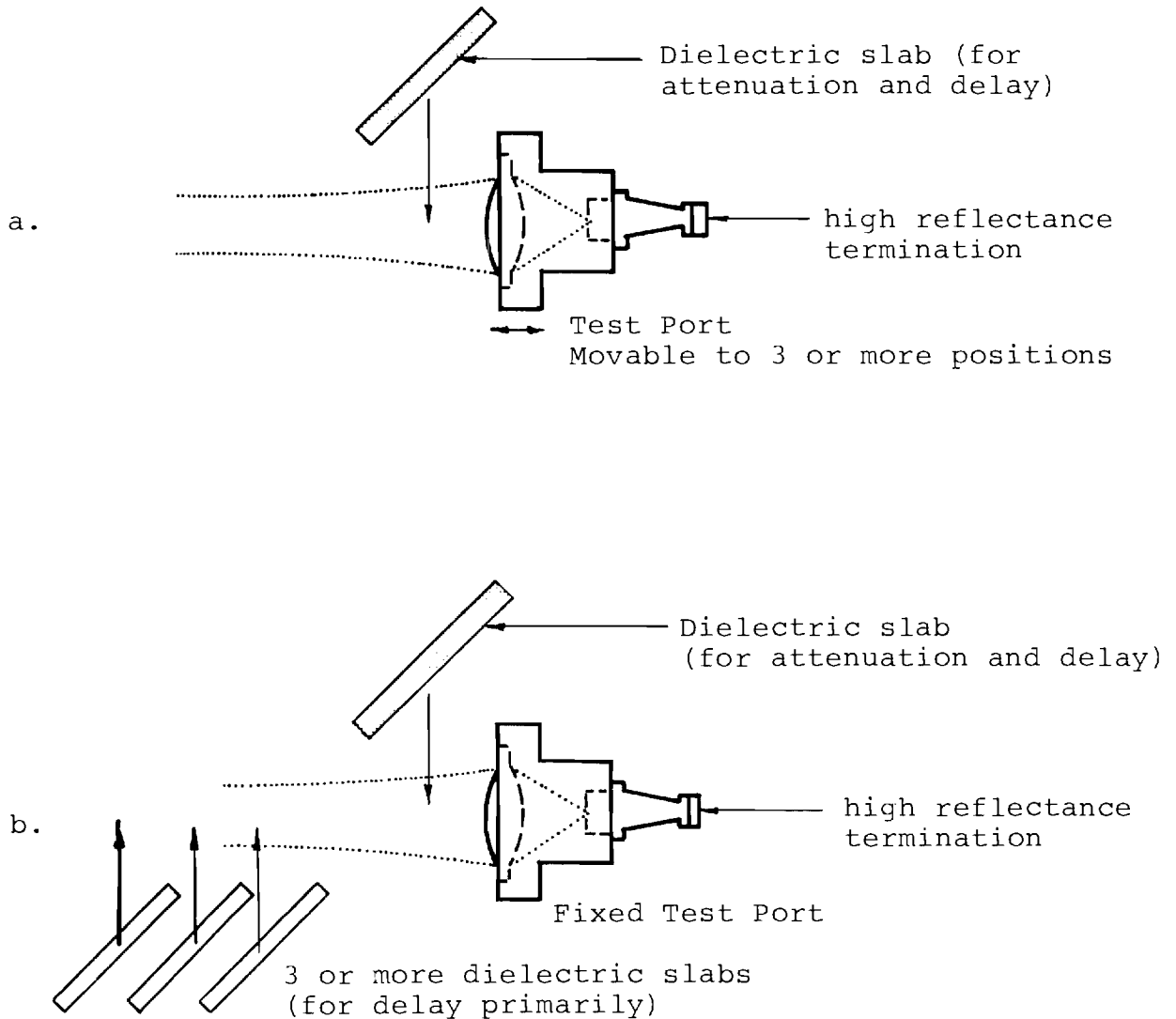


Figure 2.10 Two ways in which a sliding transmission line with two terminations can be emulated in the QUOSM. In a) the test port as a whole is moved to three or more reproducible positions. The termination is effectively modified by introducing a dielectric slab which in two passes gives ~ 3 db attenuation and 45° phase shift. In (b) the test port is fixed and the equivalent delays introduced by switching in low loss dielectric slabs of different thicknesses.

the first method could be used.

With a six-port, there is a requirement for a set of four power measurements to be made with a matched load mounted on the test-port, as discussed earlier. If the horn-lens transition in the test port of the QUOSM did not partially reflect radiation passing through it, all that would be necessary to meet the analogous requirement would be to mount a tapered load on the flange of the horn and make power measurements with the principal detector (for three mirror positions) and one with the reference detector. Such loads have been fabricated for use with the QUOSM in earlier work [3]. However, the fact that the lens and horn may be expected to reflect energy back toward the principal beam splitter, appears to mean that an additional calibration absorber is needed. This would be an absorbing pad (like that shown in Figure 1 of reference [3]) that could be inserted in the optical beam between the reference detector's beam splitter and the test port lens and could thus eliminate all reflection from the test port. Used as part of a calibration procedure analogous to that for a six-port, this would permit one to determine the complex reflectance* of the whole test port. One would then determine the complex reflectance of the port with the DUT mounted and make a second determination with a tapered load mounted. The latter would determine the amplitude and phase of the reflection from the lens-horn and could be used to remove the effect of this reflection from the results obtained when the DUT is mounted. This correction would closely parallel that described in an earlier report [1].

Since this type of correction is well-established, it was not dwelt on in the present work. Instead, as a simplification for the following discussions and for the simulations which will

* The term "reflectance" is interchangeable with "reflection coefficient", but generally refers to reflection from something other than a simple surface.

be described, the reflectance of the test port's lens-horn is taken to be zero. This significantly facilitated the simulations and focused attention on the main issues while the work was underway. In future work, the calibration step can be added, as described above, to correct for the lens-horn reflectance, which according to previous estimates [1] may be of the order of ten percent (in terms of power).

Finally, as with a six-port, an absolute reflectance and a reference for phase can be determined by the comparison of results obtained for a DUT with those for a near perfect reflector (high-reflectance short) mounted on the waveguide flange of the test port.

It has been shown above that the QUOSM either has, or can be provided with, capabilities that are analogous to those possessed by a six-port network analyzer. As a result the calibration procedure outlined for six-ports in Figure 2.7 corresponds to an analogous procedure for the QUOSM shown in Figure 2.11. In the following sections, descriptions are given of the numerical algorithms and simulations which have been prepared to test this procedure.

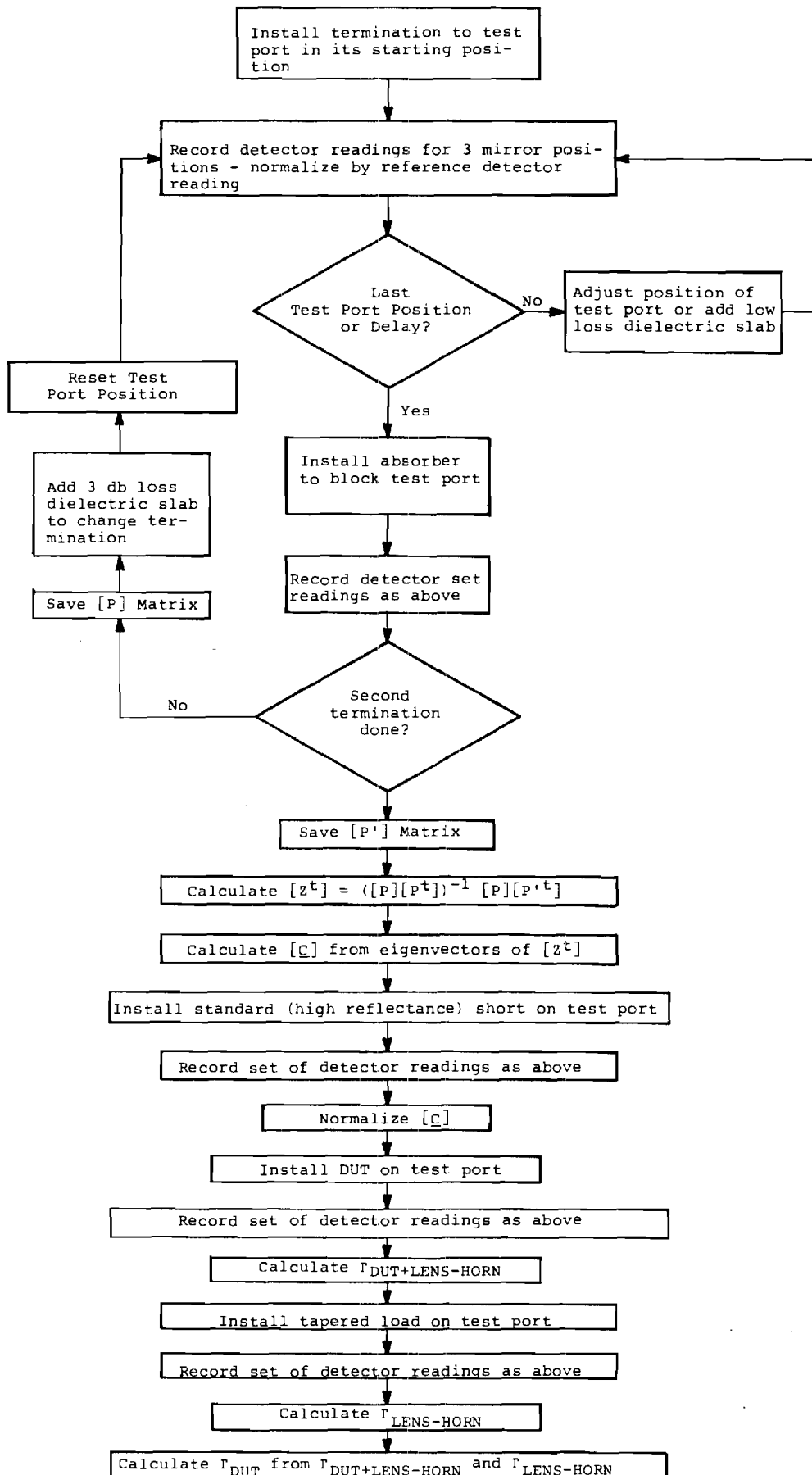


Figure 2.11 Procedure for Calibration of QUOSM

2.4 Eigenvalue/vector Analysis

As discussed above, the new calibration procedure for the QUOSM involves calculation of the eigenvalues and eigenvectors of the matrix $[Z]$, where

$$[Z] = [P'] [P^t] ([P] [P^t])^{-1}$$

and where the matrices $[P]$ and $[P']$ contain power measurements for prescribed calibration conditions. The rows of the calibration matrix $[C]$ described earlier are the left-hand form of eigenvectors of $[Z]$, since

$$[C] [Z] = [L] [C].$$

As it happens, right-hand eigenvectors are more commonly found in numerical analysis literature, and so for compatibility with standard practice, the above equation must be transformed by transposition so that the eigenvectors are of the right-hand form:

$$[Z^t] [C^t] = [C^t] [L]$$

Now the columns of the transposed calibration matrix are the right-hand eigenvectors of the matrix

$$[Z^t] = ([P] [P^t])^{-1} [P] [P'^t]$$

The eigenvalues in the diagonal matrix $[L]$ are unaffected by the above transposition.

The actual numerical procedures to derive eigenvector solutions and to calibrate the QUOSM have been developed independently of the work of Cronson and Susman. In the main, well-established numerical methods have been used which were available either from published algorithms and literature or from the library of the HP-85 computer that is included in the QUOSM as a controller and automatic data processor. The published routines selected were translated into the form of BASIC language used in the HP-85 and tested as will be described below. In general, for the present purpose of demonstrating the eigensolution approach to the calibration of a QUOSM, numerical procedures were selected which appeared to offer maximum

insensitivity to numerical ill-conditioning and to noise. Compactness of coding was given little consideration at this stage.

The first step in the eigenvector solution is the calculation of $[Z^t]$ from $[P]$ and $[P']$, and this appears at first glance to require the calculation of the inverse of $[P][P^t]$. The HP-85 computer in the QUOSM system is equipped with a ROM package of matrix routines as an extension of the BASIC language. This recognizes a one-statement command for calculating the inverse of square matrices and can be applied to finding the inverse of the 4×4 square matrix ($[P][P^t]$). This inverse can then be used to premultiply the matrix result of $[P][P^t]$. However, it is more accurate to calculate $[Z^t]$ by a method that avoids the explicit calculation of the above inverse. In general, the product of an inverse matrix $[A^{-1}]$ and another matrix $[B]$ can be expressed as the solution matrix in the familiar general problem of simultaneous linear equations whose coefficients are the elements of $[A]$:

$$\begin{aligned} [A][X] &= [B] \\ [X] &= [A^{-1}][B] \end{aligned}$$

Well-established numerical methods are available which can be used to calculate $[A^{-1}][B]$ directly and with greater accuracy than the calculation of $[A^{-1}]$ followed by multiplication by $[B]$ (see e.g., refs. [8,9]). The HP-85 package of firmware makes available a command, $X = \text{MAT SYS } (A,B)$ which implements such a solution. (According to the manufacturer, the method of UL decomposition is used [10]). Thus one may substitute $[P][P^t]$ for $[A]$ and $[P][P']^t$ for $[B]$ in the above and obtain $[Z^t]$.

The difference in results was demonstrated in a test that calculated $[X] = [A^{-1}][A]$ for various trial matrices $[A]$ containing values in the range 0 to 1, and then compared $[X]$ with $[I]$, the identity matrix. In the case where $[A^{-1}]$ was calculated explicitly and then multiplied by $[A]$ the diagonal elements of $[X]$ differed from 1 by at most 3×10^{-12} , and the off-diagonal

elements differed from 0 by at most 3.2×10^{-12} . When the system of equations was solved using the MAT SYS command the diagonal elements were found to be identically equal to 1 (for the 12 significant digits displayed). The off-diagonal elements were reduced to the order of 10^{-16} . The results of tests of this type depend to some extent on the values used to define the matrix [A], so the results described above should be taken only qualitatively as an indication of the difference between the two methods of solution.

The optimum procedure for calculation of the eigenvectors of a matrix depends in general on the nature of the matrix. According to a number of reviews which are available [e.g. 10-12], matrices are frequently poorly conditioned for eigenvector solutions and the choice of algorithm can have a significant impact on the quality of the results. In the case of interest here the matrix $[Z^t]$ is real and unsymmetric, and in general such matrices can present special problems of ill-conditioning [11]. However, if as recommended above, one chooses calibration terminations such that $|\lambda|^2$ is approximately 0.5, the eigenvalues will be reasonably well-separated in magnitude, and in such a case, more accurate eigenvector solutions can be found [11]. (The fact that two eigenvalues λ and λ^* and the corresponding eigenvectors are complex conjugates does not affect this assessment.)

The method of solution selected for the present work is believed to be optimum or near-optimum for real, unsymmetrical matrices as regards accuracy [10,11]. In outline, the procedure involves (1) balancing the matrix using similarity transformations that nearly equalize the norms of corresponding rows and columns, (2) reducing the matrix to upper-Hessenberg form (nearly upper-triangular) by means of orthogonal,

Householder transformations*, (3) further decomposing the matrix by what is known as the double-QR algorithm to obtain the eigenvalues, and finally (4) solving for the eigenvectors by inverse iteration. A FORTRAN program written by Grad and Brebner [13] and tested by several workers [14,15,16] implements the above steps and has been translated here into BASIC for use on the HP-85. An annotated listing of this program named EIGEN is given in Appendix B. Several matrices for which the eigenvalues and eigenvectors are known, including three suggested by Grad and Brebner, were used as test cases to verify that the translated version was working correctly. Agreement with expected values was obtained to at least 9 significant figures, where the computer normally displays up to 12. The test matrices are believed to have been of equal or greater difficulty by comparison with the matrices $[Z^t]$ expected to be encountered in practice, in the sense that some of the eigenvalues of the test matrices had magnitudes which were pathologically close to each other.

Two tests for the correctness of the eigenvalues have also been added to the program that apply even for matrices with unknown solutions. The first checks for the expected [17] equality between the sum of the calculated eigenvalues and the trace of the original matrix. The imaginary parts of the complex eigenvalues should cancel in the addition process to yield a number equal to the sum of the diagonal elements of the real matrix. The second test checks that the product of the eigenvalues equals the determinant of the matrix as expected [17]. Agreement under these tests has generally been found to at least 11 significant figures.

* One may note that in previous work involving the least squares method [1], orthogonal Householder transformations were also selected for similar qualities of robustness.

After the eigenvalues are calculated and verified as described above, the eigenvectors are also subjected to an additional routine test that verifies that

$$[Z^t][C^t] = [L][C^t].$$

When $[C]$ is formed by transposition, it is further tested by multiplication with the columns of power measurements in $[P]$. The matrix product $[B_Q] = [C][P]$ should indicate values consistent with the parameters used in the simulation. In particular the complex reflection parameter Γ_i

$$\Gamma_i = \frac{a_i b_i^*}{|b_i|^2}$$

for one of the sliding terminations in position i , can be found from

$$\Gamma_i = \frac{B_{Q,2,i}}{B_{Q,1,i}}$$

and compared with what was specified in the simulation.

The following sections will describe procedures that have been developed to simulate signals recorded by the detectors in the QUOSM and thus to make it possible to construct examples of the $[P]$ and $[P']$ matrices. For convenience, the programs for simulation and for the calculation of the calibration matrix are separate, and communication between them is through data files stored on cartridge tapes in the built-in facility of the HP-85 computer. The simulation program RFLCTN stores the columns of the $[P]$ and $[P']$ matrices on data files, and the program EIGEN which accesses these data then reconstructs $[P]$ and $[P']$, calculates $[Z^t]$, performs the eigenvector/value analysis, and calculates $[C^t]$ and hence $[C]$. EIGEN in turn stores $[C]$ on a file, and a final program CTIMEP can be used to calculate columns of $[B_Q]$ or $[B_Q']$ from

$$\begin{aligned} [B_Q] &= [C][P] \\ \text{or } [B_Q'] &= [C][P']. \end{aligned}$$

Annotated listings of these programs are given in Appendices A, B, and C.

2.5 Simulation of QUOSM Signals

The purpose of the RFLCTN program is to simulate QUOSM detector signals as a function of the positions and reflectivity values assigned to various components including the source and detector. This has resulted both in a better understanding of the standing wave condition and in vital, controlled data for the development of the matrix calibration technique.

As mentioned in an earlier section, when multiple reflections occur in the QUOSM, the number of paths by which radiation can reach the detector is infinite, but for finite component reflectances, significant energy is transmitted over only a finite (though not necessarily small) number of paths. For convenience, it is possible to record first the amplitude and phase of the signals which arrive by the most direct route to any port where an output (desirable or otherwise) can occur. These ports are at the source, the principal detector, the reference detector, and the device under test. At each of these ports a certain amount of the signal is not output (or absorbed) but is instead reflected and redirected back into the QUOSM. (As a simplification in the simulation, one may without loss of generality assign zero reflectance to the reference detector.) Then all of the reflected radiation returns on a path back to the principal beam splitter where it recombines and continues back to the output ports, and so on. In each iteration more signal arrives at each output port, and the part not reflected is added vectorially to that so far accumulated. When the calculated output power on each of the ports has converged, the iterations can be halted. Appendix D discusses the fact that conservation of energy requires that the sum of the powers absorbed or output must equal the power input by the source. This was useful as a cross-check on the detailed calculations during the development of the simulation package. In Figures 2.12 to 2.15 "optical flow charts" are given which diagram the paths taken by the radiation

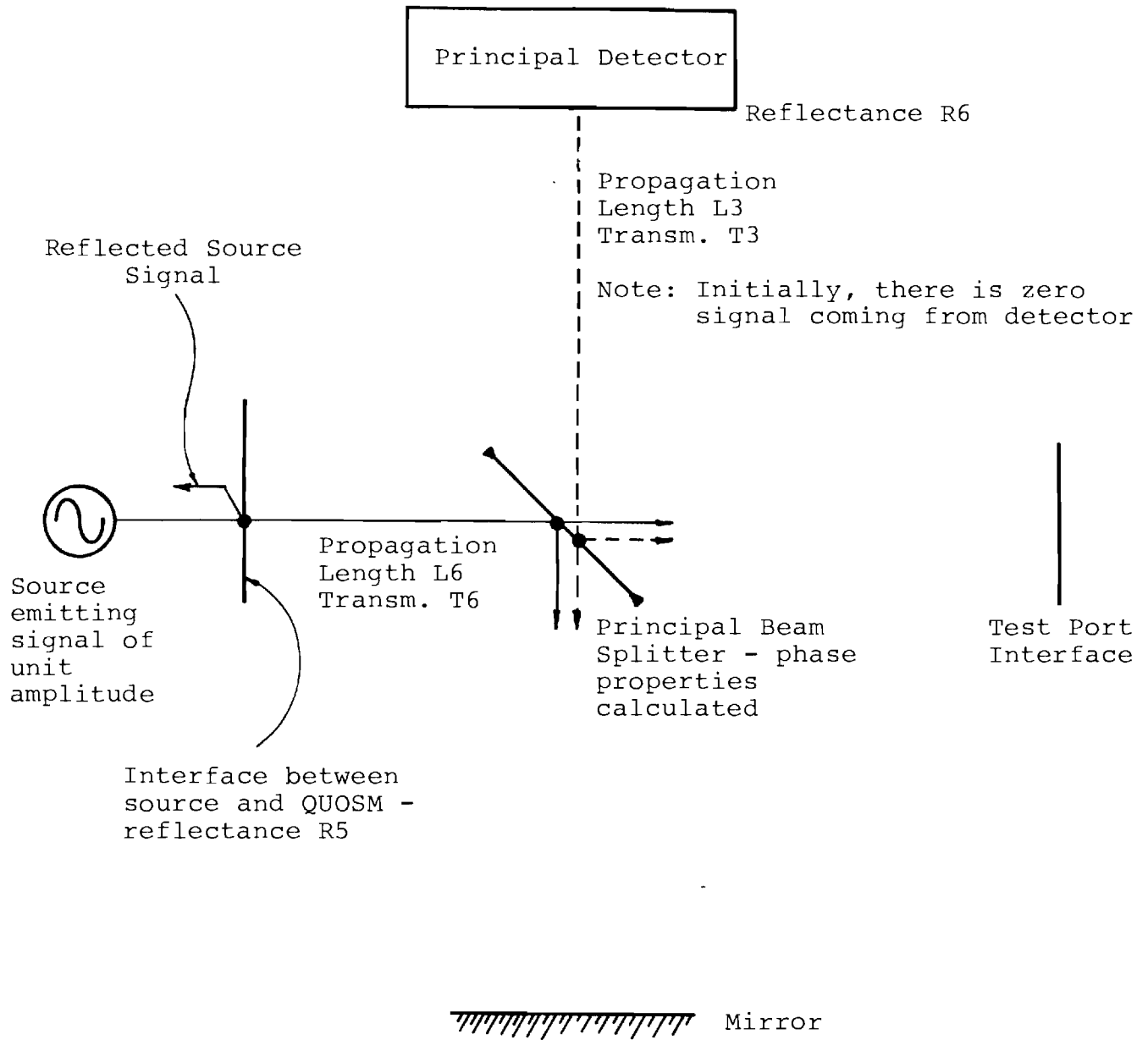


Figure 2.12 Optical Flow Chart for Initial Optical Paths from Source and Detector. Parameter labels given are those used in RFLCTN program (see Appendix A).

Principal Detector

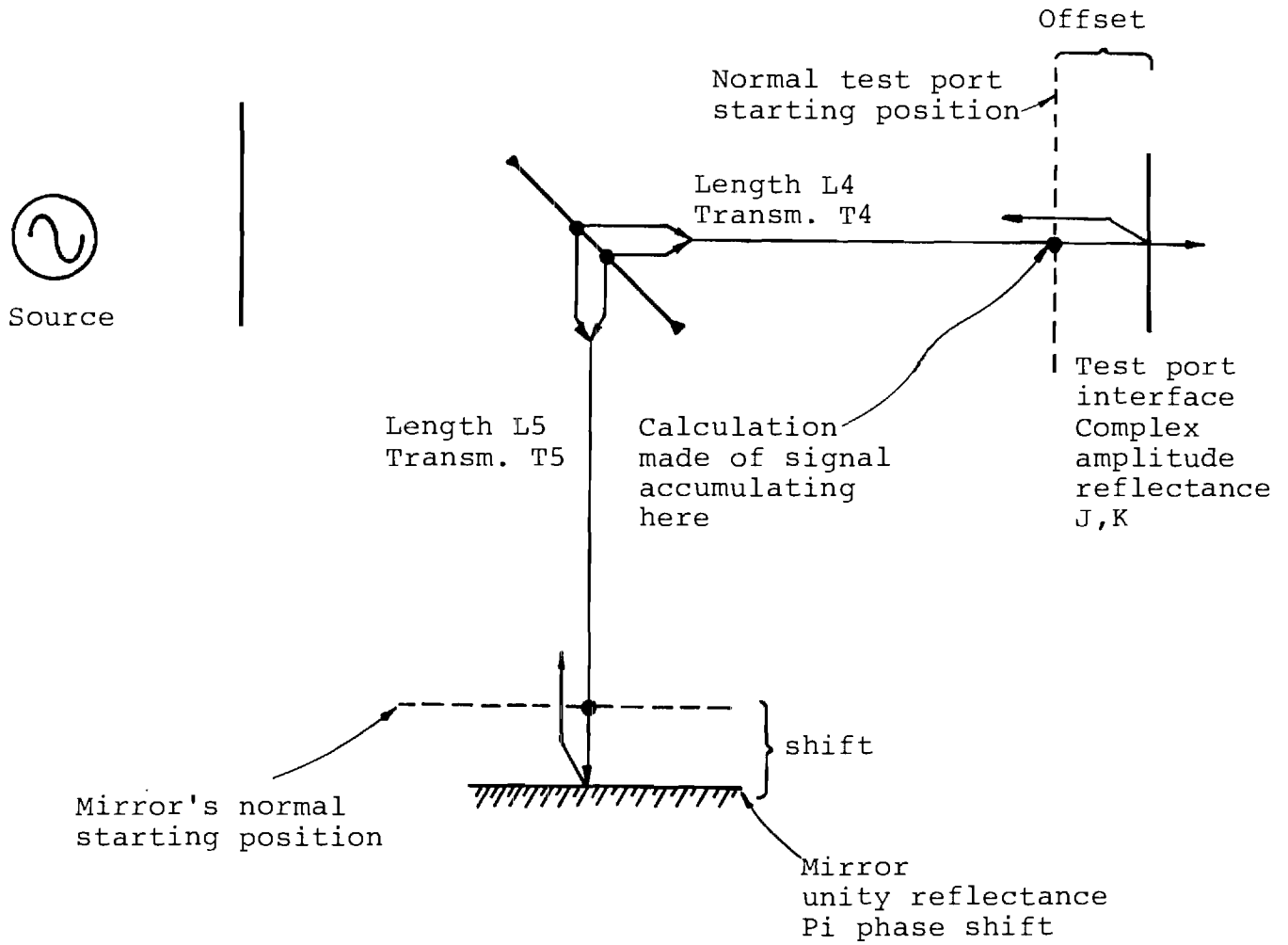


Figure 2.13 Optical Flow Chart for Optical Paths from Beam Splitter to Mirror and Test Port.

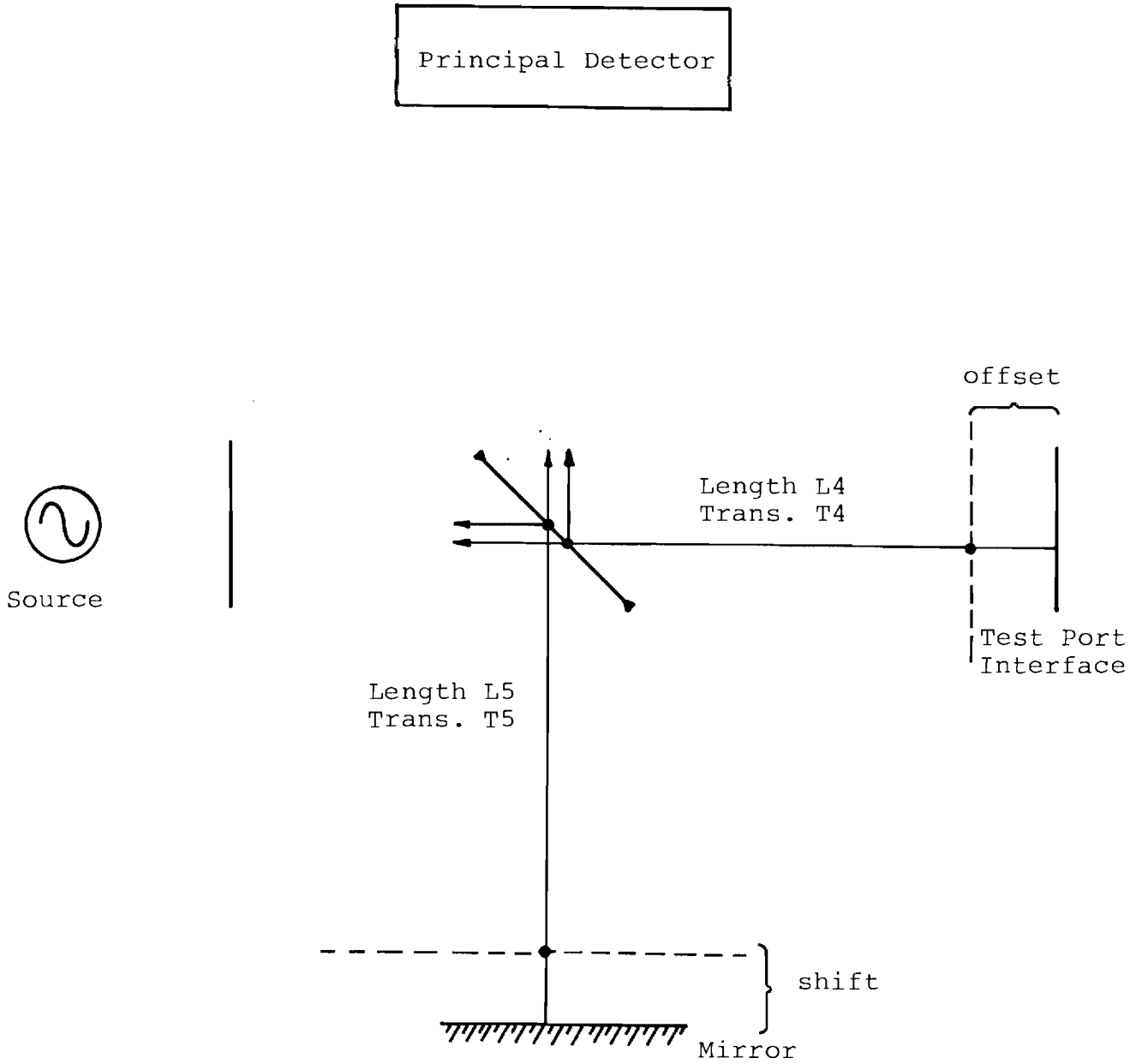


Figure 2.14 Optical flow chart for optical paths from mirror and test port back to the beam splitter.

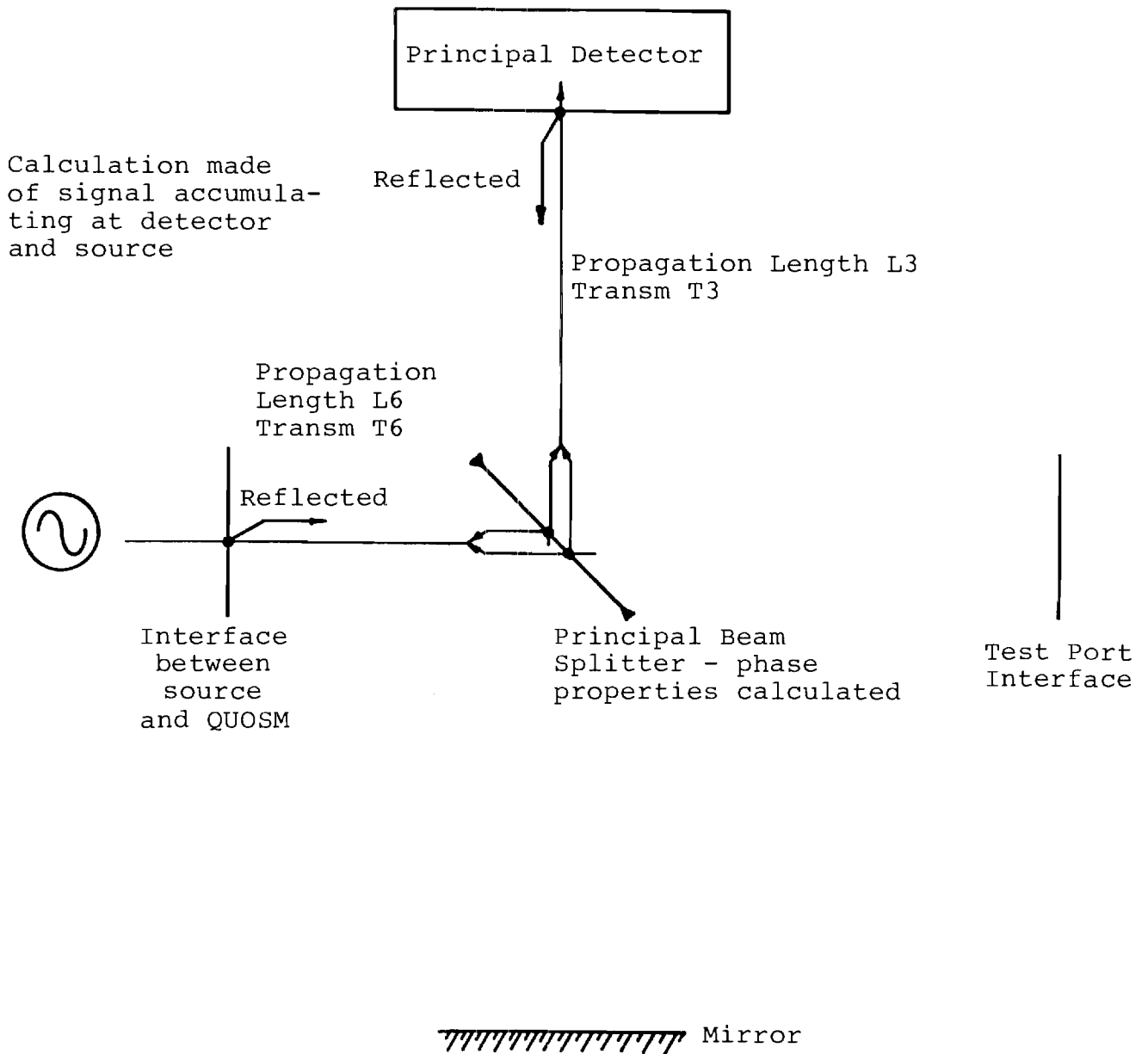


Figure 2.15 Optical flow chart for optical paths back to source and detector. Reflections at source and detector are start of next iteration.

and outline most of the details included in the calculation of the various signal amplitudes.

Figure 2.12 describes the starting conditions. Values of reflection coefficients for the source, detector, and Device Under Test (DUT) are input from the keyboard. The same is true for the source frequency and the beam splitter thickness. The indicated path lengths (L_3 , L_4 , L_5 , and L_6) are stored within the program along with path transmission values which simulate the effect of attenuators. Since BASIC programs are easily amended, these values can be readily changed. The calculation is initialized such that the source emits a signal of unit amplitude toward the QUOSM. A portion of this signal, determined by the selected source reflectivity, enters the QUOSM going toward the beam splitter. The rest is reflected toward the source at the Source/QUOSM interface. Of course no radiation is coming from the detector at this stage, and the initial detector signal is explicitly set equal to zero. This sets the conditions for the computer to begin its iterative procedure. The effects (phase change and possible amplitude change) of propagating through the path lengths L_3 and L_6 are calculated. Then the effects of the beam splitter are taken into account. The beam splitter (assumed lossless) divides the amplitude of the signal from the source into transmitted and reflected components, and calculable phase changes occur [18]. The same happens for the signal (initially zero) reflected by the detector. The four resulting signals are shown in Figure 2.12 as four short arrows originating at the beam splitter, two going toward the DUT and two toward the movable mirror.

Figure 2.13 indicates that each pair of signals propagating in the same direction are vectorially added. The effects of propagating through paths L_4 and L_5 are then calculated. The previously entered values of DUT reflection and phase shift are utilized to calculate the amplitude and phase of the signal reflected from the DUT (shown as a short arrow at the DUT). The

mirror displacement introduces an additional phase shift of the signal coming to the mirror from the beam splitter. The mirror itself is assumed to have unity reflectance and a phase shift of π radians.

Figure 2.14 illustrates the calculations performed that treat the propagation of the signals from the DUT and mirror to the beam splitter. The effects of propagating through the path lengths are once again accounted for, as are the effects of the beam splitter.

Figure 2.15 shows that the parallel beams from the beam splitter have been combined, the propagation through the paths accounted for, and the detector and source reflections applied to calculate the values for the signals from the source and detector in the next iteration.

As mentioned earlier, the signals which pass through the output ports are vectorially added and accumulated over all iterations. In the program as implemented, the power at the DUT is not formally accumulated and stored. Tests based on conservation of energy are restricted then to the case of 100 percent DUT reflectance, but such a test gives an adequate verification that the simulation is working correctly.

The complex numbers representing the signal to the main detector and to the source are converted to power readings at the end of each iteration. These power readings are compared with those of the previous iteration. When the percent difference between iterations, for both the source and the detector powers, becomes less than a selected small value, the detector power reading is normalized (i.e., divided by the power on the reference detector, as required by theoretical considerations discussed earlier).

To obtain the data necessary to form a column of [P] or [P'], the simulation program repeats the calculation of the normalized detector level for three unique mirror positions stored in the program. The fourth element of such a column is of

course unity, as it represents the reference detector signal divided by itself as discussed previously. The QUOSM has a great deal of flexibility in terms of the mirror positions used, and hence in the phase shifts, available, whereas the relative phases seen by the detectors in the six-port analyzer are normally fixed by the hardware configuration. Simple program modifications or parameter inputs are all that is required to change the mirror positions selected by the QUOSM, and hence optimization of the kind described by Engen [4] is more easily implemented, in principle, in the QUOSM.

2.6 Simulated Calibration

2.6.1 Case of Standing Waves

The calibration process described in Sections 2.3 and 2.4 has been tested with simulated data, and the the results of one such test are explained here. The source frequency was set to 94 GHz. The source and the detector were each simulated as having a power reflectance of 0.2. This is an order of magnitude larger than the value measured [3] for the detector in previous work, and is a plausible upper limit. The two fixed, but uncalibrated, terminations required for the relative calibration were assigned amplitude reflectances of 1.0 and 0.7. The phase-shift difference between the two devices was set at 45° . (The program actually asks for the value of half the phase shift). Table 2.2 shows what calibration devices are in place, the position of the scanning mirror, and the status of the position or effective shift of the test port for each element of the [P] and [P'] matrices that were calculated.

The eigenvalues of the square matrix derived from the power readings were tested on the basis that the largest eigenvalue should be unity and the smallest should be the ratio of the power reflectances of the two calibration shorts. The two intermediate eigenvalues are a complex conjugate pair found from the ratio of the amplitude reflection coefficients. The calculated eigenvalues, rounded to four decimal places, were: 1, 0.4901, $0.4951 + i 0.4951$. Thus the largest eigenvalue was correctly found to be unity. The smallest, 0.4901, was acceptably close to $0.7^2 = 0.4900$, the ratio of the power reflectances. The magnitude of the complex values is 0.7002 and the polar angle is 45° . Therefore, the calculated eigenvalues were in excellent agreement with expectation.

The calibration matrix [C] was then formed by assembling the complex eigenvectors as rows, and was tested for consistency by multiplication with each of the eight sets of power measurements.

That is, the $[B_Q]$ and $[B'_Q]$ matrices were calculated by

$$[B_Q] = [C] [P]$$

and

$$[B'_Q] = [C] [P'].$$

These results are compiled in Table 2.3 along with the values expected in accordance with equations (9a) and (9b) and the input parameters of the simulation. One may see that the rows of $[B_Q]$ and $[B'_Q]$ differ from expectation by a factor depending on the row. As previously explained, the rows in $[C]$ can only be found by eigenvector analysis to within a constant factor, and the magnitude of each row must be normalized by results obtained when a termination of unity reflectance is used. In this case one of the terminations used in the calibration has unity reflectance $|\Gamma| = 1$, and one may define the phase of its reflection to be zero when the DUT is unshifted. Thus, one may normalize each row of $[C]$ by the reciprocal of the values in the first column of the unnormalized $[B_Q]$; that is, the rows of $[C]$ from one through four are multiplied by -1 , $1/(.193-3.6 \times 10^{-5}i)$, $1/(.193+3.6 \times 10^{-5}i)$, and $-1/.1644$ respectively. In Table 2.3 the normalized values for elements of $[B_Q]$ and $[B'_Q]$ were found with the normalized $[C]$ and show excellent agreement with expectation. In addition to the correctness of the relative amplitudes, the calculated phase shifts were found to be accurate to better than .05 degrees. The accuracy with which an unknown reflectance of a DUT can be found would be expected to be similar to the normalized values in the second row of $[B_Q]$ and $[B'_Q]$ as illustrated in Table 2.3. One may note, however, that instrumental noise has not as yet been introduced, and preliminary discussion of this will be given later.

2.6.2 Case of No Standing Waves

The preceding test results are representative of the case where significant standing waves are present due to the significant power reflectances of the source and detector. The case of a QUOSM without any standing waves can be simulated by

Table 2.3 Calculated Test Port Parameters B_Q and B'_Q for Case of Standing Waves

B_Q		TEST PORT POSITION			MATCHED LOAD
		1	2	3	
1	UNNORMALIZED	-1.000	-1.000	-1.000	-1.000
	NORMALIZED	1.000	1.000	1.000	1.000
	EXPECTED	1.000	1.000	1.000	1.000
a	UNNORMALIZED	$.193-3.6 \times 10^{-5}i$	$-.09635+.16736i$	$-.09664-.1670i$	$+1 \times 10^{-12}+2 \times 10^{-13}i$
	NORMALIZED	1.000	$-.4994+.8666i$	$-.5006-.8654i$	$+8 \times 10^{-12}+1 \times 10^{-12}i$
	EXPECTED	1.000	$-.5000+.8660i$	$-.5000-.8660i$	0.000
a*	UNNORMALIZED	$.193+3.6 \times 10^{-5}i$	$-.09635+.16736i$	$-.09664-.1670i$	$+1 \times 10^{-12}-2 \times 10^{-13}i$
	NORMALIZED	1.000	$-.4994-.8666i$	$-.5006+.8654i$	$+8 \times 10^{-12}-1 \times 10^{-12}i$
	EXPECTED	1.000	$-.5000-.8660i$	$-.5000+.8660i$	0.000
$ a ^2$	UNNORMALIZED	-.1664	-.1664	-.1664	-9×10^{-13}
	NORMALIZED	1.000	.9995	.9996	1×10^{-11}
	EXPECTED	1.000	1.000	1.000	0.000
B'_Q	UNNORMALIZED	-1.000	-1.000	-1.000	-1.000
	NORMALIZED	1.000	1.000	1.000	1.000
	EXPECTED	1.000	1.000	1.000	1.000
a'	UNNORMALIZED	$.09556+.09552i$	$-.1305+.03511i$	$.03482-.1305i$	$+1 \times 10^{-12}+2 \times 10^{-13}i$
	NORMALIZED	$.4951+.4951i$	$-.6763+.1818i$	$.1806-.6763i$	$+8 \times 10^{-12}+1 \times 10^{-12}i$
	EXPECTED	$.4950+.4950i$	$-.6761+.1812i$	$.1812-.6761i$	0.000
a'*	UNNORMALIZED	$.09556-.09552i$	$-.1305-.03511i$	$.03482+.1305i$	$+1 \times 10^{-12}-2 \times 10^{-13}i$
	NORMALIZED	$.4951-.4951i$	$-.6763-.1818i$	$.1806+.6763i$	$+8 \times 10^{-12}-1 \times 10^{-12}i$
	EXPECTED	$.4950-.4950i$	$-.6761-.1812i$	$.1812+.6761i$	0.000
$ a' ^2$	UNNORMALIZED	-.08157	-.08153	-.08154	-9×10^{-13}
	NORMALIZED	.4901	-.4901	-.4899	1×10^{-11}
	EXPECTED	.4900	.4900	.4900	0.000

setting these reflectances equal to zero so that radiation can follow only two paths through the interferometer.

A slight improvement in the precision of the eigenvalues was found when the standing waves were eliminated. Whereas agreement with expectation was good to three significant figures with standing waves, at least 10 significant figures of agreement were found with no standing waves. However, since three significant figures appear to be sufficient, this dependence on the standing waves is not particularly significant. Indeed, the root of this small inaccuracy may not be in the eigenvector method at all. When standing waves are introduced, the iterative simulation of QUOSM signals is truncated before the solution is exact, as mentioned earlier, and this corresponds to a residual inaccuracy of about five parts in 10^4 . It is not unreasonable to suppose that this would affect the eigenvector solution.

The eigenvectors for the case of no standing waves appeared at first glance to be substantially different than for the first case in which standing waves were present. However, the difference was only due to the need for normalization of the rows of $[C]$ and the fact that a different normalization was needed in the present case. By using the unnormalized results for the first column of $[B_Q]$ as in the previous example, one finds that the rows of $[C]$ in order, starting at the top, are multiplied by 1, $1/ (.4959 + 5 \times 10^{-12} i)$, $1/ (.4959 - 5 \times 10^{-12} i)$, and $-1/.2753$. Table 2.4 gives expected, unnormalized, and normalized values of the elements of both $[B_Q]$ and $[B_Q']$. Agreement between the expected and normalized values is again excellent and good to at least 10 significant figures.

2.6.3 All-dielectric shifted DUT calibration

The calibration procedures simulated above have been consistent with physical shifts of the whole DUT port, including its lens and horn, as the means of obtaining the required DUT

Table 2.4 Calculated Test Port Parameters B_Q and B'_Q for Case of No Standing Waves

B_Q		TEST PORT POSITION			MATCHED LOAD
		1	2	3	
1	UNNORMALIZED	1.000	1.000	1.000	1.000
	NORMALIZED	1.000	1.000	1.000	1.000
	EXPECTED	1.000	1.000	1.000	1.000
a	UNNORMALIZED	$.4959+5 \times 10^{-12}i$	$-.248+.4295i$	$.2480-.4295i$	$-8 \times 10^{-12}+6 \times 10^{-12}i$
	NORMALIZED	1.000	$-.5000+.8660i$	$-.5000-.8660i$	$-2 \times 10^{-11}+1 \times 10^{-11}i$
	EXPECTED	1.000	$-.5000+.8660i$	$-.5000-.8660i$	0.000
a*	UNNORMALIZED	$.4959-5 \times 10^{-12}i$	$-.248-.4295i$	$.2480+.4295i$	$-8 \times 10^{-12}-6 \times 10^{-12}i$
	NORMALIZED	1.000	$-.5000-.8660i$	$-.5000+.8660i$	$-2 \times 10^{-11}+1 \times 10^{-11}i$
	EXPECTED	1.000	$-.5000-.8660i$	$-.5000+.8660i$	0.000
$ a ^2$	UNNORMALIZED	-.2753	-.2753	-.2753	4×10^{-12}
	NORMALIZED	1.000	1.000	1.000	-2×10^{-11}
	EXPECTED	1.000	1.000	1.000	0.000
B'_Q					
1	UNNORMALIZED	1.000	1.000	1.000	1.000
	NORMALIZED	1.000	1.000	1.000	1.000
	EXPECTED	1.000	1.000	1.000	1.000
a'	UNNORMALIZED	$.2445+.2445i$	$-.3353+.08985i$	$.08985-.3353i$	$-8 \times 10^{-12}+6 \times 10^{-12}i$
	NORMALIZED	$.4950+.4950i$	$-.6761+.1812i$	$.1812-.6761i$	$-2 \times 10^{-11}+1 \times 10^{-11}i$
	EXPECTED	$.4950+.4950i$	$-.6761+.1812i$	$.1812-.6761i$	0.000
a'*	UNNORMALIZED	$.2455-.2455i$	$-.3353-.08985i$	$.08985+.3353i$	$-8 \times 10^{-12}-6 \times 10^{-12}i$
	NORMALIZED	$.4950-.4950i$	$-.6761-.1812i$	$.1812+.6761i$	$-2 \times 10^{-11}+1 \times 10^{-11}i$
	EXPECTED	$.4950-.4950i$	$-.6761-.1812i$	$.1812-.6761i$	0.000
$ a' ^2$	UNNORMALIZED	-.1349	-.1349	-.1349	4×10^{-12}
	NORMALIZED	.4900	.4900	.4900	-2×10^{-11}
	EXPECTED	.4900	.4900	.4900	0.000

port delays (indicated e.g. in Table 2.2). An alternative method mentioned earlier is to insert rigid dielectric plates of varying thicknesses between the beam splitter and the DUT port. This would allow the DUT port to remain rigidly mounted and yet accomplish the desired phase shifts.

This method has been simulated to get a preliminary assessment of its effectiveness in calibration. Table 2.5 gives the parameters of the simulation. One may note that some loss has been included in the dielectric plates used for phase shifts. Although low-loss dielectrics are available, inclusion of some loss gives the simulation greater generality. All the eigenvalues were found to be calculated correctly. Also, the values of the magnitude and phase of the reflection coefficients used to derive the calibration matrix were recovered correctly from the operation of multiplying the associated sets of power data by the normalized $[C]$. The largest error in the magnitude was 0.02%. The largest phase error was 0.07 degrees.

2.6.4 Noise

An arbitrary amount of noise has been added to the simulated power data of Section 2.6.1 and the calibration matrix recalculated. The peak-to-peak size of the noise was set at 10^{-4} compared with detected signals whose maximum values were of the order unity, and this is crudely consistent with previous discussions of expected detector noise [1] in the QUOSM. The noise used was obtained simply from the random number function incorporated in the BASIC language of the HP-85 computer. The results of premultiplying the "noisy" power data sets by the "noisy" calibration matrix are shown in Table 2.6 along with the noise-free and expected results for comparison. The effects of the noise may be seen in this table and are not of a surprising magnitude. Similar tests with varying noise amplitude have shown the expected increase in error as the noise level is increased.

Table 2.5 Parameters Used in Simulation in Which All Test Port Delays Achieved with Dielectric Plates

All parameters identical to those in Table 2.2 except that the dielectric plates used to introduce the test port delays reduce the apparent test port power reflectances. Accordingly the following are the calibration conditions corresponding to each element P_{ij} of the [P] matrix (Same key as in Table 2.2):

i	j	1	2	3	4
2		M1, D1, 1	M1, D2, .8	M1, D3, .64	M1, D1, 0
3		M2, D1, 1	M2, D2, .8	M2, D3, .64	M1, D1, 0
4		M3, D1, 1	M3, D2, .8	M3, D3, .64	M1, D1, 0

For the [P'] matrix:

i	j	1	2	3	4
2		M1, D4, .9	M1, D5, .72	M1, D6, .576	M1, D1, 0
3		M2, D4, .9	M2, D5, .72	M2, D6, .576	M2, D1, 0
4		M3, D4, .9	M3, D5, .72	M3, D6, .576	M3, D1, 0

Table 2.6 Calculated Test Port Parameters B_Q and B'_Q With and Without Noise

B_Q		TEST PORT POSITION			MATCHED LOAD
		1	2	3	
1	NOISE	1.000	1.000	1.000	.9998
	WITHOUT NOISE	1.000	1.000	1.000	1.000
	EXPECTED	1.000	1.000	1.000	1.000
a	NOISE	$1.000+1 \times 10^{-11}i$	$-.4997+.8673i$	$-.5010-.8652i$	$-1 \times 10^{-4}-2 \times 10^{-4}i$
	WITHOUT NOISE	1.000	$-.4994+.8666i$	$-.5006-.8654i$	$-1 \times 10^{-11}+2 \times 10^{-12}i$
	EXPECTED	1.000	$-.5000+.8660i$	$-.5000-.8660i$	0.000
a*	NOISE	$1.000-1 \times 10^{-12}i$	$-.4997-.8673i$	$-.5010+.8652i$	$-1 \times 10^{-4}+2 \times 10^{-4}i$
	WITHOUT NOISE	1.000	$-.4994-.8666i$	$-.5006+.8654i$	$-1 \times 10^{-11}-2 \times 10^{-12}i$
	EXPECTED	1.000	$-.5000-.8660i$	$-.5000+.8660i$	0.000
$ a ^2$	NOISE	1.000	1.000	.9995	-4×10^{-4}
	WITHOUT NOISE	1.000	.9995	.9996	3×10^{-11}
	EXPECTED	1.000	1.000	1.000	0.000
<hr/>					
B'_Q	NOISE	.9999	.9999	.9999	.9999
	WITHOUT NOISE	1.000	1.000	1.000	1.000
	EXPECTED	1.000	1.000	1.000	1.000
a'	NOISE	$.4950+.4951i$	$-.6764+.1821i$	$.1805-.6764i$	$2 \times 10^{-4}-2 \times 10^{-4}i$
	WITHOUT NOISE	$.4951+.4951i$	$-.6763+.1818i$	$.1806-.6763i$	$-1 \times 10^{-11}+2 \times 10^{-12}i$
	EXPECTED	$.4950+.4950i$	$-.6761+.1812i$	$.1812-.6761i$	0.000
a'*	NOISE	$.4950-.4951i$	$-.6764-.1821i$	$.1805+.6764i$	$2 \times 10^{-4}+2 \times 10^{-4}i$
	WITHOUT NOISE	$.4951-.4951i$	$-.6763-.1818i$	$.1806+.6763i$	$-1 \times 10^{-11}-2 \times 10^{-12}i$
	EXPECTED	$.4950-.4950i$	$-.6761-.1812i$	$.1812-.6761i$	0.000
$ a' ^2$	NOISE	.4900	.4900	.4896	-7×10^{-5}
	WITHOUT NOISE	.4901	.4898	.4899	3×10^{-11}
	EXPECTED	.4900	.4900	.4900	0.000

However, the rate of increase in the error for a given increase in noise does not indicate a pathological sensitivity to noise in the power measurements. A more systematic study of the effects of different kinds of noise and error, such as was done in earlier simulations [1], will be recommended for further work involving the eigenvector method.

3.0 Reduction of Standing Waves

Another aspect of the present study has been the investigation of ways to reduce the magnitude of standing waves. In numerical methods designed to apply a correction for an undesirable phenomenon, it is often the case that accuracy is served if the size of the phenomenon can be kept reasonably small compared to the quantity of principal interest. Such was the motivation for the tests reported in this section. These occupied only a relatively small part of the effort for two reasons. First, during the course of the work, the emphasis on the numerical methods side shifted away from an extension of the phasor method, which was used earlier and which clearly is more tractable if the standing wave phenomenon is smaller. Second, in the new eigenvector method, no assumptions appear to be necessary concerning the size of the standing wave effect. As of yet, no important relationship between uncertainty and the magnitude of the standing waves is known, but a further systematic investigation of this would be prudent. Should a reduction of standing waves be required in the future, the results discussed in the following sections will be of interest. As a by-product of this study, a preliminary evaluation of pyroelectric detectors is also reported.

3.1 Experiments with the Detector

As mentioned in Section 2.1, previous attempts [3] to suppress reflections from the Golay cell detectors, by tilting them away from the optical axis of the QUOSM, failed. The apparent reason was retroreflection by the metal surrounding the detector window or by the cavity inside the detector. Alternative pyroelectric detector elements come in a variety of packages, but the most common, shown in Figure 3.1 has the pyroelectric crystal mounted in a standard transistor can.

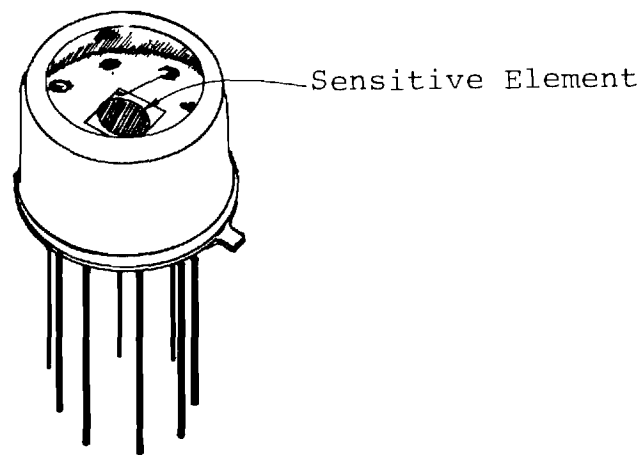


Figure 3.1 Type of Pyroelectric Detector Element Tested.

Georgia Tech-owned versions of this have been tested at a frequency of 94 GHz in the present work, and the same or slightly higher levels of standing waves were found in tests similar to those previously conducted with Golay cells. Apparently the metal can around the sensitive crystal is similarly retroreflective. Alternative forms of pyroelectric elements are commercially available in which the crystals are large discs and are not surrounded by metal. It was not in the scope of the present work to pursue this further, but such detectors may be a good choice for future systems.

What was shown in the present work is that while the pyroelectric detector has less sensitivity than a Golay cell, the signal levels available from klystron sources are high enough to offset this. Pyroelectric detectors possess the advantage of being solid-state, rugged, compact, and somewhat less expensive by comparison with Golay cells. Thus the option of using such detectors should be taken seriously for future designs. This may require some testing of several models and makes of elements, however, since they are made primarily for infrared use, and the millimeter wave performance is often poorly known by the manufacturer.

3.2 Isolation by Attenuation

It was realized that the quasi-optical attenuators [2,3] in the QUOSM could, in principle, provide a simple form of isolation. Waveguide-type isolators are neither readily available in the frequency range of the QUOSM nor well suited. Low-loss quasi-optical isolation schemes are known, for example ones involving the use of a circular polarizer [19], but they are not able to cover a wide frequency range, are not trivial to construct, and were not within the scope of the present work. Therefore, the only apparent option was to use loss as a mechanism of isolation.

Since it was found in previous work [3] that detector reflection was the primary cause of standing waves at 94 GHz, attenuation by the quasi-optical attenuator nearest the detector would be expected to reduce their magnitude. Up to 28 dB of attenuation (for a single-pass) is available from this unit [3]. For this amount the depth of modulation found in the interference pattern, when the test port was blocked by an absorber and the mirror was scanning, was only a few percent of the maximum power recorded. This may be compared with a depth of modulation of sixty percent found [3] without the attenuation. Since the klystron emits so much more power than the maximum power which the detector can handle (a factor of 10^5), such attenuation need not reduce the accuracy of the QUOSM; in other words, if the detector attenuator is not used, attenuation must be introduced at the source anyway. The problem with putting all of the required attenuation in the detector port is that this necessarily means that the power level at the test port will be high. This would be intolerable for some devices that might burn out, such as mixers for example.

Therefore one must view these results from larger perspectives. A reduction of the standing wave effects by more than an order of magnitude, while impressive, is not enough to permit one to neglect them. Secondly, the eigenvector method appears to work well enough that such drastic measures as described above are not needed, and thus it will still be possible to reduce source powers and the power to the DUT to safe levels.

4.0 Status of Hardware and Software.

In the foregoing discussion of calibration techniques, a few hardware changes or additions to the QUOSM were shown to be needed. These may be summarized as follows:

- 1) The reference detector and its beam splitter coupler must be relocated in the test port arm. The present design can readily be adapted to this configuration provided that the quasi-optical attenuator is removed from the test port arm and either omitted or moved to the source port arm. As the calibration procedure is presently understood, there is no longer a need for the attenuator in the test port arm.
- 2) A choice must be made between two alternative mechanisms of test port delays described earlier. One would require a method of translating the test port along the optical axis that preserves alignment and provides three or more reproducible positions. The other would require the selection and fabrication of some low-loss dielectric plates of appropriate thicknesses and a holder to place them reproducibly in the beam in front of the test port. Both appear to be practical but will require additional hardware to be designed and fabricated.
- 3) When during the calibration procedure the high reflectance termination is installed and the power readings for the matrix $[P']$ must be measured, a somewhat lossy dielectric slab must be mounted in front

of the test port. The arrangement for mounting would probably be similar to that in the second option on (2) above. For both cases the plate should be angled to suppress multiple reflections between the plate and other optical components.

- 4) Another high-loss absorber must be made that can block the test port beam. One similar to the type in the quasi-optical attenuators [3] is appropriate, although the type which incorporates epoxy-based material, rather than rubber-based, would probably be preferred as it is believed to give somewhat more absorption [3]. Attenuation values of 40db are believed possible.

None of these new requirements have been implemented. No problems of feasibility have been identified, but some further design work should be done to establish the best alternative in (2) and to work out the details for each of the items. The only new hardware items added in the present work have been two new horns made for use with WR-10 components.

All of the software is at present in an experimental state and requires considerable operator attention and involvement. The longest program EIGEN occupies 22,244 bytes out of the available 30,219 bytes in the HP-85. The running time for this program is dominated by the time for diagnostic printing of numerous intermediate calculations. Without input-output, the calibration calculations take approximately 30 seconds. As mentioned earlier, neither the program contents nor the run-time have been streamlined. Further work on this is envisioned along with efforts to structure the programs for ease of use.

5.0 Summary

There have been a number of significant accomplishments in the present work, such as the following:

1. A program has been developed that simulates the phenomenon of standing waves in the QUOSM and has provided tests of new calibration procedures.
2. A method of calibration previously developed for use with six-port network analyzers has been shown to be adaptable for use with the QUOSM. The calibration devices needed are a standard short, two standard matched loads (one quasi-optical), and two uncalibrated terminations along with a mechanism for creating reproducible delays in the test port arm of the QUOSM. Proposed implementations of each of the new requirements have been briefly described and in many cases differ from previous implementations with six-port network analyzers. Quasi-optical techniques are stressed here as they are likely to offer advantages of greater accuracy and ease of use and fabrication throughout the frequency range of the QUOSM. For example, there is relatively greater facility with the QUOSM for establishing the phase relationships between the source and reflected signals which are believed to be optimum [4, 6].
3. Numerical techniques for calculating eigenvectors have been implemented as an integral part of the calibration procedure which ultimately defines the relationship between recorded detector signals and the reflection parameters of a device under test. Simulated data have been used to show that the recommended optical and numerical procedures together provide a valid calibration, whether or not standing waves exist in the QUOSM. Very preliminary

investigations with simulated instrumental noise have found no pathological sensitivities to noise in the numerical methods employed.

4. Not of primary importance, but of some significance, have been the efforts to reduce the magnitude of standing waves. As expected the quasi-optical attenuators in the QUOSM can provide crude isolation and reductions in standing wave effects. Tests with pyroelectric detectors were significant in demonstrating that they can have adequate sensitivity, but the type tested did not reduce VSWR from the detector. Nonetheless, their smaller, more rugged construction make them desirable in future systems similar to the QUOSM.

6.0 Future Work

It is Georgia Tech's desire to continue to work on the QUOSM network analyzer in order to make necessary modifications and to carry out thorough tests involving further simulations and measurements. It is believed that this is justified by the indications of success thus far achieved and by the continuing need for network analyzers operating in the 90-340 GHz range. The need by the Army and the Army's contractors to test discrete millimeter wave components may be expected to continue for several years since millimeter wave intergrated circuits still require considerable research and development before they will have a dominant role in systems. The advantages of a quasi-optical metrology instrument are still extremely attractive; namely, ease of fabrication and use, and possibly greater accuracy since the fabrication requirements are not subject as much to compromise.

Some specific steps that would be proposed are the following:

- 1) Study the sensitivity of the QUOSM to the effects of noise and known errors through the use of more detailed simulations. This would include but not be limited to the effects of detector non-linearity as well as noise, of uncertainty in mirror position, and of imperfect calibration loads. In addition, cases of varying amounts of standing waves and varying test device parameters would be investigated. Any factors which may be postulated to improve accuracy will be tested.
- 2) Make selections among alternatives, develop detailed designs, and implement the hardware additions and changes necessary for the new calibration procedure. These items were listed in Section 4.0. In general, new hardware would be as compatible as possible with the present breadboard approach to the QUOSM; no major overhaul of the format is envisioned until a thorough test has been completed.
- 3) Write software that will efficiently accomplish measurements and calibration and that can be readily operated by the staff of the TMDE Support Group.
- 4) Conduct fairly extensive measurements of test devices to be agreed with the sponsor. In addition, tests can be devised to elucidate typical amounts of reflections from flange connections. Flange reflections are recognized as a greater problem for systems operating in the short millimeter wavelength range, and demonstration of such effects would be a useful beginning with the QUOSM.

When a single QUOSM has been demonstrated to work as a reliable reflectometer, it is envisioned that a dual-QUOSM system can be designed, analogous to dual six-port systems, that will permit devices to be tested both for their reflection and transmission properties. The simulation and numerical analysis tools developed in the present program can contribute to the planning and design of such a system.

7.0 References

1. R. A. Bohlander, A. McSweeney, and R. G. Shackelford, "Quasi-Optical Scanning Multiport (QUOSM) Network Analyzer," Interim Report No. 1, GT/Project A-2751, Contract DAAH01-80-C-1634, U.S. Army Missile Command (13 April 1981).
2. R. A. Bohlander, A. McSweeney, J. M. Newton, V. T. Brady, and R. G. Shackelford, "Quasi-Optical Scanning Multiport (QUOSM) Network Analyzer," Interim Report No. 2, GT/Project A-2751, Contract DAAH01-80-C-1634, U.S. Army Missile Command (23 September 1981).
3. R. A. Bohlander, A. McSweeney, V. T. Brady, O. A. Simpson, and R. G. Shackelford, "Quasi-Optical Scanning Multiport (QUOSM) Network Analyzer," Final Report, GT/Project A-2751, Contract No. DAAH01-80-C-1634, U.S. Army Missile Command (26 April 1982).
4. G. F. Engen, "The Six-Port Reflectometer: An Alternative Network Analyzer," IEEE Trans. Microwave Theory and Techniques, MTT-25, 1075-80 (1977).
5. See for example, S. Y. Liao, Microwave Devices and Circuits, Englewood Cliffs, New Jersey: Prentice-Hall, Inc. (1980).
6. H. M. Cronson and L. Susman, "Automated Six-Port Microwave Calibration System," Final Technical Report SCRC-CR-77-32, Contract No. DAAH01-75-C-1112, U.S. Army Missile Command (April 1977).
7. H. M. Cronson and L. Susman, "Dual Six-Port Microwave Calibration System," Interim Report SCRC-CR-78-12, Contract No. DAAH01-77-C-0693, U.S. Army Missile Command (March 1978).
8. S. D. Conte and C. deBoor, Elementary Numerical Analysis: An Algorithmic Approach, New York: McGraw-Hill Book Co. pp.166-167 (1980).
9. Hewlett-Packard, "HP-85 Matrix ROM Manual," Manual No. 00085-90144, p. 33 (1980).
10. J. H. Wilkinson and C. Reinsch, Linear Algebra, Berlin: Springer Verlag, pp. 191-201 (1971).
11. J. H. Wilkinson, "Calculation of Eigensystems of Matrices," in Numerical Analysis, an Introduction, J. Walsh ed., Washington, D.C.: Thompson Book Co., pp. 27-61 (1967).
12. J. H. Wilkinson, The Algebraic Eigenvalue Problem, Oxford: Clarendon Press (1965).
13. J. Grad and M. A. Brebner, "Eigenvalues and Eigenvectors of a Real General Matrix," Algorithm 343, Comm. ACM 11, 820-26 (Dec. 1968).

14. H. D. Knoble, "Certification of Algorithm 343 [F1] Eigenvalues and Eigenvectors of a Real General Matrix," Comm. ACM 13, 122-4 (Feb. 1970).
15. W. Knight and W. Mersereau "Certification of Algorithm 343 [F1] Eigenvalues and Eigenvectors of a Real General Matrix" Collected Algorithms from CACM, 343-P8-R1 (1970).
16. H. Niessner, "Remark on Algorithm 343 [F2], Collected Algorithms from CACM, 343-P9-R1 (1971).
17. B. Noble, Applied Linear Algebra, Englewood Cliffs, New Jersey: Prentice-Hall, Inc., p. 280 (1969).
18. G. W. Chantry, Submillimetre Spectroscopy, London: Academic Press, pp. 317-319 (1971).
19. R. W. McMillan, R. A. Bohlander, D. S. Ladd, R. E. Forsythe, A. McSweeney, J. M. Newton, O. A. Simpson, M. J. Sinclair, and J. C. Butterworth, "Near Millimeter Wave Radar Technology," Vol. 1, Interim Technical Report Phase III, GT/Project A-2445, Contract No. DAAK70-79-C-0108, U.S. Army Mobility Equipment and Development Command, Night Vision and Electro-Optics Laboratory (11 October 1982).

Appendix A. Software to Simulate QUOSM Signals Including the
Effects of Standing Waves

An annotated copy of the program RFLTCN, described in the
text follows. It occupies 9,690 bytes of memory.

PROGRAM NAME: RFLCTN

```

100 REM This program calculates
110 REM the signal at the photo-
120 REM diode detector of the
130 REM Quasi-Optical Scanning
140 REM Multipoint network ana-
150 REM lyzer
160 REM it takes into account
170 REM any number of reflect-
180 REM ions through the
190 REM system.
200 OPTION BASE 1
210 DIM R(41),S(41),X(41),T(41)
220 DIM D(4)
222 D(4)=1
225 DATA 0,60,120
230 CLEAR @ PRINT
240 N9=3 : # DATA PTS. <42
250 PRINT "# MIRROR POSITIONS: "
      N9
260 CLEAR @ PRINT
270 DISP "Insert CASSETTE for da-
      ta."
280 DISP "It must be set to RECO-
      RD."
290 DISP
300 DISP "Type CREATE 'name--' N
      '8#'"
305 DISP "where N is Number col-
      le e. 12"
310 DISP "and # is # of mirror p-
      ositions."
320 DISP "Press CONT when ready."
      "
330 PAUSE
340 CLEAR @ PRINT
350 DISP "Enter FILE NAME:"
360 DISP "( 1-6 characters )"
370 INPUT F#
380 PRINT "File name: " F#
390 L6=200 ! (mm) SOURCE to E.S.
400 T6=1 ! SQR amp xmtn. SOURCE
410 L3=200 ! (mm) DET to E.S.
420 T3=1 ! SQR amp xmtn. DET
430 L4=200 ! (mm) E.S. to OUT
440 T4=1 ! SQR amp xmtn. OUT
450 L5=200 ! (mm) B.S. to MIRROR
460 T5=1 ! SQR amp xmtn. MIRROR
470 CLEAR @ PRINT
480 PRINT @ PRINT @ PRINT
490 DISP "Enter SOURCE"
500 DISP "POWER reflectivity:"
510 DISP "( 0 < R < 1 )"
520 INPUT R5
530 S9=1-R5 ! SOURCE PWR xmtn
540 PRINT "SOURCE powr reflectivi-
      ty:"
550 PRINT R5
560 L=-SQR(R5) @ M=0
570 CLEAR @ PRINT
580 DISP "Enter DETECTOR"

```

Preset shifts of mirror in degrees
(i.e., 1 wavelength=360°)
Set number of mirror positions

Load tape to receive data

Create data file

Set distances between optical
components LX
Set the one-way amplitude trans-
mission factor between optical
components TX

Enter power reflectance of source

Enter power reflectance of detector

```

590 DISP "POWER reflectivity:"
600 DISP "(0.0 < R < 1.0)"
610 INPUT R5
620 Q9=1-R5 ! DET. PWR XMTN
630 PRINT "DET. power reflectivi
ty:"
640 PRINT R6
650 A=-SQRT(P6) @ B=0
660 CLEAR @ PRINT
670 DISP "Enter value for FREQ.(
GHz):"
680 DISP "(e.g. 90-340 GHz)"
690 INPUT F
700 PRINT "FREQ.=":F:"GHz"
710 L1=300/F
720 PRINT "Wavelength=":L1:"mm"
730 DEF FNF(L) = 2*PI*FP(L)/L1
740 F8=FNF(L6)
750 G6=T6*COB(F6) @ H6=-T6*SIN(F
6)
760 F3=FNF(L3)
770 G3=T3*COB(F3) @ H3=-T3*SIN(F
3)
780 F4=FNF(L4)
790 G4=T4*COB(F4) @ H4=-T4*SIN(F
4)
800 F5=FNF(L5)
810 G5=T5*COB(F5) @ H5=-T5*SIN(F
5)
820 CLEAR @ PRINT
830 DISP "Enter value for beamspl
itter"
840 DISP "THICKNESS (mils)"
850 DISP "(25.4 micron = 1 mil)"
860 INPUT T
870 PRINT "Beamsplitter thicknes
s:"
880 PRINT T:"mils"
890 CLEAR @ PRINT
900 GOSUB 2570 ! Calc.B.S. R&T
910 CLEAR @ PRINT
920 DISP "Enter complex number p
air"
930 DISP "in POLAR form (R,ANGLE
in DEG)"
940 DISP "for OUT reflect. coeff
"
950 DISP "(e.g. 1 0.0)"
960 INPUT G,H
970 PRINT "Polar OUT reflect.coe
ff.:"
980 PRINT G,H
990 H=H*PI/180
1000 RAD
1010 J=G*COB(H) @ K=G*SIN(H)
1020 PRINT "Rect. OUT reflect.co
eff.:"
1030 PRINT J,K
1040 CLEAR @ PRINT
1050 DISP "Enter OUT OFFSET (deg
)"

```

Enter Frequency (GHz)

Calculate Wavelength in mm

Convert each distance between optical components to FX radians. Then compute the factor $(GX, I = TX \exp(-i FX))$ by which a signal phasor changes in traveling between the optical components.

Enter beam splitter thickness

Calculate beam splitter complex reflection and transmission amplitude factors.

Enter magnitude of DUT amplitude reflectance and the angle by which the wave is delayed on reflection.

Enter half the delay (in degrees) caused by off-setting the test port from its initial position.

1060 INPUT F7	
1070 PRINT "OUT OFFSET: ".F7 "deg"	
1080 F7=F7*PI/180	Convert to radians-F7
1090 G7=COS(F7) @ H7=-SIN(F7)	Calculate exp(-iF7)
1100 CLEAR @ PRINT	
1110 DISP "Enter MIRROR offset (deg)."	
1120 INPUT M0	
1130 PRINT "MIRROR OFFSET: ".M0:"deg."	Enter any change desired in the mirror starting position, and convert to radians.
1140 M0=M0*PI/180	Read shift of mirror position.
1145 RESTORE	
1150 FOR I=1 TO N9	
1160 READ S	
1170 I1=1 @ CLEAR	
1180 ! MIRROR PHASE	
1200 S=2*S*PI/180+PI+M0	Calculate delay S in radians caused by shift in mirror position and by reflection from mirror.
1210 N=COS(S)	
1220 O=SIN(S)	
1230 U0=0 @ S0=0	Initialize
1240 U0=0 @ U1=0	
1250 CLEAR	
1260 REM From SOURCE	Initial signal from source Amplitude V:REAL
1270 V=1*SOR(S9) @ W=0	W:IMAG
1280 REM From DETECTOR	Initial signal from detector Amplitude X:REAL
1290 X=0 @ Y=0	Y:IMAG
1300 V0=1*SOR(R5/S9) @ W0=0	Initial signal reflected back into source
1310 X0=0 @ Y0=0	Initial signal reflected back into detector
1320 ! SOURCE-BS phase	START OF ITERATIVE PROCEDURE
1330 P=V @ Q=W	
1340 V=P*G5-Q*H5 @ W=P*H5+Q*G5	Calculate change in signal propagating from source and detector to B.S.
1350 ! DET.-BS phase	
1360 P=X @ Q=Y	
1370 X=P*G3-Q*H3 @ Y=P*H3+Q*G3	
1380 DISP I, I1	
1390 REM From BEAMSPLITTER:	Transmission through and reflection from B.S.
1400 GOSUB 3000 ! *B.S. R & T	
1410 ! From B.S. to OUT:	
1420 P=U1+X1 @ Q=W1+Y1	Combination of signals going to DUT
1430 ! Phase shift, BS TO DUT	
1440 V=P*G4-Q*H4 @ W=P*H4+Q*G4	
1450 ! Accumulated vector @ DUT	
1460 U0=U0+V @ U1=U1+W	Signal accumulated that impinges on DUT.
1470 ! Power at DUT.	DUT power calculated. (Used as REF. Detector Signal)
1480 P9=U0^2+U1^2	Propagation through DUT offset
1490 ! Prop thru DUT OFFSET	
1500 P=V*G7-W*H7 @ Q=V*H7+W*G7	Propagation through DUT offset
1510 ! Signal reflected by OUT:	Calculate effects of DUT reflection
1520 V=P*J-Q*K @ W=P*K+Q*J	
1530 ! Prop thru DUT OFFSET	
1540 P=V*G7-W*H7 @ Q=V*H7+W*G7	Propagation back through DUT offset
1550 ! Phase shift, DUT to BS:	Propagation back to Beam Splitter
1560 V=P*G4-Q*H4 @ W=P*H4+Q*G4	
1570 ! From BS to MIRROR:	Combination of signals going to mirror
1580 P=U2+X2 @ Q=W2+Y2	
1590 ! Phase shift, BS to MIRROR	Propagation to normal mirror starting position
1600 X=P*G5-Q*H5 @ Y=P*H5+Q*G5	
1610 ! Reflect from MIRROR:	
1620 P=X*N-Y*O @ Q=X*O+Y*N	Combined effect of reflection from mirror and mirror shift.

```

1630 ! Phase shift, MIRROR to BS
1640 X=P*G5-Q*H5 @ Y=P*H5+Q*G5
1650 REM From BEAMSPLITTER:
1660 GOSUB 3000 ! *B.S. R & T
1670 REM To SOURCE:
1680 P=V1+X1 @ Q=W1+Y1
1690 ! Phase shift, BS to SOURCE
1700 V=P*G6-Q*H6 @ W=P*H6+Q*G6
1710 REM To DETECTOR:
1720 P=V2+X2 @ Q=W2+Y2
1730 ! Phase shift, BS to DET.
1740 X=P*G3-Q*H3 @ Y=P*H3+Q*G3
1750 V0=V0+V @ W0=W0+W
1760 X0=X0+X @ Y0=Y0+Y
1770 P=V0^2+W0^2 ! Pwr to SOURCE
1780 P=S9*P
1790 Q=X0^2+Y0^2 ! Pwr to DET.
1800 Q=D9*Q
1810 D2=Q @ S2=P ! Save PWR val
1820 P=V @ Q=W
1830 ! From SOURCE:
1840 V=P*L-Q*M @ W=Q*L+P*M
1850 P=X @ Q=Y
1860 ! From DETECTOR:
1870 X=P*A-Q*B @ Y=Q*A+P*B
1880 I1=I1+1
1890 IF D2<>0 THEN 1920
1900 IF Q0<>0 THEN 1920
1910 GOTO 1950
1920 E=ABS(D2-Q0)/((D2+Q0)/2)
1930 IF E<.0005 THEN 1950
1940 Q0=D2 @ S0=S2 @ GOTO 1330
1950 IF S2<>0 THEN 1980
1960 IF S0<>0 THEN 1980
1970 GOTO 2010
1980 E=ABS(S2-S0)/((S2+S0)/2)
1990 IF E<.0005 THEN 2010
2000 GOTO 1940
2010 D(I)=D2 @ S(I)=S2 ! D&S PWR
2020 T(I)=D2+S2 ! DET+SOURCE PWR
2030 R(I)=P9
2040 NEXT I
2050 GOTO 2090
2060 PRINT
2070 PRINT "DET+SOURCE power:"
2080 GOSUB 3060 ! Plot TOTAL Pwr
2090 FOR I=1 TO N9 @ T(I)=D(I)/R
(I)
2100 NEXT I
2110 PRINT
2120 PRINT " NORM DETECTOR power
:"
2130 GOSUB 3060 ! Plot DET pwr.
2140 CLEAR @ PRINT
2150 DISP "Instal CASSETTE for d
ata "
2160 DISP
2170 DISP "Enter RECORD NUMBER."
2180 DISP "(0-8, 0=do NOT save)"
2190 INPUT R9

```

Return propagation to B.S.

Transmission through and reflection from B.S.

Combination of signals going to source- followed by propagation

Combination of signals going to detector- followed by propagation

Accumulation of signal returning to source and to detector

Calculation of powers

Save power values for convergence test

Calculate complex amplitudes reflected by source and detector.

Increment iteration counter

Convergence tests

If not converged, do next iteration

Further convergence tests

Save detector and power back to source

Save sum of these

Save power impinging on DUT.

Plot total power normalized by DUT power

Plot normalized detector power

The [P] and [P'] matrices are stored in the same file. The [P] matrix occupies record 1-m of the file, and [P'], records m+1 through 2m (where m defined in Section 2.3.1)

```

2200 PRINT "RECORD # " : R9
2210 IF R9=0 THEN 2300
2220 FOR I=1 TO N9
2230 D(I)=D(I)/R(I)
2240 PRINT I:D(I)
2250 NEXT I
2255 PRINT 4:D(4)
2260 ASSIGN# 1 TO F$
2270 PRINT# 1,R9 : D()
2280 ASSIGN# 1 TO *
2290 GOTO 2400
2300 FOR I=1 TO N9 @ T(I)=S(I)
2310 NEXT I
2320 PRINT
2330 PRINT "SOURCE power:"
2340 GOSUB 3060 ! Plot SOURCE
2350 FOR I=1 TO N9 @ T(I)=R(I)
2360 NEXT I
2370 PRINT
2380 PRINT "DUT power:"
2390 GOSUB 3060 ! Plot DUT
2400 CLEAR @ PRINT
2410 DISP "New MIRROR offset? 1=
YES"
2420 INPUT C
2430 IF C=1 THEN 1100 ! END
2440 CLEAR
2450 DISP "New DUT? 1=YES"
2460 INPUT C
2470 IF C=1 THEN 910
2480 CLEAR
2490 DISP "New FREQUENCY? 1=YES"
2500 INPUT C
2510 IF C=1 THEN 660
2520 CLEAR
2530 DISP "New DETECTOR? 1=YES"
2540 INPUT C
2550 IF C=1 THEN 570
2560 GOTO 470 ! New SOURCE
2570 REM Subroutine to calculate
2580 REM complex beamsplitter
2590 REM reflection & xmtn
2600 REM amplitude coefficients
2610 RAD
2620 N1=1.0003
2630 N2=1.7
2640 U=PI/4
2650 C1=COS(ASN(SIN(U)*N1/N2))
2660 REM Wavenumber (mils-1)
2670 N3=10*2.54/(1000*L1)
2680 D2=4*PI*N2*T*N3*C1
2690 C0=COS(U)
2700 R4=(N1*C0-N2*C1)/(N1*C0+N2*
C1)
2710 C2=COS(D2)
2720 S3=SIN(D2/2)*(1+R4^2)
2730 C3=COS(D2/2)*(1-R4^2)
2740 Z1=2*R4^2*(1-C2)
2750 Z2=1-2*R4^2*C2+R4^4
2760 Z6=-SIN(D2)*(1-R4^2)

```

Record normalized detector signals

Plot power returned to source

Plot power impinging on DUT

This section prepares the operator to use RFLCTN again and change only one or a few of the parameters.

The usual thing with the new calibration procedure is to set a new DUT offset and/or new DUT reflection parameters and calculate a new column of the [P] or [P'] matrices.

Subroutine to calculate beam splitter complex transmission and reflection coefficients. See text for reference.

```

2770 Z7=(1-C2)*(1+R4^2)
2780 Z8=ATN2(Z6,Z7)
2790 Z4=(1-R4^2)^2
2800 Z8=R4^2*SIN(D2)
2810 Z9=1-R4^2*C2
2820 Z5=ATN2(Z8,Z9)
2830 R1=-SQR(Z1/Z2)*COS(Z3)
2840 R2=-SQR(Z1/Z2)*SIN(Z3)
2850 T1=SQR(Z4/Z2)*COS(D2/2+Z5)
2860 T2=SQR(Z4/Z2)*SIN(D2/2+Z5)
2870 A3=PI-ATN2(C3,S3)
2880 A4=ATN2(S3,C3)
2890 PRINT "Complex refl. coeff.
:"
2900 PRINT R1,R2
2910 PRINT "Complex xmtn. coeff
:"
2920 PRINT T1,T2
2930 PRINT "Reflectivity:"
2940 PRINT R1^2+R2^2
2950 PRINT "Transmissivity:"
2960 PRINT T1^2+T2^2
2970 PRINT "REFL. PHASE= ";A3;" R
ADIANS"
2980 PRINT "TRANS. PHASE= ";A4;"
ADIANS"
2990 RETURN ! To approx. 830
3000 REM From beamsplitter.
3010 V1=T1*W-T2*W @ W1=T1*W+T2*W
3020 V2=R1*W-R2*W @ W2=R1*W+R2*W
3030 X1=R1*X-R2*Y @ Y1=R1*Y+R2*X
3040 X2=T1*X-T2*Y @ Y2=T1*Y+T2*X
3050 RETURN
3060 ! This subroutine PLOTS
3070 ! data in array T(I)
3080 PEN 1 @ GOCLEAR
3090 SCALE 0,400,0,1.2
3100 XAXIS 0,45,0,400
3110 YAXIS 0, 1,0,1
3120 XAXIS 1 2,45,0,400
3130 YAXIS 400, 1,0,1
3140 MOVE 0,T(1)
3150 FOR I=1 TO N9
3160 DRAW 360/N9*(I-1),T(I)
3170 NEXT I
3180 BEEP @ PRINT
3190 PAUSE
3200 RETURN
3210 CLEAR @ PRINT
3220 DISP "THE END"
3230 PRINT "THE END"
3240 END
4546 PLIST 1160,1190

```

Return to 900

Subroutine that applies B.S. complex transmission and reflection factors to signals impinging on it.

Return

Subroutine for graph plots on screen

Pause to copy to paper; if desired press "COPY" key, then press "CONTINUE".

Appendix B. Software to Calculate Eigenvalues and Eigenvectors
for Calibrating the QUOSM

An annotated copy of the program EIGEN, described in the text, follows. It occupies 22,244 bytes of memory and has a run time of about thirty seconds apart from all input/output operations.

PROGRAM NAME: EIGEN

```

100 OPTION BASE 1
110 INTEGER IS
120 DIM A(4,4),B(4,4),D(4),E(4)
130 DIM F(4),H(4,4),I(4),J(4)
140 DIM L(100),P(4,4),Q(4),R(4)
150 DIM S(4),T(4,4),V(4,4)
160 DIM W(4),X(4,4),Y(4,4),Z(4,4)
170 CLEAR @ PRINT
180 BEEP
190 DISP "Insert DATA cartridge."
200 DISP
210 DISP "Enter data FILE NAME:"
220 INPUT F$
230 PRINT "File name: ";F$
240 ASSIGN# 1 TO F$
250 FOR J=1 TO 4
260 READ# 1,J ; D()
270 FOR I=1 TO 4
280 P(I,J)=D(I)
290 NEXT I
300 NEXT J
310 FOR J=5 TO 8
320 K=J-4
330 READ# 1,J ; D()
335 FOR I=1 TO 4
340 B(I,K)=D(I)
350 NEXT I
360 NEXT J
390 ASSIGN# 1 TO *
400 CLEAR @ PRINT
410 PRINT "Matrix P:" @ PRINT
420 FOR J=1 TO 4
430 FOR I=1 TO 4
440 PRINT I;J:P(I,J)
450 NEXT I
460 PRINT
470 NEXT J
480 PRINT @ PRINT
490 PRINT "Matrix P':"
500 PRINT
510 FOR J=1 TO 4
520 FOR I=1 TO 4
530 PRINT I;J:B(I,J)
540 NEXT I
550 PRINT
560 NEXT J
570 CLEAR @ PRINT
580 DISP "CALCULATING"
590 MAT T=TRN(P) ! P transpose
600 MAT Y=P*T ! P*Pt
605 D1=DET(Y)
610 MAT X=B*T ! P'*Pt
611 MAT Y=TRN(Y)
612 MAT X=TRN(X)
613 PRINT @ PRINT "(PPt)*(PPt)in
v" @ PRINT
614 MAT P=Y
615 MAT H=SYS(Y,P)

```

Enter name of file containing matrices [P]
and [P']

Read matrices column by column

Print matrix [P] column by column

Print matrix [P'] column by column

```

616 MAT H=TRN(A) ! H=(PPt)*A*(PPt)
    inv
617 MAT PRINT USING "MD.E.X" ; H
618 PRINT
630 MAT A=SYS(Y,X) ! TRANS(P'Pt)
    *(PPt)inv
660 MAT Z=A
662 PRINT
663 PRINT "Matrix A:"
664 PRINT
666 MAT PRINT USING "MD.DDE.2X"
    ; A
668 PRINT
670 D2=DET(A)
680 PRINT "D1=":D1
681 T=0
682 FOR I=1 TO 4
683 T=T+A(I,I)
684 NEXT I
685 PRINT "TRACE A:";T
690 PRINT "DET A:";D2
700 T=39
710 N=4
720 GOSUB 890
730 CLEAR @ PRINT
740 PRINT "STATUS INFO:"
750 MAT PRINT COL @/
760 CLEAR @ PRINT
770 PRINT "REAL EigenVALUES:"
780 MAT PRINT R/
790 CLEAR @ PRINT
800 PRINT "IMAG. EigenVALUES:"
810 MAT PRINT I/
811 CLEAR @ PRINT
812 R=0 @ C=0
813 FOR I=1 TO N
814 R=R+R(I) @ C=C+I(I)
815 NEXT I
816 PRINT "SUM of eigenVALUES:"
817 PRINT R;"1";C
818 CLEAR @ PRINT
819 R=1 @ C=0
820 FOR I=1 TO N @ A=R @ B=C
821 R=A*R(I)-B*I(I)
822 C=A*I(I)+B*R(I)
823 NEXT I
824 PRINT "PROD. of eigenVALUES:"
    "
825 PRINT R;"1";C
826 CLEAR @ PRINT
830 PRINT "REAL part of vectors:"
    "
840 MAT PRINT COL W/
850 CLEAR @ PRINT
860 PRINT "IMAG. part of vectors:"
    "
870 MAT PRINT COL H/
880 GOTO 8010

```

Calculation of matrix $[z^t]$

Print it

Print determinant of $[P][P^t]$ to show it is not singular
 Print trace and determinant of $[z^t]$ for 1 comparison with sum of its eigenvalues, and with eigenvectors.

Go to Eigensolution subroutine written by Grad and Brebner with modifications suggested by Niessner. (See text for references).

Print eigenvalues

Print sum of eigenvalues

Print product of eigenvalues

Print eigenvectors

Skip over EIGENP and continue program at statement 8010.

```

890 REM SUBROUTINE EIGENP
900 IF N<1 THEN 970
910 R(1)=A(1,1)
920 I(1)=0
930 W(1,1)=1
940 H(1,1)=0
950 Q(1)=2
960 RETURN ! FROM SUBROUTINE EIG
ENP
970 GOSUB 2260 ! CALL SCALE FROM
EIGENP
980 REM COMPUTE EIGENVALUES OF N
ORMALIZED MATRIX
990 E3=EXP(-T*LOG(2))
1000 GOSUB 2740 ! CALL HESOR
1010 ! POSSIBLE DECOMP OF UPPER
HESS MATRIX INTO SUBMATRICE
S OF LOWER ORDER IS INDICAT
ED IN
1020 ! ARRAY L( ), DECOMP. OCCUR
S WHEN SOME SUBDIAG. ELEMENT
S ARE IN MODULUS <EQ.
1030 ! THIS DIMINISHES EIGENVECT
OR WORK
1040 J=N
1050 I=1
1060 L(1)=1
1070 IF J=1 THEN 1150
1080 IF ABS(S(J-1))>E0 THEN 1110
1090 I=I+1
1100 L(I)=0
1110 J=J-1
1120 L(I)=L(I)+1
1130 IF J<>1 THEN 1080
1140 REM EIGENVECTOR PROBLEM
1150 K4=1
1160 K0=0
1170 L4=L(1)
1180 M=N
1190 FOR I4=1 TO N
1200 I0=N-I4+1
1210 IF I4<=L4 THEN 1250
1220 K4=K4+1
1230 M=N-L4
1240 L4=L4+L(K4)
1250 IF Q(I0)=0 THEN 1440
1260 IF I(I0)<>0 THEN 1390
1270 ! TRANSFER UPPER-HESS MAT O
F ORDER M FROM ARRAYS H AND
S INTO A
1280 FOR K1=1 TO M
1290 FOR L1=K1 TO M
1300 A(K1,L1)=H(K1,L1)
1310 NEXT L1
1320 IF K1=1 THEN 1340
1330 A(K1,K1-1)=S(K1-1)
1340 NEXT K1
1350 ! COMPUTATION OF REAL EIGEN
VECTOR I0 OF UPPER-HESS MAT
RIX CORRESP TO EIGENVALUE R
(I0)
1360 GOSUB 4860 ! CALL REALVE
1370 GOTO 1440
1380 ! COMPUTATION OF COMPLEX EI
GENVECTOR I0 OF UPPER-HESS
CORRESP. TO COMPLEX EIGENVA
LUE W(I0)
1390 IF K0<>0 THEN 1430
1400 K0=1
1410 GOSUB 5960 ! CALL COMPE
1420 GOTO 1440
1430 K0=0
1440 NEXT I4
1450 ! RECONSTRUCTION OF MATRIX
USED IN REDUCTION OF MATRIX
A TO UPPER-HESS FORM BY HO
USEHOLDER
1460 ! METHOD
1470 MAT A=IDN
1480 IF N<=2 THEN 1640
1490 M=N-2
1500 FOR K=1 TO M
1510 L=K+1
1520 FOR J=2 TO N
1530 D1=0
1540 FOR I=L TO N
1550 D2=H(I,K)
1560 D1=D1+D2*A(J,I)
1570 NEXT I
1580 FOR I=L TO N
1590 A(J,I)=A(J,I)-H(I,K)*D1
1600 NEXT I
1610 NEXT J
1620 NEXT K
1630 ! COMPUTATION OF EIGENVECTO
RS OF ORIGINAL NON-SCALED M
ATRIX
1640 K0=1
1650 FOR I=1 TO N
1660 I8=Q(I)-1
1670 IF I8<0 THEN 2240
1680 L=0
1690 IF I(I)=0 THEN 1740
1700 L=1
1710 IF K0=0 THEN 1740
1720 K0=0
1730 GOTO 2240
1740 IF I8<0 THEN 2240
1750 IF I8>0 THEN 1780
1760 IF L=0 THEN 2000
1770 IF L<>0 THEN 2190
1780 FOR J=1 TO N
1790 D1=0 @ D2=0
1800 FOR K=1 TO N
1810 D3=A(J,K)
1820 D1=D1+D3*V(K,I)
1830 IF L=0 THEN 1850
1840 D2=D2+D3*V(K,I-1)
1850 NEXT K
1860 W(J)=D1/F(J)
1870 IF L=0 THEN 1890

```

```

1880 S(J)=D2/F(J)
1890 NEXT J
1900 ! NORMALIZATION OF EIGENVECTORS AND COMPUTATION OF ORIGINAL NONNORM MATRIX
1910 IF L=1 THEN 2020
1920 D1=0
1930 FOR M=1 TO N
1940 D1=D1+W(M)^2
1950 NEXT M
1960 D1=SQR(D1)
1970 FOR M=1 TO N
1980 H(M,I)=0 @ W(M,I)=W(M)/D1
1990 NEXT M
2000 R(I)=R(I)*E2
2010 GOTO 2240
2020 R=0
2030 FOR J=1 TO N
2040 R1=W(J)^2+S(J)^2
2050 IF R>R1 THEN 2080
2060 R=R1
2070 L=J
2080 NEXT J
2090 D3=W(L)
2100 R1=S(L)
2110 FOR J=1 TO N
2120 D1=W(J)
2130 D2=S(J)
2140 W(J,I)=(D1*D3+D2*R1)/R
2150 H(J,I)=(D2*D3-D1*R1)/R
2160 W(J,I-1)=W(J,I)
2170 H(J,I-1)=-H(J,I)
2180 NEXT J
2190 K0=1
2200 R(I)=R(I)*E2
2210 R(I-1)=R(I)
2220 I(I)=I(I)*E2
2230 I(I-1)=-I(I)
2240 NEXT I
2250 RETURN ! FROM SUBROUTINE EI
GENF
2260 MAT H=R ! SUBROUTINE SCALE
2270 MAT F=(1)
2280 B1=.75
2290 B2=1.33
2300 I1=0
2310 C1=0
2320 FOR I=1 TO N
2330 C2=0
2340 C3=0
2350 FOR J=1 TO N
2360 IF I=J THEN 2390
2370 C2=C2+ABS(A(J,I))
2380 C3=C3+ABS(A(I,J))
2390 NEXT J
2400 IF C2=0 THEN 2450
2410 IF C3=0 THEN 2450
2420 Q=C2/C3
2430 IF Q<B1 THEN 2470
2440 IF Q>B2 THEN 2470
2450 C1=C1+1
2460 GOTO 2540
2470 F1=SQR(Q)
2480 FOR J=1 TO N
2490 IF I=J THEN 2520
2500 A(I,J)=A(I,J)*F1
2510 A(J,I)=A(J,I)/F1
2520 NEXT J
2530 F(I)=F(I)*F1
2540 NEXT I
2550 I1=I1+1
2560 IF I1>30 THEN 2700
2570 IF C1<N THEN 2310
2580 F2=0
2590 FOR I=1 TO N
2600 FOR J=1 TO N
2610 IF I=J=0 THEN 2630
2620 A(I,J)=H(I,J)*F(I)/F(J)
2630 Q=A(I,J)
2640 F2=F2+Q*Q
2650 NEXT J
2660 NEXT I
2670 MAT A=(1/F2)*A
2680 E2=F2
2690 RETURN ! FROM SUBROUTINE SC
ALE
2700 MAT A=H
2710 MAT F=(1)
2720 E2=1
2730 RETURN ! FROM SUBROUTINE SC
ALE
2740 ! SUBROUTINE HESQR
2750 IF N>2 THEN 2790
2760 IF N<2 THEN 3360
2770 S(1)=A(2,1)
2780 GOTO 3360
2790 M=N-2
2800 FOR K=1 TO M
2810 L=K+1
2820 S0=0
2830 FOR I=L TO N
2840 H(I,K)=A(I,K)
2850 S0=S0+ABS(A(I,K))
2860 NEXT I
2870 IF S0<>ABS(A(K+1,K)) THEN 2910
2880 S(K)=A(K+1,K)
2890 H(K+1,K)=0
2900 GOTO 3300
2910 S2=0
2920 FOR I=L TO N
2930 S1=A(I,K)
2940 S1=S1/S0
2950 A(I,K)=S1
2960 S2=S2+S1*S1
2970 NEXT I
2980 S1=SQR(S2)
2990 IF A(L,K)<0 THEN 3010
3000 S1=-S1
3010 S2=S2-S1*A(L,K)

```

```

3020 H(L,K)=H(L,K)-S1
3030 H(L,K)=H(L,K)-S1*S0
3040 S(K)=S1*S0
3050 X=S0*SQR(S2)
3060 FOR I=L TO N
3070 H(I,K)=H(I,K)/X
3080 S(I)=A(I,K)/S2
3090 NEXT I
3100 ! PREMULTIPLICATION BY MATR
    IX PR
3110 FOR J=L TO N
3120 S1=0
3130 FOR I=L TO N
3140 S1=S1+A(I,K)*A(I,J)
3150 NEXT I
3160 FOR I=L TO N
3170 A(I,J)=A(I,J)-S(I)*S1
3180 NEXT I
3190 NEXT J
3200 ! POST MULTIPLICATION BY MA
    TRIX PR
3210 FOR J=1 TO N
3220 S1=0
3230 FOR I=L TO N
3240 S1=S1+A(J,I)*A(I,K)
3250 NEXT I
3260 FOR I=L TO N
3270 A(J,I)=A(J,I)-S(I)*S1
3280 NEXT I
3290 NEXT J
3300 NEXT K
3310 FOR K=1 TO M
3320 A(K+1,K)=S(K)
3330 NEXT K
3340 ! TRANSFER UPPER HALF OF MA
    TRIX A TO ARRAY H AND CALCUL
    ATION OF SMALL NO. E0
3350 S(N-1)=A(N,N-1)
3360 E0=0
3370 FOR K=1 TO N
3380 Q(K)=0
3390 IF K<>N THEN E0=E0+S(K)^2
3400 FOR I=K TO N
3410 H(K,I)=A(K,I)
3420 E0=E0+A(K,I)^2
3430 NEXT I
3440 NEXT K
3450 E0=E3*SQR(E0)
3460 ! QR ITERATIVE PROCESS. UPP
    ER-HESS MATRIX H IS REDUCED
    TO UPPER MODIFIED TRIANGUL
    AR
3470 ! DETERMINATION OF SHIFT OF
    ORIGIN FOR THE FIRST STEP
    OF QR ITERATIVE PROCESS
3480 S3=A(N,N-1)
3490 IF N<=2 THEN S3=0
3500 IF A(N,N)<>0 THEN S3=0
3510 IF A(N-1,N)<>0 THEN S3=0
3520 IF A(N-1,N-1)<>0 THEN S3=0
3530 M=N
3540 N0=0
3550 M0=N*10
3560 ! TESTING IF UPPER HALF HES
    S MATRIX =0. IF SO, QR PROC
    ESS UNNECESSARY
3570 FOR I=2 TO N
3580 FOR K=I TO N
3590 IF A(I-1,K)<>0 THEN 3690
3600 NEXT K
3610 NEXT I
3620 FOR I=1 TO N
3630 Q(I)=1
3640 R(I)=A(I,I)
3650 I(I)=0
3660 NEXT I
3670 RETURN ! FROM SUBROUTINE HE
    SQR
3680 ! START MAIN LOOP OF QR PRO
    CESS IN HESQR
3690 K=M-1
3700 M1=K
3710 I=K
3720 ! FIND ANY DECOMPOSITIONS O
    F THE MATRIX
3730 REM GOTO 4300 IF LAST SUBMA
    T OF DECOMP OF ORDER 1
3740 REM GOTO 4360 IF LAST SUBMA
    T OF DECOMP OF ORDER 2
3750 IF K=0 THEN 4580
3760 IF K<0 THEN RETURN
3770 IF ABS(A(M,K))<=E0 THEN 458
    0
3780 IF M=2 THEN 4640
3790 I=I-1
3800 IF ABS(A(K,I))<=E0 THEN 383
    0
3810 K=I
3820 IF K>1 THEN 3790
3830 IF K=M1 THEN 4640
3840 ! TRANSFORMATION OF MATRIX
    OF ORDER >2
3850 S0=A(M,M)+A(M1,M1)+S3
3860 S1=A(M,M)*A(M1,M1)-A(M,M1)*
    A(M1,M)+.25*S3*S3
3870 A(K+2,K)=0
3880 ! CALCULATE X1,Y1,Z1 FOR SU
    BMATRIX OBTAINED BY DECOMP
3890 X=A(K,K)*(A(K,K)-S0)+A(K,K+
    1)*A(K+1,K)+S1
3900 Y=A(K+1,K)*(A(K,K)+A(K+1,K+
    1)-S0)
3910 R=ABS(X)+ABS(Y)
3920 IF R/E0-E0/E3>0 THEN 3960
3930 IF S3-A(M,M-1)=0 THEN 3960
3940 S3=A(M,M-1)
3950 GOTO 3830
3960 Z=A(K+2,K+1)*A(K+1,K)
3970 S3=0
3980 N0=N0+1

```

```

3990 ! LOOP FOR ONE STEP OF QR P
      PROCESS
4000 FOR I=K TO M1
4010 IF I=K THEN 4080
4020 ! CALCULATE XR,YR,ZR
4030 X=A(I,I-1)
4040 Y=A(I+1,I-1)
4050 Z=0
4060 IF I+2>M THEN 4080
4070 Z=A(I+2,I-1)
4080 S2=ABS(X)+ABS(Y)+ABS(Z)
4090 IF S2=0 THEN 4130
4100 X=X/S2
4110 Y=Y/S2
4120 Z=Z/S2
4130 S0=SQR(X*X+Y*Y+Z*Z)
4140 IF X<0 THEN 4160
4150 S0=-S0
4160 IF I=K THEN 4180
4170 A(I,I-1)=S0*S2
4180 IF S2<>0 THEN 4200
4190 IF I+3>M THEN 4540 ELSE 451
      0
4200 S1=1-X/S0
4210 S0=X-S0
4220 X=Y/S0
4230 Y=Z/S0
4240 ! PREMULTIPLICATION BY MATR
      IX PR
4250 FOR J=I TO M
4260 S0=A(I,J)+A(I+1,J)*X
4270 IF I+2>M THEN 4290
4280 S0=S0+A(I+2,J)*Y
4290 S0=S0*S1
4300 A(I,J)=A(I,J)-S0
4310 A(I+1,J)=A(I+1,J)-S0*X
4320 IF I+2>M THEN 4340
4330 A(I+2,J)=A(I+2,J)-S0*Y
4340 NEXT J
4350 ! POST MULTIPLICATION BY MA
      TRIX PR
4360 L=I+2
4370 IF I<M1 THEN 4390
4380 L=M
4390 FOR J=K TO L
4400 S0=A(J,I)+A(J,I+1)*X
4410 IF I+2>M THEN 4430
4420 S0=S0+A(J,I+2)*Y
4430 S0=S0*S1
4440 A(J,I)=A(J,I)-S0
4450 A(J,I+1)=A(J,I+1)-S0*X
4460 IF I+2>M THEN 4480
4470 A(J,I+2)=A(J,I+2)-S0*Y
4480 NEXT J
4490 IF I+3>M THEN 4540
4500 S0=-A(I+3,I+2)*Y*S1
4510 A(I+3,I)=S0
4520 A(I+3,I+1)=S0*X
4530 A(I+3,I+2)=S0*Y+A(I+3,I+2)
4540 NEXT I
4550 IF N0>M0 THEN 4840
4560 GOTO 3690
4570 ! COMPUTE THE LAST EIGENVAL
      UE
4580 R(M)=A(M,M)
4590 I(M)=0
4600 Q(M)=1
4610 M=K
4620 GOTO 3690
4630 ! COMPUTE EIGENVALUES OF LA
      ST 2X2 MATRIX OBTAINED BY Q
      ECOMPOSITION
4640 R=.5*(A(K,K)+A(M,M))
4650 S0=.5*(A(M,M)-A(K,K))
4660 S0=S0*S0+A(K,M)*A(M,K)
4670 Q(K)=1
4680 Q(M)=1
4690 IF S0<0 THEN 4770
4700 T0=SQR(S0)
4710 R(K)=R-T0
4720 R(M)=R+T0
4730 I(K)=0
4740 I(M)=0
4750 M=M-2
4760 GOTO 3690
4770 T0=SQR(-S0)
4780 R(K)=R
4790 I(K)=T0
4800 R(M)=R
4810 I(M)=-T0
4820 M=M-2
4830 GOTO 3690
4840 RETURN ! FROM SUBROUTINE HE
      SQ
4850 ! END OF SUBROUTINE HESQR
4860 ! SUBROUTINE REALVE
4870 V(1,I0)=1
4880 IF M=1 THEN 5890
4890 E1=R(I0)
4900 IF I0=M THEN 4990
4910 K=I0+1
4920 R=0
4930 FOR I=K TO M
4940 IF E1<>R(I) THEN 4970
4950 IF I(I)<>0 THEN 4970
4960 R=R+3
4970 NEXT I
4980 E1=E1+R*E3
4990 FOR K=1 TO M
5000 A(K,K)=A(K,K)-E1
5010 NEXT K
5020 ! GAUSSIAN ELIMINATION OF U
      PPER-HESS MATRIX A. ALL ROW
      CHANGES ARE INDICATED IN T
      HE ARRAY J
5030 ! ALL MULTIPLIERS ARE SAVED
      AS SUBDIAGONAL ELEMENTS OF
      A.
5040 K=M-1
5050 FOR I=1 TO K

```

```

5060 L=I+1
5070 J(I)=0
5080 IF A(I+1,I) <> 0 THEN 5120
5090 IF A(I,I) <> 0 THEN 5240
5100 A(I,I)=E0
5110 GOTO 5240
5120 IF ABS(A(I,I)) >= ABS(A(I+1,I)) THEN 5190
5130 J(I)=1
5140 FOR J=I TO M
5150 R=A(I,J)
5160 A(I,J)=A(I+1,J)
5170 A(I+1,J)=R
5180 NEXT J
5190 R=-A(I+1,I)/A(I,I)
5200 A(I+1,I)=R
5210 FOR J=L TO M
5220 A(I+1,J)=A(I+1,J)+R*A(I,J)
5230 NEXT J
5240 NEXT I
5250 IF A(M,M) <> 0 THEN 5280
5260 A(M,M)=E0
5270 ! VECTOR (1,1,...,1) IS STORED IN RIGHT HAND COLUMN VECTOR
5280 FOR I=1 TO M
5290 IF I>M THEN W(I)=0 ELSE W(I)=1
5300 NEXT I
5310 ! INVERSE ITERATION IS PERFORMED ON MATRIX UNTIL INFINITE NORM ON RIGHT HAND VECTOR > BOUND
5320 ! = .01/(N*E3)
5330 B3=.01/(N*E3)
5340 N0=0
5350 I1=1
5360 ! BACK SUBSTITUTION
5370 R=0
5380 FOR I=1 TO M
5390 J=M-I+1
5400 S0=W(J)
5410 IF J=M THEN 5470
5420 L=J+1
5430 FOR K=L TO M
5440 S1=W(K)
5450 S0=S0-S1*A(J,K)
5460 NEXT K
5470 W(J)=S0/A(J,J)
5480 T0=ABS(W(J))
5490 IF R>=T0 THEN 5510
5500 R=T0
5510 NEXT I
5520 ! COMPUTATION OF RIGHT HAND SIDE VECTOR FOR NEW ITERATION STEP
5530 FOR I=1 TO M
5540 W(I)=W(I)/R
5550 NEXT I
5560 ! TEST FOR CONVERGENCE--SEE SOURCE
5570 R1=0
5580 FOR I=1 TO M
5590 T0=0
5600 FOR J=I TO M
5610 T0=T0+A(I,J)*W(J)
5620 NEXT J
5630 T0=ABS(T0)
5640 IF R1>=T0 THEN 5660
5650 R1=T0
5660 NEXT I
5670 IF I1=1 THEN 5690
5680 IF P0<=R1 THEN 5890
5690 FOR I=1 TO M
5700 W(I,I0)=W(I)
5710 NEXT I
5720 P0=R1
5730 IF N0=1 THEN 5890
5740 IF I1>6 THEN 5900
5750 I1=I1+1
5760 IF R<B3 THEN 5790
5770 N0=1
5780 ! GAUSSIAN ELIMINATION OF RIGHT HAND SIDE VECTOR
5790 K=M-1
5800 FOR I=1 TO K
5810 R=W(I+1)
5820 IF J(I)=0 THEN 5860
5830 W(I+1)=W(I)+W(I+1)*A(I+1,I)
5840 W(I)=R
5850 GOTO 5870
5860 W(I+1)=W(I)+W(I)*A(I+1,I)
5870 NEXT I
5880 GOTO 5370
5890 Q(I0)=2
5900 IF M=N THEN 5950
5910 J=M+1
5920 FOR I=J TO N
5930 W(I,I0)=0
5940 NEXT I
5950 RETURN ! FROM REALVE
5960 ! SUBROUTINE COMPVE
5970 F4=R(I0)
5980 E4=I(I0)
5990 ! MODIFICATION OF EIGENVALUE IF MORE EIGENVALUES ARE EQUAL
6000 IF I0=M THEN 6120
6010 K=I0+1
6020 R=0
6030 FOR I=K TO M
6040 IF F4 <> R(I) THEN 6070
6050 IF ABS(E4) <> ABS(I(I)) THEN 6070
6060 R=R+3
6070 NEXT I
6080 R=R/E3
6090 F4=F4+R
6100 E4=E4+R
6110 ! MATRIX ((H-F4*I)*(H-F4*I)+(E4*E4*I)

```

```

6130 P=F4^2+E4^2
6130 S0=2*F4
6140 L=M-1
6150 FOR I=1 TO M
6160 FOR J=I TO M
6170 D=0
6180 A(J,I)=0
6190 FOR K=I TO J
6200 D=D+H(I,K)*H(K,J)
6210 NEXT K
6220 A(I,J)=D-S0*H(I,J)
6230 NEXT J
6240 A(I,I)=A(I,I)+R
6250 NEXT I
6260 FOR I=1 TO L
6270 R=S(I)
6280 A(I+1,I)=-S0*R
6290 I2=I+1
6300 FOR J=1 TO I2
6310 A(J,I)=A(J,I)+R*H(J,I+1)
6320 NEXT J
6330 IF I=1 THEN 6350
6340 A(I+1,I-1)=R*S(I-1)
6350 FOR J=I TO M
6360 A(I+1,J)=A(I+1,J)+R*H(I,J)
6370 NEXT J
6380 NEXT I
6390 ! GAUSSIAN ELIMINATION OF M
MATRIX ((H-F4*I)*(H-F4*I)+(E
4^2)*I) IN ARRAY A.
6400 ! ROW INTERCHANGES THAT OCC
UR, INDICATED IN ARRAY J.
6410 ! ALL MULTIPLIERS USED ARE
STORED IN FIRST AND SECOND
DIAGONAL OF A
6420 K=M-1
6430 FOR I=1 TO K
6440 I2=I+1
6450 I3=I+2
6460 J(I)=0
6470 IF I=K THEN 6490
6480 IF A(I+2,I) <> 0 THEN 6530
6490 IF A(I+1,I) <> 0 THEN 6530
6500 IF A(I,I) <> 0 THEN 6760
6510 A(I,I)=E0
6520 GOTO 6760
6530 IF I=K THEN 6590
6540 IF ABS(A(I+1,I)) >= ABS(A(I+2
,I)) THEN 6590
6550 IF ABS(A(I,I)) >= ABS(A(I+2,I
)) THEN 6690
6560 L=I+2
6570 J(I)=2
6580 GOTO 6620
6590 IF ABS(A(I,I)) >= ABS(A(I+1,I
)) THEN 6670
6600 L=I+1
6610 J(I)=1
6620 FOR J=I TO M
6630 R=A(I,J)
6640 A(I,J)=A(L,J)
6650 A(L,J)=R
6660 NEXT J
6670 IF I <> K THEN 6690
6680 I3=I2
6690 FOR L=I2 TO I3
6700 R=-A(L,I)/A(I,I)
6710 A(L,I)=R
6720 FOR J=I2 TO M
6730 A(L,J)=A(L,J)+R*A(I,J)
6740 NEXT J
6750 NEXT L
6760 NEXT I
6770 IF A(M,M) <> 0 THEN 6810
6780 A(M,M)=E0
6790 ! VECTOR (1,1,...,1) STORED
IN RIGHT-HAND SIDE VECTORS
V( ,I0)&V( ,I0-1) REPRESEN
TING
6800 ! COMPLEX RIGHT-HAND SIDE V
ECTORS
6810 FOR I=1 TO M
6820 IF I > M THEN 6860
6830 V(I,I0)=1
6840 V(I,I0-1)=1
6850 GOTO 6880
6860 V(I,I0)=0
6870 V(I,I0-1)=0
6880 NEXT I
6890 ! INVERSE ITERATION PERFORM
ED ON THE MATRIX UNTIL INFI
NITE NORM OF RIGHT-HAND SID
E VECTOR
6900 ! IS GREATER THAN BOUND=.01
/(N*E3)
6910 B3=.01/(N*E3)
6920 N0=0
6930 I1=1
6940 FOR I=1 TO M
6950 W(I)=H(I,I)-F4
6960 NEXT I
6970 ! SEQUENCE OF COMPLEX VECTO
RS Z(S)=P(S)+I*Q(S) & W(S+1
)=V(S+1)+I*W(S+1) GIVEN BY
RELATIONS
6980 REM (A-(F4-I*E4)*I)*W(S+1)=
Z(S) & Z(S+1)=W(S+1)/MAX(W(
S+1))
6990 ! THE FINAL W(S) TAKEN AS C
OMPUTED EIGENVECTOR
7000 ! COMPUTATION OF RIGHT-HAND
SIDE VECTOR (A-F4*I)*P(S)-
E4*Q(S). A IS UPPER-HESS MA
TRIX.
7010 FOR I=1 TO M
7020 D=W(I)*V(I,I0)
7030 IF I=1 THEN 7050
7040 D=D+S(I-1)*V(I-1,I0)
7050 L=I+1
7060 IF L > M THEN 7100

```

```

7070 FOR K=L TO M
7080 D=D+H(I,K)*V(K,I0)
7090 NEXT K
7100 V(I,I0-1)=D-E4*V(I,I0-1)
7110 NEXT I
7120 ! GAUSSIAN ELIMINATION OF R
      !IGHT-HAND SIDE VECTOR
7130 K=M-1
7140 FOR I=1 TO K
7150 L=I+J(I)
7160 R=V(L,I0-1)
7170 V(L,I0-1)=V(I,I0-1)
7180 V(I,I0-1)=R
7190 V(I+1,I0-1)=V(I+1,I0-1)+A(I
+1,I)*R
7200 IF I=K THEN 7220
7210 V(I+2,I0-1)=V(I+2,I0-1)+A(I
+2,I)*R
7220 NEXT I
7230 ! COMPUTATION OF REAL PART
      W(S+1) OF COMPLEX VECTOR W(
      S+1).
7240 ! VECTOR V(S+1) IS OBTAINED
      AFTER BACK SUBSTITUTION.
7250 FOR I=1 TO M
7260 J=M-I+1
7270 D=V(J,I0-1)
7280 IF J=M THEN 7340
7290 L=J+1
7300 FOR K=L TO M
7310 D1=A(J,K)
7320 D=D-D1*V(K,I0-1)
7330 NEXT K
7340 V(J,I0-1)=D/A(J,J)
7350 NEXT I
7360 ! COMPUTATION OF IMAG PART
      W(S+1) OF VECTOR W(S+1).
7370 ! WHERE V(S+1)=(P(S)-(A-F4*
      I)*U(S+1))/E4
7380 FOR I=1 TO M
7390 D=W(I)*V(I,I0-1)
7400 IF I=1 THEN 7420
7410 D=D+S(I-1)*V(I-1,I0-1)
7420 L=I+1
7430 IF L>M THEN 7470
7440 FOR K=L TO M
7450 D=D+H(I,K)*V(K,I0-1)
7460 NEXT K
7470 V(I,I0)=(V(I,I0)-D)/E4
7480 NEXT I
7490 ! COMPUTATION OF (INFINITE
      NORM OF W(S+1))^2
7500 L=1
7510 S0=0
7520 FOR I=1 TO M
7530 R=V(I,I0)^2+V(I,I0-1)^2
7540 IF R<=S0 THEN 7570
7550 S0=R
7560 L=I
7570 NEXT I
7580 ! COMPUTATION OF VECTOR Z(S
+1) WHERE Z(S+1)=W(S+1)/COM
PONENT OF W(S+1) WITH LARGE
ST ABS VAL
7590 U=V(L,I0-1)
7600 V=V(L,I0)
7610 FOR I=1 TO M
7620 B=V(I,I0)
7630 R=V(I,I0-1)
7640 V(I,I0)=(R*U+B*V)/S0
7650 W(I,I0-1)=(B*U-R*V)/S0
7660 NEXT I
7670 ! TEST FO CONVERGENCE--SEE
      SOURCE
7680 B=0
7690 FOR I=1 TO M
7700 R=W(I)*V(I,I0-1)-E4*V(I,I0)
7710 U=W(I)*V(I,I0)+E4*V(I,I0-1)
7720 IF I=1 THEN 7750
7730 R=R+S(I-1)*V(I-1,I0-1)
7740 U=U+S(I-1)*V(I-1,I0)
7750 L=I+1
7760 IF L>M THEN 7810
7770 FOR J=L TO M
7780 R=R+H(I,J)*V(J,I0-1)
7790 U=U+H(I,J)*V(J,I0)
7800 NEXT J
7810 U=R^2+U^2
7820 IF B>=U THEN 7840
7830 B=U
7840 NEXT I
7850 IF I1=1 THEN 7870
7860 IF P0<=B THEN 7960
7870 MAT D(1:N)=V(1:N,I0)
7880 MAT E(1:N)=V(1:N,I0-1)
7890 P0=B
7900 IF N0=1 THEN 7980
7910 IF I1>6 THEN 8000
7920 I1=I1+1
7930 IF B3>SQR(S0) THEN 7010
7940 N0=1
7950 GOTO 7010
7960 MAT V(1:N,I0)=D(1:N)
7970 MAT V(1:N,I0-1)=E(1:N)
7980 Q(I0-1)=2
7990 Q(I0)=2
8000 RETURN ! FROM COMPVE

```

```

8010 CLEAR @ PRINT
8020 IMAGE MD.DDDE,2X,"I",SD.000
      E
8030 MAT A=Z
8040 FOR I=1 TO N
8050 PRINT "EigenVALUE #",I,": "
8060 PRINT USING 8020 : R(I),I(
      )
8070 PRINT
8080 PRINT "EigenVECTOR:"
8090 PRINT
8100 FOR J=1 TO N
8110 PRINT USING 8020 : V(J,I),H
      (J,I)
8120 NEXT J
8130 PRINT
8140 PRINT "[A]v(I):"
8150 FOR J=1 TO N
8160 R=0 @ C=0
8170 FOR K=1 TO N
8180 R=R+A(J,K)*V(K,I)
8190 C=C+A(J,K)*H(K,I)
8200 NEXT K
8210 PRINT USING 8020 : R,C
8220 F(I)=R @ Q(I)=C
8230 NEXT J
8240 PRINT
8250 PRINT "L(I)*v(I):"
8260 FOR K=1 TO N
8270 D(I)=R(I)*V(K,I)-I(I)*H(K,I
      )
8280 E(I)=R(I)*H(K,I)+I(I)*V(K,I
      )
8290 PRINT USING 8020 : D(I),E(I
      )
8300 NEXT K
8310 PRINT
8320 FOR J=1 TO N
8330 M=R(J)*R(J)+I(J)*I(J)
8340 IF ABS(F(J)-D(J))>.001*M TH
      EN 8370
8350 IF ABS(Q(J)-E(J))>.001*M TH
      EN 8370
8360 GOTO 8380
8370 PRINT "Error at EigenVALUE
      #",I
8380 NEXT I
8390 CLEAR @ PRINT @ BEEP
8400 DISP "Insert CASSETTE for V
      ECTORS."
8410 DISP "It must be set to REC
      ORD."
8420 DISP
8430 DISP "Type: CREATE 'name--'
      ,2*N,8*N"
8440 DISP "where N is order of m
      atrix.e.g.4"
8450 DISP "Press CONT when ready
      "
8460 PAUSE

```

For each eigenvalue

and the corresponding eigenvector

Check that the basic equation defining the eigenvalue/vector problem is true: compare matrix times eigenvector

with eigenvalue times eigenvector

If not nearly equal, indicate an error.

Load cassette to dump eigenvector to a file.

```

8470 CLEAR @ PRINT
8480 DISP "Enter FILE NAME."
8490 DISP "( 1-6 characters )"
8500 INPUT F#
8510 PRINT "VECTOR File Name:":F
#
8520 CLEAR @ PRINT
8530 ASSIGN# 2 TO F#
8540 FOR J=1 TO N
8550 FOR I=1 TO N
8560 D(I)=V(I,J)
8570 NEXT I
8580 PRINT# 2,J : D()
8590 NEXT J
8600 FOR J=N+1 TO 2*N
8610 FOR I=1 TO N
8620 D(I)=H(I,J-N)
8630 NEXT I
8640 PRINT# 2,J : D()
8650 NEXT J
8660 ASSIGN# 2 TO #
8670 BEEP @ PRINT @ PRINT "END"
8680 DISP "END"
8690 END

```

Save column eigenvector (real part)
on a file record

Save column eigenvector (imaginary part)
on a file record.

Stop.

Appendix C. Software to Calculate Termination Parameters

An annotated copy of the program CTIMEP described in the text, follows. It occupies 2,946 bytes of memory.

PROGRAM NAME: CTIMEP

```
100 OPTION BASE 1
110 DEG
120 DIM D(4),M(4,4),H(4,4),Q(4),
    P(4,8)
125 DIM Q(4,8),R(4,8)
130 DISP "Insert 'UCTRdd' cartridge."
140 DISP
150 DISP "Enter FILE NAME:"
160 INPUT F#
170 PRINT "UCTR file name: ";F#
180 ASSIGN# 1 TO F#
190 FOR J=1 TO 4
200 READ# 1,J ; D()
210 FOR I=1 TO 4
220 M(I,J)=D(I)
230 NEXT I
240 NEXT J
250 FOR J=5 TO 8
260 READ# 1,J ; D()
270 FOR I=1 TO 4
280 H(I,J-4)=D(I)
290 NEXT I
300 NEXT J
305 ASSIGN# 1 TO #
310 CLEAR @ PRINT
315 IMAGE MD,DDDE,2X,"1",50.00DE
320 PRINT "EigenVECTORS:"
330 PRINT
340 FOR J=1 TO 4
350 PRINT "EigenVECTOR #";J
360 PRINT
370 FOR I=1 TO 4
380 PRINT USING 315 ; M(I,J),H(I
    ,J)
390 NEXT I
395 PRINT
400 NEXT J
402 MAT M=TRN(M)
404 MAT H=TRN(H)
410 PRINT @ CLEAR @ BEEP
420 DISP "Insert 'POWadd' cartridge."
430 DISP
440 DISP "Enter FILE NAME:"
450 INPUT F#
460 PRINT "POWER file name: ";F#
470 ASSIGN# 1 TO F#
475 FOR R8=1 TO 8
480 READ# 1,R8 ; Q()
490 PRINT "POWER vector:"
510 PRINT
520 FOR I=1 TO 4
530 PRINT Q(I)
535 P(I,R8)=Q(I)
540 NEXT I
545 NEXT R8
548 ASSIGN# 1 TO #
550 CLEAR @ PRINT
560 PRINT "[C]*[P]:"
```

Read in file containing calibration matrix $[C^t]$ column by column

Real part

Imaginary part

Print out Eigenvectors

Transpose $[C^t]$ to $[C]$

Read in file containing the matrices $[P]$ and $[P']$ column by column. Store internally in a 4x8 augmented matrix

Print each column

```

570 MAT R=W*P
580 MAT L=H*P
590 FOR J=1 TO 8
600 PRINT
610 FOR I=1 TO 4
630 PRINT USING 315 ; R(I,J),C(I
    ,J)
635 NEXT I
640 NEXT J
700 FOR I=1 TO 4
710 D=R(I,1)^2+C(I,1)^2
720 FOR J=1 TO 4
730 V=(R(I,1)*V(I,J)+C(I,1)*H(I
    ,J))/D
740 H=(R(I,1)*H(I,J)-C(I,1)*V(I
    ,J))/D
741 V(I,J)=V
742 H(I,J)=H
745 NEXT J
747 NEXT I
750 CLEAR @ PRINT
760 PRINT "NORMALIZED [C]*[P]:"
765 MAT R=W*P
766 MAT C=H*P
770 FOR J=1 TO 8
780 PRINT
790 FOR I=1 TO 4
800 PRINT USING 315 ; R(I,J),C(I
    ,J)
810 NEXT I
820 NEXT J
830 PRINT @ PRINT "MAG & PHASE:"
840 FOR J=1 TO 8
850 PRINT
860 FOR I=1 TO 4
870 D=R(I,J)^2+C(I,J)^2
880 A=ATN2(C(I,J),R(I,J))
890 PRINT USING 900 ; SQR(D),A
900 IMAGE MD,00DE,3%,S00D,00
910 NEXT I
920 NEXT J
930 PRINT "END"
9998 RAD
9999 END

```

Form matrices for real and imaginary parts of $[C]*[P \ \& \ P']$ where $[P \ \& \ P']$ is the augmented matrix.

Print results

Normalize $[C]$ by the method described in the text.

Print normalized complex results of $[C] * [P \ \& \ P']$ in cartesian form

Express normalized complex results in polar form.

Appendix D. Energy Conservation in the QUOSM

There are no particularly significant occurrences of absorption within the QUOSM, except when the quasi-optical attenuators are used. In the simulations actually made absorption was neglected. In this case and in the steady state, the source power entering the QUOSM must equal the sum of the powers leaving all of the QUOSM ports. The authors have occasionally noted discussions of Michelson interferometers in which it is argued that the power coming out of a particular port can exceed the input power for a particular path difference so long as the average over all path differences agrees with energy conservation. This is clearly nonsense since one could leave the instrument set at a particular path difference and get more power out than is put in. As described in the text, the simulation program written for the QUOSM was provided with the facility to check for energy conservation, and this was helpful in the identification and elimination of several errors during the development of the program.

One particularly interesting requirement in the simulation was exposed in this way; namely, that all partial reflections must be modeled with a certain degree of realism or else energy conservation will appear to fail. Partial reflection (and transmissions) occur at the beam splitters and at the interfaces between the QUOSM and the source and detector, and the key properties are the phase changes introduced at these surfaces. Chantry recognized this fact [see p.67 ref.18] and stated that what is required is for a π phase change to occur somewhere in the system. A more complete statement is given by the Stoke's relations [D1, D2] for a non-absorbing interface between non-absorbing media; namely, if t and r are the complex amplitude transmission and reflection coefficients for incidence on one side of the interface and t' and r' , for the other side, then

$$tt'^* = 1 - rr'^*$$

$$r' = -r$$

Provided these conditions are met, the expected energy conservation should occur in the system.

In the simulation program described elsewhere, the phase behavior of the Mylar film beam splitter was modeled in detail, following reference [18]. However, it is more difficult to specify and describe the source and detector interfaces in similar detail, and so a simplification has been made, one which satisfies the above Stokes' relations. In both cases, all phase shifts at the interface are set equal to zero with this exception: the waves travelling from the principal beam splitter toward the source or detector ports are shifted by π at the interface when they are reflected. Although such details are important in the matter of energy conservation, they have a trivial effect on the standing wave patterns, and thus there is no loss of generality in such an oversimplification. In the simulations of the QUOSM which have been described, the operator controls the remaining significant parameters of the detector and source interfaces, their power reflectance values, and thereby establishes the magnitude of the standing wave effects.

References for Appendix D

- D1. G.G. Stokes, Mathematical and Physical Papers, Vol. II, New York: Johnson Reprint Corp., pp. 89-103 (1966).
- D2. E.Hecht and A. Zajac, Optics, Reading, Massachusetts: Addison-Wesley Publishing Co., p.91ff (1974).
- 18. See reference list with main text.